

NATIONAL CENTER FOR EARTHQUAKE
ENGINEERING RESEARCH

State University of New York at Buffalo

Empirical Analysis of
Horizontal Ground Displacement
Generated by Liquefaction-Induced Lateral Spreads

by

S.F. Bartlett and T.L. Youd
Department of Civil Engineering
Brigham Young University
Provo, Utah 84602

Technical Report NCEER-92-0021

August 17, 1992

This research was conducted at Brigham Young University and was partially supported by the National Science Foundation under Grant No. BCS 90-25010 and the New York State Science and Technology Foundation under Grant No. NEC-91029.

NOTICE

This report was prepared by Brigham Young University as a result of research sponsored by the National Center for Earthquake Engineering Research (NCEER) through grants from the National Science Foundation, the New York State Science and Technology Foundation, and other sponsors. Neither NCEER, associates of NCEER, its sponsors, Brigham Young University, nor any person acting on their behalf:

- a. makes any warranty, express or implied, with respect to the use of any information, apparatus, method, or process disclosed in this report or that such use may not infringe upon privately owned rights; or
- b. assumes any liabilities of whatsoever kind with respect to the use of, or the damage resulting from the use of, any information, apparatus, method or process disclosed in this report.

Any opinions, findings, and conclusions or recommendations expressed in this publication are those of the author(s) and do not necessarily reflect the views of the National Science Foundation, the New York State Science and Technology Foundation, or other sponsors.



**Empirical Analysis of Horizontal Ground Displacement
Generated by Liquefaction-Induced Lateral Spreads**

by

S.F. Bartlett and T.L. Youd

August 17, 1992

Technical Report NCEER-92-0021

NCEER Project Number 90-1505

NSF Master Contract Number BCS 90-25010

and

NYSSTF Grant Number NEC-91029

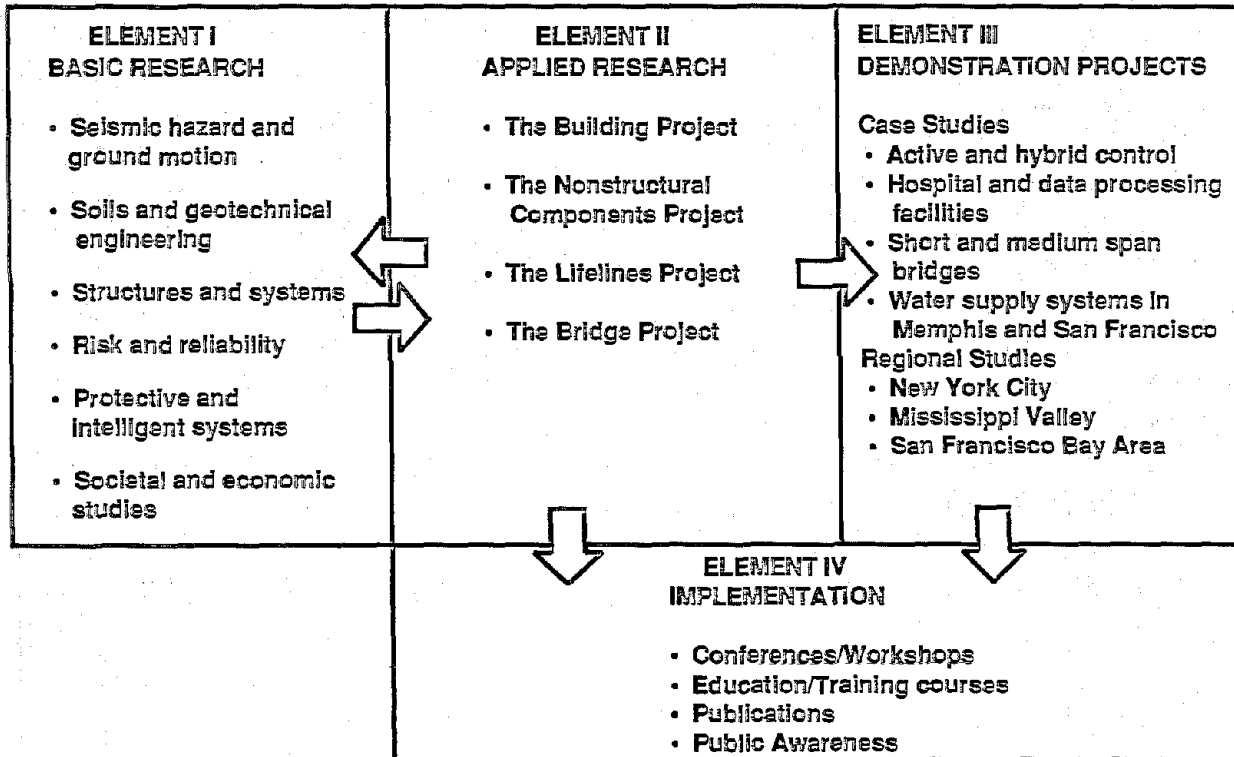
- 1 Research Assistant, Civil Engineering Department, Brigham Young University
- 2 Professor, Civil Engineering Department, Brigham Young University

NATIONAL CENTER FOR EARTHQUAKE ENGINEERING RESEARCH
State University of New York at Buffalo
Red Jacket Quadrangle, Buffalo, NY 14261

PREFACE

The National Center for Earthquake Engineering Research (NCEER) was established to expand and disseminate knowledge about earthquakes, improve earthquake-resistant design, and implement seismic hazard mitigation procedures to minimize loss of lives and property. The emphasis is on structures in the eastern and central United States and lifelines throughout the country that are found in zones of low, moderate, and high seismicity.

NCEER's research and implementation plan in years six through ten (1991-1996) comprises four interlocked elements, as shown in the figure below. Element I, Basic Research, is carried out to support projects in the Applied Research area. Element II, Applied Research, is the major focus of work for years six through ten. Element III, Demonstration Projects, have been planned to support Applied Research projects, and will be either case studies or regional studies. Element IV, Implementation, will result from activity in the four Applied Research projects, and from Demonstration Projects.



Tasks in Element I, **Basic Research**, include research in seismic hazard and ground motion; soils and geotechnical engineering; structures and systems; risk and reliability; protective and intelligent systems; and societal and economic impact.

The soils and geotechnical engineering program constitutes one of the important areas of research in Element I, **Basic Research**. Major tasks are described as follows:

1. Perform site response studies for code development.
2. Develop a better understanding of large lateral and vertical permanent ground deformations associated with liquefaction, and develop corresponding simplified engineering methods.
3. Continue U.S. - Japan cooperative research in liquefaction, large ground deformation, and effects on buried pipelines.
4. Perform soil-structure interaction studies on soil-pile-structure interaction and bridge foundations and abutments, with the main focus on large deformations and the effect of ground failure on structures.
5. Study small earth dams and embankments.

This report describes an empirical model for estimating the horizontal ground displacement caused by liquefaction-induced lateral spreads. The model was developed from multiple linear regression analyses of data pertaining to earthquake, topographical, and geological variables for Japanese and U.S. earthquakes. Two types of lateral spreads are distinguished in the model: lateral spread toward a free face; and lateral spread down gentle ground slopes. Horizontal movement associated with free face lateral spreads was found to correlate with the logarithm of the free face ratio, which is the height of the free face divided by horizontal distance from the free face. In contrast, displacement associated with ground slope failure is strongly correlated with the steepness of the ground slope. The model is expressed as a multiple linear regression equation linking lateral movement with moment magnitude of the earthquake, distance from the seismic source, free face ratio, ground slope, thickness of saturated granular soil with a modified standard penetration value $[(N_1)_{60}]$ less than or equal to 15, $(N_1)_{60}$ of the soil with lowest factor of safety against liquefaction, and depth to the soil with lowest safety factor against liquefaction. Because the model was developed for a wider range of seismic and site conditions than utilized in previously proposed empirical models, it is more general and will result in better estimates. The model appears to give the best predictions for earthquakes with moment magnitudes of 6.5 to 8.0 at sites underlain by sands and silty sand layers with $(N_1)_{60} \leq 15$ and thickness greater than 0.3 m at depths less than 15 m. The model does not appear to work well for gravels with mean grain sizes greater than 2 mm. Because the model was primarily developed from western U.S. and Japanese data, it is best suited to regions that have high to moderate ground motion attenuation.

ABSTRACT

Liquefaction-induced ground failure is responsible for considerable damage to engineered structures during major earthquakes. Presently, few empirical techniques exist for estimating the amount of horizontal ground displacement resulting from liquefaction-induced lateral spread. None of these techniques fully addresses all the earthquake and site conditions known to influence ground displacement.

This study compiles earthquake, geological, topographical, and soil factors that affect ground displacement and develops empirical models from these factors. Case histories of lateral spread are gathered from the 1906 San Francisco, 1964 Alaska, 1964 Niigata, 1971 San Fernando, 1979 Imperial Valley, 1983 Nihonkai-Chubu, 1983 Borah Peak, Idaho, and 1987 Superstition Hills earthquakes. Multiple linear regression (MLR) is used to develop empirical models from the compiled data. Two general models are derived herein, one for free face failures and one for ground slope failures. The predictive performance of the proposed empirical models is determined by comparing predicted displacements with those actually measured at the case history sites.

ACKNOWLEDGEMENTS

This study was funded by the National Center for Earthquake Engineering Research (NCEER), State University of New York at Buffalo. Also, an earlier statistical study was supported by the U.S. Army Corps of Engineers, Washington, D.C., under contract DACW39-87-M-2007 (Bartlett and Youd, 1990). We are grateful to these two organizations for their financial support and technical interest. We also express our appreciation to Dr. Masanori Hamada of Tokai University, Shimizu, Japan, for providing data and maps from his case studies of displacements generated by the 1964 Niigata and 1983 Nihonkai-Chubu, Japan, earthquakes. These extensive data made our regression analyses possible. We also acknowledge the assistance of Dr. Bruce Collins of Brigham Young University in reviewing the statistical analyses in this report.

TABLE OF CONTENTS

SECTION	TITLE	PAGE
1	INTRODUCTION	1-1
2	LIQUEFACTION, LATERAL SPREAD, AND DISPLACEMENT MODELS	2-1
2.1	Liquefaction	2-1
2.2	Lateral Spread	2-1
2.3	Modeling Lateral Spread Displacement	2-1
2.4	Static Models from Elastic Theory	2-2
2.5	Dynamic Models	2-2
2.6	Sliding Block Analysis	2-3
2.7	Empirical Models	2-4
2.7.1	Liquefaction Severity Index	2-4
2.7.2	Hamada et al. (1986) Equation for Lateral Spread Displacement	2-5
2.7.3	Summary of Empirical Models	2-7
2.7.4	Towards a More Comprehensive, Empirical Model	2-7
3	EMPIRICAL ANALYSIS OF LATERAL SPREAD FOR NIIGATA AND NOSHIRO, JAPAN	3-1
3.1	Multiple Linear Regression	3-1
3.2	Compilation of Case History Data for MLR Analyses	3-3
3.3	Strategy for Development of MLR Models	3-5
3.4	Free Face MLR Model for Lateral Spreads in Niigata, Japan	3-8
3.5	Ground Slope Model for Niigata and Noshiro, Japan	3-14
4	COMBINED MLR MODEL FOR JAPANESE AND U.S. CASE HISTORIES	4-1
4.1	Earthquake Factors	4-1
5	APPLICATION AND LIMITATIONS OF MLR MODEL	5-1
5.1	Ground Motion Attenuation	5-1
5.2	Earthquake Magnitude	5-5
5.3	Distance to the Fault Rupture or Zone of Seismic Energy Release	5-6
5.4	Free Face Ratio and Ground Slope	5-7
5.5	Gravelly Soils	5-8
5.6	Fines Content and Layered Profiles	5-8
5.7	Soils with $(N_1)_e$ Values Greater than 15	5-10
5.8	Thickness and Depth of the Liquefiable Layer	5-11
5.9	Residual Strength and SPT N Measures	5-11
5.10	Boundary Effects	5-12
5.11	Flow Chart for the Application of Equation 4.1.9	5-12
5.12	Calculation of the Upper Prediction Limit for Displacement	5-14
5.13	Comparison of Equation 4.1.9 with Other Empirical Models	5-16
6	CONCLUSIONS	6-1
7	REFERENCES	7-2
APPENDIX 1	DISCUSSION OF INDEPENDENT VARIABLES USED IN MLR ANALYSES	A1-1
A1.1	Earthquake Independent Variables	A1-1
A1.1.1	Earthquake Magnitude	A1-1
A1.1.2	Distance to Seismic Energy Source or Fault Rupture	A1-4
A1.1.3	Peak Ground Acceleration	A1-4
A1.1.4	Duration of Strong Ground Motion	A1-5
A1.2	Topographical Independent Variables	A1-6
A1.2.1	Ground Slope	A1-6
A1.2.2	Distance to and Height of Free Face	A1-6
A1.3	Geological and Soil Independent Variables	A1-7
A1.3.1	Geological and Soil Measures from the Simplified Procedure	A1-10
A1.3.2	Liao's Probability Curves for the Simplified Procedure	A1-14
A1.4	Weighted Averaging Routine	A1-18

TABLE OF CONTENTS

SECTION	TITLE	PAGE
APPENDIX 2	MINITAB ANALYSES	A2-1
A2.1	Minitab Analysis for Equation 3.4.10	A2-1
A2.2	Minitab Analysis for Equation 3.5.3	A2-4
A2.3	Minitab Analysis for Equation 4.1.9	A2-7

LIST OF ILLUSTRATIONS

FIGURE	TITLE	PAGE
2-1	Block diagram of a lateral spread before and after failure. Liquefaction occurs in the cross-hatched zone. Surface layer displaces laterally downslope (after Youd, 1984).	2-2
2-2 (a)	Illustration of slope and thickness measurements used in equation 2.7.2.8 (after Hamada et al., 1986).	2-5
2-2 (b)	Technique used by Hamada et al. to measure the ground slope for lateral spreads along the Shinano River (after Hamada et al., 1986).	2-6
2-3	Observed displacements plotted against displacements calculated from Equation 2.7.2.8 (after Hamada et al., 1986).	2-7
3-1	Examples of standard residual plots.	3-2
3-2	A section of working maps developed by Hamada et al. (1986) showing displacement vectors and locations of SPT boreholes from an area along the Shinano River near the Echigo Railway Bridge in Niigata, Japan.	3-6
3-3	Plot of ground displacement, Y , versus distance from the free face, L , for lateral spreads along the Shinano River, Niigata, Japan.	3-8
3-4	Plot of ground displacement, D_H , versus free face ratio, W , for lateral spreads along the Shinano River, Niigata, Japan. . .	3-9
3-5	Diagram showing that the shear force acting along the base of slide block is proportional to $\sin (H/L)$	3-9
3-6	Plot of $\text{LOG } D_H$ versus $\text{LOG } W$ for lateral spread displacements along the Shinano River, Niigata, Japan showing an approximately linear relationship.	3-10
3-7	Standardized residuals, e_i 's, from model 3.4.4 plotted against $\text{LOG } D_H$ showing no evidence of nonconstant variance.	3-10
3-8	Definition of free face factors, L and H , and ground slope, S , for free face failures.	3-12
3-9	Standardized residuals for models 3.4.4, 3.4.6, 3.4.7, and 3.4.8	13
3-10	Plot of measured displacements, D_H , versus predicted displacements, D_{Hmat} , for Equation 3.4.10, Shinano River, Niigata.	3-14
3-11	Case 1. Definition of ground slope, S , for long uniform slopes. Cases 2 - 4. Definition of S for nonuniform slopes.	3-15
3-12	Typical topography and ground displacement pattern for ground slope failures in Noshiro, Japan, (after Hamada et al., 1986). . .	3-16
3-13	Plot of log of displacement, $\text{LOG } D_H$, versus log of ground slope, $\text{LOG } S$, for ground slope failures indicating an approximately linear trend.	3-17

LIST OF ILLUSTRATIONS

FIGURE	TITLE	PAGE
3-14	Plot of measured displacements, D_H , versus predicted displacements, D_{Hhat} , for Equation 3.5.3, ground slope failures, Niigata and Noshiro.	3-17
4-1	Plot of measured displacements, D_H , versus predicted displacements, D_{Hhat} , for model 4.1.5 using Japanese and U.S. case history data.	4-3
4-2	Performance of MLR model prior to including Ambraseys' data and adding a R term.	4-4
4-3	Performance of MLR model after including Ambraseys' data and adjusting for R.	4-5
4-4	Plot of measured displacements, D_H , versus predicted displacements, D_{Hhat} , for Equation 4.1.9 using Japanese, U.S., and Ambraseys' data.	4-6
5-1	Histograms for (1) displacement, D_H , (2) magnitude, M , (3) distance to seismic energy source, R , (4) peak ground acceleration, A .	5-2
5-2	Histograms for (1) duration, D , (2) free face ratio, W , (3) ground slope, S , and, (4) thickness with $(N1)_{60} < 15$, T_{15}	5-3
5-3	Histograms for (1) fines content, F_{15} , (2) mean grain size, $D50_{15}$, (3) depth to low FS, Z_s , (4) lowest $N1_{60}$	5-4
5-4	Graph for Determining Equivalent Source Distance, R_{eq} , from Magnitude and Peak Acceleration.	5-5
5-5	Approximate Curve for Estimating A for Stiff Soil Sites (Modified from Idriss, 1990).	5-6
5-6	Standardized residuals, e_i 's, plotted against the average mean grain size, $D50_{15}$, in T_{15} , showing outliers in gravelly soils.	5-8
5-7	Plot of ranges of F_{15} versus $D50_{15}$ for which Equation 4.1.9 has been verified (data from 267 boreholes).	5-9
5-8	Plot of measured displacements versus displacements predicted by Equation 4.1.9 for displacements that are less than 2 meters.	5-10
5-9	Flow chart for the application of Equation 4.1.9	5-13
5-10	Comparison of D_H versus D_{Hhat} for LSI model, Hamada et al. thickness-slope model, and Equation 4.1.9 showing improved performance of Equation 4.1.9.	5-18
A1-1	A sample SPT borehole taken at Railroad Bridge Mile Post 147.1, Matanuska River, Alaska.	A1-8
A1-2	Chart for evaluation of CSRL of sands for earthquakes of different magnitudes (NRC, 1985).	A1-11
A1-3	Relationship between CSRL and $N1_{60}$ values for silty sands for $M = 7.5$ earthquakes (NRC, 1985).	A1-12
A1-4	SPT $(N1)_{60}$ values and cyclic stress ratios (CSR) for SPT borehole at Railroad Bridge Milepost 147.1, Matanuska River, Alaska.	A1-13

LIST OF ILLUSTRATIONS

FIGURE	TITLE	PAGE
A1-5	Contours of equal probability of liquefaction for: (a) clean sands (i.e. fines content $\leq 12\%$), and (b) silty sands (i.e., fines content $> 12\%$) (Liao, 1986).	A1-16
A1-6	Weighted average used to assign borehole measurements to displacement vectors.	A1-18

LIST OF TABLES

TABLE	TITLE	PAGE
3-1	Earthquake and Lateral Spread Sites Used in this Study. . . .	3-4
3-2	Summary of Independent Variables Considered in MLR Analysis.	3-7
3-2 (cont.)	Summary of Independent Variables Considered in MLR Analysis.	3-8
4-1	Average Site Conditions for Case Studies Tabulated by Earthquake	4-8
4-2	Observations from Ambraseys' Study Used to Adjust MLR Models	4-8
5-1	Minimum Values of R for Various Earthquake Magnitudes	5-7
5-2	Critical t Values for Confidence Limits.	5-16
A1-1	Example Summary Sheet showing Case History Information and Liquefaction Analyses	A1-2
A1-2	Names of Data Files Found in Appendix 4.	A1-3
A1-3	Summary of Earthquake Independent Variables Used in MLR . . .	A1-4
A1-4	Summary of Topographical Independent Variables Used in MLR .	A1-6
A1-5	Summary of Geological Independent Variables Used in MLR . . .	A1-8
A1-6	Summary of Soil Independent Variables Used in MLR	A1-10
A1-7	Example of SPT Data and Liquefaction Analysis Found in Appendix 4	A1-16

SECTION 1 INTRODUCTION

Lateral spread on gently sloping ground is generally the most pervasive and damaging type of liquefaction-induced ground failure generated by earthquakes (NRC, 1985). Lateral spread generated by the 1906 San Francisco earthquake damaged several buildings, bridges, roads, and pipelines (Youd and Hoose, 1978). Most notably, lateral spread along Valencia Street between 17th and 18th Street severed water lines to downtown San Francisco. The resulting loss of water greatly hampered fire fighting efforts during the ensuing fire. Lateral spread during the 1964 Alaska earthquake caused \$80 million damage (1964 value) to 266 bridges and numerous sections of embankment along the Alaska Railroad and Highway (McCulloch and Bonilla, 1970; Kachadoorian, 1968). Liquefaction and lateral spread also produced widespread damage during the 1964 Niigata, Japan earthquake (Hamada et al., 1986). In Niigata, liquefaction of loose, channel deposits caused the banks of the Shinano River to displace as much as 10 meters toward the center of the channel.

Two general questions must be answered when evaluating the liquefaction hazard for a given site: (1) "Are the sediments susceptible to liquefaction?"; and (2) "If liquefaction does occur, what will be the ensuing amount of ground deformation?" Generally accepted empirical and analytical criteria have been developed to evaluate liquefaction susceptibility (Seed and Idriss, 1971; Seed et al., 1983, 1985; NRC, 1985; Liao, 1986). However, little progress has been made in developing methods for estimating the amount of horizontal ground displacement. This need was noted by the National Research Council in outlining new initiatives in liquefaction research: "Methods of evaluating the magnitude of permanent soil deformations induced by earthquake shaking, while considered in the past, have emerged as a pressing need to understand the dynamic behavior of structures and soil deposits. Both triggering and dynamic soil strength must be considered in studying the effect of liquefaction or high pore pressure on deformations. Calculations based on realistic constitutive models are needed to help comprehend the development of permanent deformations and progressive failure (NRC, 1985, p. 217)."

This paper presents a statistical analysis of liquefaction-induced, ground displacement resulting from lateral spread on gently sloping ground. Multiple linear regression (MLR) is used to develop empirical models from earthquake, topographical, geological, and soil conditions associated with lateral spreads from 8 major earthquakes. The MLR models developed herein provide a means of predicting the amount of horizontal ground displacement at potentially liquefiable sites in earthquake-prone regions.

SECTION 2 LIQUEFACTION, LATERAL SPREAD, AND DISPLACEMENT MODELS

2.1 Liquefaction

In this study, we use "liquefaction" to describe any significant loss of shear strength in a saturated, cohesionless soil due to a transient rise in excess pore pressure generated by strong ground motion. Flow failure, lateral spread, ground oscillation, differential settlement, loss of bearing strength, ground fissures, and sand boils are evidences of excess pore pressure generation and liquefaction.

Unconsolidated fluvial, deltaic, loess, flood plain, fan delta, lacustrine, playa, colluvial, dune, sebka, estuarine, and lagoonal sediments may be moderately to highly susceptible to liquefaction (Youd and Perkins, 1978). Saturated, granular soils found in these depositional environments consist mainly of interbedded layers of loose, sand, silt, and fine gravel. Saturated, poorly compacted, artificial fills are also moderately to highly susceptible to liquefaction (Youd and Perkins, 1978).

Dense, consolidated, or well-cemented, granular soils are not usually susceptible to liquefaction. These soils do not incur significant collapse and pore pressure generation during strong ground motion. Consequently, the loss of shear strength in these soils is negligible. Similarly, liquefaction does not usually occur in nonsensitive, clayey soils. Seed and Idriss (1982) give the following criteria to identify clayey soils that are not normally susceptible to liquefaction: (1) soils with a clay content greater than 15 percent, (2) soils with a liquid limit greater than 35 percent, and (3) soils with a moisture content less than 0.9 times the liquid limit.

2.2 Lateral Spread

Lateral spread is the most common type of liquefaction-induced, ground failure. During lateral spread, blocks of intact, surficial soil displace along a shear zone that has formed within the liquefied layer (Figure 2-1). Upon reaching mobilization, the surficial blocks are transported downslope or in the direction of a free face (i.e., channel or abrupt topographical depression) by earthquake and gravitational forces. Horizontal ground displacement resulting from lateral spread ranges from a few centimeters to several meters. This displacement typically occurs on gentle slopes that range from 0.3 to 5 percent (Youd, 1978). Although, ground displacements as large as 5 to 6 m have occurred on a 0.2 percent slope during the 1964 Niigata, Japan earthquake (Hamada, 1992) and displacements as large as 0.3 m occurred on 0.05 to 0.10 percent slopes during the 1964 Alaska earthquake (Bartlett and Youd, 1992).

Ground deformation resulting from lateral spread typically forms a graben or extensional fissures at the head of the failure, shear deformations along the side margins, and buckling or compression of the soil at the toe. Rigid structures at the head of the failure are commonly pulled apart; those at the toe are compressed or buckled. Buried objects, such as pipelines and piles, are often sheared by differential movement within or at the side margins of the lateral spread.

2.3 Modeling Lateral Spread Displacement

Predicting the amount of ground displacement resulting from dynamic and static forces acting upon a composite system of liquefied and non-liquefied soil is a challenging problem. Ultimately, horizontal ground displacement is controlled by: (1) the degree of shear strength loss in the liquefied layer, (2) the continuity and boundary conditions surrounding the failure, (3) the magnitude and direction of the dynamic and static shear forces acting upon the mobilized soil, and (4) the time interval that these forces exceed the shear strength of the liquefied soil. A rigorous solution of this problem requires a dynamic, 3-D,

analysis of a nonlinear, anisotropic, heterogeneous material.

Several analytical and numerical models have been proposed for calculating liquefaction-induced, ground displacement. However, these models have not been applied to a wide range of earthquake and site conditions. More validation and calibration studies are needed before the practicing engineer can place a high degree of confidence in these techniques.

2.4 Static Models from Elastic Theory

Hamada et al. (1987), Towhata et al. (1990), and Yasuda et al. (1990) have used static, 2-D, elastic models to estimate the amount of lateral spread displacement resulting from the 1964 Niigata and 1983 Nihonkai-Chubu earthquakes. Hamada et al. (1987) propose that upon reaching liquefaction, the frictional resistance between the liquefied, subsurface layer and the nonliquefied, surface layer approaches zero. The nonliquefied, surface layer is then modeled as a 2-D, elastic beam that is deformed by pre-earthquake, static shear stresses. Likewise, the model proposed by Towhata et al. (1990) treats the nonliquefied, surface layer as an 2-D, elastic beam that is deformed by static shear stresses. The resulting strain is approximated as a sinusoidal curve with zero displacement assigned to the base of the liquefied layer and the maximum displacement assigned at the ground surface. An analytical, closed-form solution is used to calculate the displacement at the ground surface by minimizing the potential energy of the system.

In the first step of a static, 2-D, elastic, finite element procedure proposed by Yasuda et al. (1990), the pre-earthquake, static shear stresses and pre-liquefaction strains are calculated for each element using the elastic modulus of the nonliquefied soil. In the next step, the post-liquefaction strains are calculated for the mesh by holding the pre-earthquake static stresses constant and by reducing the shear modulus of the soil to represent liquefaction. Finally, the strains from the second analysis are subtracted from those of the first to calculate ground displacement vectors.

2.5 Dynamic Models

Prevost (1981), Finn and Yogendrakumar (1989), and Finn (1990) have developed dynamic, 2-D and 3-D models that can be used to predict liquefaction-induced ground displacement. For example in a finite element model, TARA-3FL, proposed by Finn and Yogendrakumar (1989), the pre-earthquake, static, stress-strain state is calculated for each element in the finite-element mesh. In the subsequent, dynamic part of the analysis, as liquefaction is triggered in specific elements according to the criteria developed by Seed (1983) and Seed et al. (1985), the shear strength of these elements is allowed to drop to its steady-state value.

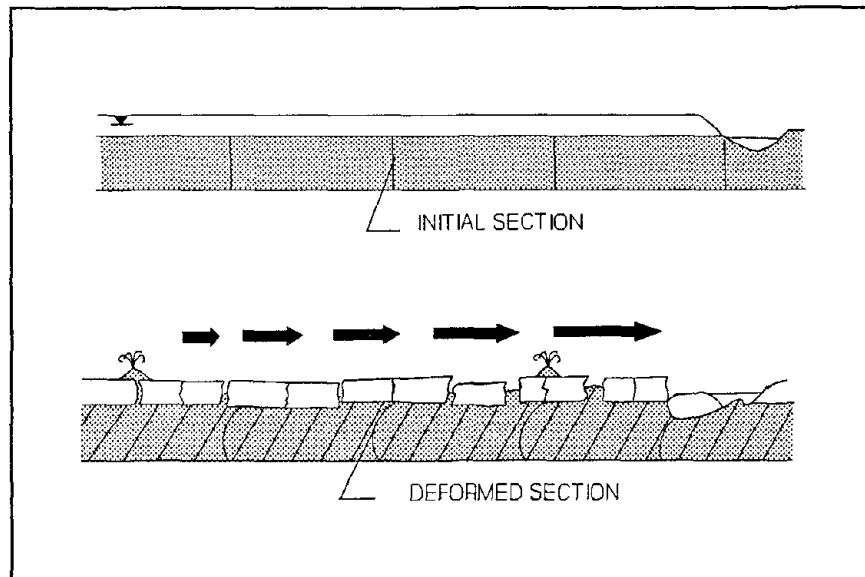


Figure 2-1 Block diagram of a lateral spread before and after failure. Liquefaction occurs in the cross-hatched zone. Surface layer displaces laterally downslope (after Youd, 1984).

The post-liquefaction shear strength of these elements is unable to sustain the imposed static and dynamic shear stresses, and the mesh is allowed to progressively deform until equilibrium is restored between the final stress state and the steady-state strength of the liquefied soil. Because deformation can become large, the finite element mesh has to be progressively updated. Calculation of the incremental deformation is done on the current shape of the soil mass and not on the initial shape as in conventional finite element analysis. Finn (1990) also recommends that a static stability analysis be performed on the final soil configuration to verify that the factor of safety is equal to or greater than unity.

2.6 Sliding Block Analysis

Newmark (1965), Goodman and Seed (1966) and Makdisi and Seed (1978), Dobry and Baziar (1990), Byrne (1990), Yegian, et al. (1991), and Mabey (1992) have developed various methods of estimating liquefaction-induced, ground failure displacement from sliding block analysis. In these dynamic, 1-D models, a rigid, soil block is allowed to displace along a planar failure surface during time intervals when the earthquake inertial force, F_{di} , exceeds the yield coefficient of the soil, K_y . The value of F_{di} is calculated by multiplying the horizontal ground acceleration by the mass of the block. Also, F_{di} is assumed to act parallel to the base of the block and is not allowed to vary along the failure surface. K_y is normalized for the weight of the block and is calculated from:

$$K_y = (F_{rs} - F_{da}) / W \quad (2.6.1)$$

where:

F_{rs} = resisting force due to the dynamic shear strength of the soil

F_{da} = force acting on the block due to active earth pressure

W = weight of the block.

Typically, resisting forces due to irregularities along the failure surface are assumed to be negligible and are omitted from the analysis. Additionally, upslope translation of the block is usually small because the magnitude of the inertial force in the upslope direction seldom greatly exceeds the weight of the downslope component of the soil block.

The net downslope displacement of the block, D_r , is governed by the magnitude and time interval that F_{di} exceeds K_y . Several researchers have proposed solutions for D_r using various shapes for the base input motion. Yegian et al. (1988) have presented solutions for triangular, sinusoidal, and rectangular, base input motions. Franklin and Chang (1977), Makdisi and Seed (1978), Sarma (1979), and Whitman and Liao (1985) have proposed similar solutions for earthquakes of various magnitudes.

As originally introduced by Newmark (1965), sliding block analysis is based on the assumption that the soil within the failure plane deforms as a perfectly plastic material (i.e., F_{rs} remains constant with strain). Many researchers have incorporated the residual strength of the liquefied soil to represent F_{rs} in sliding block analysis. However, the use of a constant value, such as residual strength, to represent the nonlinear, stress-strain behavior of a liquefied soil is a simplification that remains to be validated. In addition, current laboratory and field methods for estimating residual strength are based on limited data and exhibit a great deal of scatter as noted by Marcuson et al. (1990). Thus, the ability of sliding block analysis to accurately predict liquefaction-induced ground displacement may be limited by the uncertainty associated with obtaining representative values of residual strength for the failure surface.

Byrne (1990) has proposed a more sophisticated sliding block model that incorporates shear strength degradation during cyclic loading. Instead of the

rigid-plastic spring proposed by Newmark (1965), a nonlinear spring is used to account for shear strength degradation as liquefaction develops. In Byrne's model, the stiffness of the spring is expressed as a function of both the residual strength and the limiting strain of the liquefied soil. Both of these factors are in turn strongly influenced by the relative density of the cohesionless soil (Seed and Harder, 1990; Seed et al., 1984).

2.7 Empirical Models

Hamada et al. (1986) and Youd and Perkins (1987) have proposed empirical models to predict lateral spread displacement. We will briefly review these models to provide ideas on how earthquake and site conditions can be quantified and used as predictor variables in empirical models.

2.7.1 Liquefaction Severity Index

Youd and Perkins (1987) evaluated cases of liquefaction-induced ground failure that occurred in a very specific geologic setting. They limited their study to lateral spreads that occurred on gentle slopes or into river channels having widths greater than 10 meters. Their study was also restricted to lateral spreads which occurred in saturated, cohesionless, Holocene fluvial or deltaic deposits with estimated standard penetration resistances ranging from 2 to 10 blows per foot. By restricting their study to these site conditions, Youd and Perkins postulated that ground displacement, S , becomes primarily a function of the amplitude, A , and duration of strong ground motion, D :

$$S = f(A, D). \quad (2.7.1.1)$$

Other researchers have shown that A and D are functions of earthquake magnitude, M , and distance from the seismic energy source, R , (Joyner and Boore, 1981; 1988; Krinitzky and Chang, 1988b). In general, A attenuates logarithmically with R , and D shows a slight increase with increasing R . For many of the lateral spreads in the Youd-Perkins study, strong motion records were not available; thus, they chose to express S as a function of M and $\log R$:

$$S = f(M, \log R). \quad (2.7.1.2)$$

The moment magnitude, M_w , was chosen to represent M , because it generally provides a better estimate of the total energy released during a seismic event than other measures of earthquake magnitude (Kanamori, 1978).

Youd and Perkins (1987) introduced the "Liquefaction Severity Index" or LSI as a convenient scale to represent the general maximum value of S for a given lateral spread occurring within the defined geological setting. Localities where the reported horizontal ground displacement had obviously exceeded 100 inches (2.5 m) were excluded from the formulation of the LSI equation. Youd and Perkins considered these large displacements to be so damaging and erratic in nature that extending the LSI beyond 100 inches (2.5 m) was not meaningful; thus, the LSI was chosen to range between 0 and 100 inches.

Least squares regression was used to develop the following equation:

$$\log \text{LSI} = -3.49 - 1.86 \log R + 0.98 M_w \quad (2.7.1.3)$$

where:

LSI = maximum, permanent, horizontal displacement in inches (i.e., mm divided by 25)

R = horizontal distance from the energy source in kilometers

M_w = moment magnitude.

Because the LSI equation was developed primarily from lateral spread sites in California and Alaska, it is applicable only to seismic regions with high ground motion attenuation.

2.7.2 Hamada et al. (1986) Equation for Lateral Spread Displacement

Based on pre- and post-earthquake aerial photographs, Hamada et al. (1986) published horizontal ground displacement vector maps for many areas damaged by lateral spreads in Niigata and Noshiro, Japan, during the 1964 Niigata and 1983 Nihonkai-Chubu earthquakes, respectively. Using borehole logs, they also constructed subsurface cross-sections along the longitudinal axis of many of the lateral spreads in these two cities. Guided by changes in the surface topography and breaks in the vector displacement pattern, Hamada et al. divided each cross-section into segments or blocks that appeared to have displaced as a discrete unit (Figure 2-2a and 2-2b). They averaged the displacement vectors, the thickness of the liquefied layer(s), and the slope measurements for each block and used these averages in their correlative analyses.

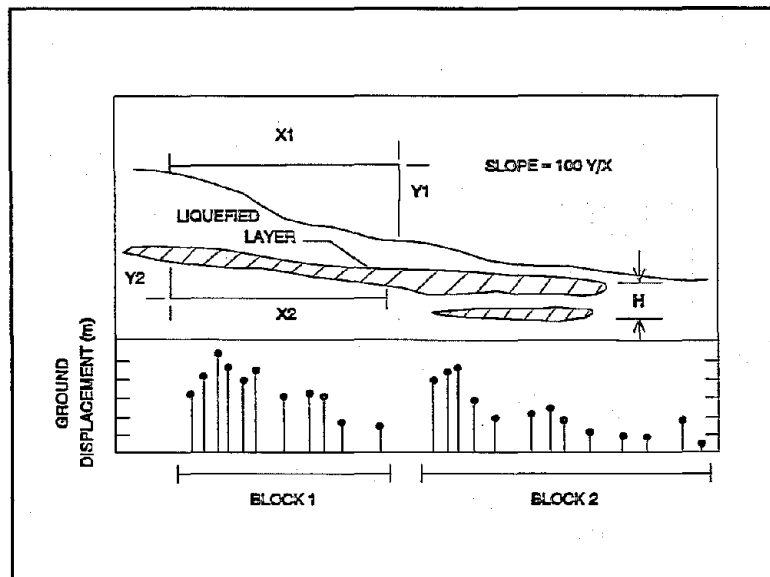


Figure 2-2 (a) Illustration of slope and thickness measurements used in equation 2.7.2.8 (after Hamada et al., 1986).

Hamada et al. used the Factor of Liquefaction Resistance, F_L , to estimate the thickness of the liquefied layer(s), H (Appendix III of Hamada et al., 1986; Iwasaki et al., 1978). F_L is a factor of safety that compares the liquefaction resistance of the soil to the dynamic shear stresses generated by the earthquake:

$$F_L = R/L. \quad (2.7.2.1)$$

Layer(s) having F_L values less than 1.0 were considered to have liquefied. The in-situ resistance of the soil, R , was calculated from empirical curves adopted by the Japanese Code of Bridge Design. R is a function of the standard penetration resistance of the soil, the effective overburden stress, σ_v' , and the mean grain size, D_{50} :

$$R = 0.0882(N/\sigma_v' + 0.7)^{1/2} + 0.19 \quad (2.7.2.2)$$

where:

N = SPT blow count in blows per foot

σ_v' = effective overburden stress in kg/cm^2 .

Equation 2.7.2.2 is used for soils with $0.02 \text{ mm} \leq D_{50} \leq 0.05 \text{ mm}$ and Equation 2.7.2.3,

$$R = 0.0882(N/\sigma_v' + 0.7)^{1/2} + 0.225 \log (0.35/D_{50}) \quad (2.7.2.3)$$

is used for soils with $0.05 \text{ mm} \leq D_{50} \leq 0.6 \text{ mm}$ and Equation 2.7.2.4,

$$R = 0.0882(N/\sigma_v' + 0.7)^{1/2} - 0.5 \quad (2.7.2.4)$$

is used for soils with $0.6 \text{ mm} \leq D_{50} \leq 1.5 \text{ mm}$. The dynamic earthquake shear stress, L , is normalized for σ_v' and is given by:

$$L = 0.65(\sigma_v/\sigma_v')r_d \quad (2.7.2.5)$$

where:

r_d = a stress reduction factor that reduces L with depth.

Hamada et al. identified the liquefied layer(s) in each cross-section by using F_L . Layers with F_L values less than 1.0 were marked as having liquefied. Boundaries for liquefied layers were interpolated between bore holes to construct a continuous profile along the longitudinal axis of the lateral spread. If liquefaction was indicated in more than one layer, the total thickness of the liquefied layer, H , included the combined thickness of liquefiable layers plus the thickness of any intermediate nonliquefiable layer(s) (Figure 2-2a).

Hamada et al. also estimated the ground slope along the longitudinal axis of each displaced block and correlated it with ground displacement. The ground slope, θ_1 , (%), was defined simply as:

$$\theta_1 = 100(Y_1/X_1) \quad (2.7.2.6)$$

where:

Y = vertical change in surface elevation across the block

X = length of the block (Figure 2-2a).

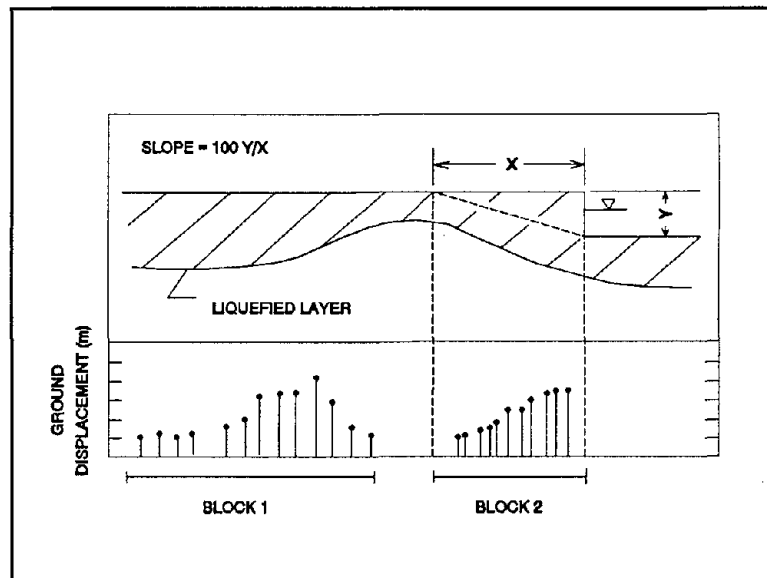


Figure 2-2 (b) Technique used by Hamada et al. to measure the ground slope for lateral spreads along the Shinano River (after Hamada et al., 1986).

For lateral spreads that occurred near the banks of the Shinano River, the measurement of θ_1 was artificially steepened to the bottom of the river channel (Figure 2-2b).

Hamada et al. also postulated that the slope of the bottom of the liquefied layer may have influenced horizontal displacement. This slope, θ_2 , (%), was measured by scaling the slope of the bottom of the liquefied layer from the constructed cross-section (Figure 2-2a):

$$\theta_2 = 100(Y_2/X_2) \quad (2.7.2.7)$$

where:

Y_2 = vertical change in subsurface elevation across the block

X_2 = length of the block.

Hamada et al. found that MLR models which included H in conjunction with the larger value of either θ_1 or θ_2 yielded the best predictions of horizontal displacement. They proposed the following regression model:

$$D = 0.75 H^{0.50} \theta^{0.33} \quad (2.7.2.8)$$

where:

D = horizontal ground displacement, (m)
H = thickness of the liquefied layer, (m),
 θ = the larger value of θ_1 or θ_2 , for the block, (%).

Figure 2-3 is a plot of observed displacements from Niigata and Noshiro, Japan, plotted against displacements predicted by this model. Predictions that fall on or near the 45 degree solid line are closely approximated by the model. The dashed line below the 45 degree solid line represents a 100 percent overprediction bound (i.e., the predicted displacements are 2 times larger than observed displacements). The dashed line above the 45 degree solid line represents a 50 percent underprediction bound (i.e., the predicted displacements are one-half times larger than the observed displacements). Approximately 80 percent of the displacements predicted by the Hamada et al. model fall between these two prediction bounds.

2.7.3 Summary of Empirical Models

The LSI equation of Youd and Perkins (1987) is based primarily on earthquake factors and is intended to provide a conservative upper bound for estimating horizontal ground displacement at sites having a moderate to high liquefaction susceptibility. In contrast to the LSI equation, the model proposed by Hamada et al. (1986) emphasizes the thickness of the liquefiable layer and slope, but it does not address the importance of earthquake factors. This thickness-slope model appears to produce reasonable estimates for $M = 7.5$ earthquakes and for highly liquefiable sediments that are located approximately 20 to 30 km from the seismic source. However, it yields less reliable results for smaller or larger seismic events occurring at varying distances (Bartlett and Youd, 1990). Additionally, the characteristics of the liquefied deposits in Niigata and Noshiro cities are relatively homogeneous (i.e., uniform, medium-to fine-grained, clean sand). Extrapolation of the regression equation to gravelly and silty sediments yields poorer predictions (Bartlett and Youd, 1990).

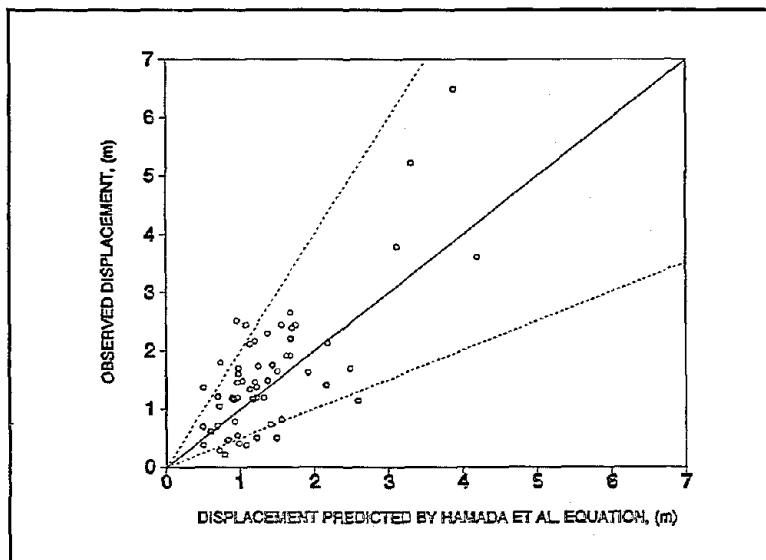


Figure 2-3 Observed displacements plotted against displacements calculated from Equation 2.7.2.8 (after Hamada et al., 1986).

2.7.4 Towards a More Comprehensive, Empirical Model

It is difficult to quantify and model all factors that contribute to liquefaction and ground displacement. Thus, the modeler is forced to select only a handful of the most influential factors and attempt to represent their complex interaction. Based on the studies by Hamada et al. (1986), Youd and Perkins

(1987), and Bartlett and Youd (1990), we believe that a more compressive empirical model should include, but not be restricted to the following: (1) earthquake factors (e.g., peak ground acceleration and duration of strong ground motion or earthquake magnitude and distance from the zone of seismic energy release), (2) topographical factors (e.g., ground slope and/or the distance to and height of a free face, if present), (3) geological factors (e.g., thickness of and depth to the liquefied layer), and (4) soil factors (e.g., residual strength, mean grain size, and the silt and clay content of the liquefied soil).

SECTION 3
EMPIRICAL ANALYSIS OF LATERAL SPREAD FOR NIIGATA AND NOSHIRO, JAPAN

3.1 Multiple Linear Regression

Multiple linear regression (MLR) is often used to predict the behavior of complex phenomena that are influenced by several factors (Draper and Smith, 1981). In applying MLR analysis, it is assumed that changes in the independent variables, $X(s)$, are accompanied by a corresponding change in the response of the dependent variable, Y . The true response, Ω , is expressed in terms of an unknown function, ϕ , which contains the $X(s)$, and the unknown parameters, $B(s)$, that accompany the $X(s)$.

$$\Omega = \phi(X_1, X_2, \dots, X_p; B_1, B_2, \dots, B_p) \quad (3.1.1)$$

For example, in this study we postulate that horizontal ground displacement is a function of several independent variables.

$$\Omega = \phi(E, G, T, S; B_E, B_G, B_T, B_S) \quad (3.1.2)$$

where:

E = Earthquake factors

G = Geological factors

T = Topographical factors

S = Soil factors

$B_E, B_G, B_T,$ and B_S = unknown parameters corresponding to E, G, T, and S

Ideally, the value of Ω for a given set of $X(s)$ is the same each time the experiment is performed. But, in reality, Ω is seldom observed due to the presence of many uncontrolled and unmeasured variables that affect Ω . The deviation of the observed response, Y , from Ω is called experimental error, ϵ .

$$\Omega - Y = \epsilon \quad (3.1.3)$$

In MLR analysis, ϕ is approximated by an additive, linear model. The values of Y and the $X(s)$ are often transformed (e.g., $1/X$, $\log X$, e^x , etc.) in order to produce a linear form.

$$Y = b_0 + b_1X_1 + b_2X_2 + \dots + b_pX_p + \epsilon \quad (3.1.4)$$

The regression coefficients, b_0, \dots, b_p are best-fit estimates of the $B(s)$, and ϵ is a best-fit estimate of ϵ . The method of ordinary least squares is commonly used to estimate the $B(s)$ by minimizing the error sum of squares:

$$S_e = \sum(\epsilon)^2 \quad (3.1.5)$$

where:

ϵ = difference between the measured response, Y , and the response predicted by the regression equation, Y_{hat} , i.e.,

$$\epsilon = Y - Y_{\text{hat}} \quad (3.1.6)$$

To provide these best-fit estimates, it is assumed: (1) the $\epsilon(s)$ are random variables with an expected value of zero (i.e., $E(\epsilon) = 0$), (2) the variance of the $\epsilon(s)$ is constant for all values of the $X(s)$ (i.e., $V(\epsilon)$ is constant), (3) the $\epsilon(s)$ are not correlated, and (4) the values of the can be measured without error. Also, if the $\epsilon(s)$ appear to be normally distributed, then partial and sequential t and F tests can be performed on each of the $b(s)$ to verify that these coefficients are statistically significant (i.e., b_0, \dots, b_p are not equal to

zero) (Draper and Smith, 1981). Standardized residual plots are commonly used to evaluate the validity of these assumptions. Also, these plots give the investigator valuable information about the general performance of the MLR model. The standardized residual, e_i , for each observation is calculated from:

$$e_i = e / (\text{standard deviation of } e) \quad (3.1.7)$$

where:

$$e = Y - Y_{\text{hat}}$$

Typically, the $e_i(s)$ from the model are plotted against the corresponding $X(s)$ and $Y_{\text{hat}}(s)$ to confirm that the $e_i(s)$ are independent and have a constant variance with a mean of zero. An acceptable standard residual plot gives the impression of a horizontal band of data centered on zero. Approximately 95 percent of the $e_i(s)$ should fall within ± 2 standard deviations of zero, and almost all $e_i(s)$ should fall within ± 3 standard deviations of zero line shown in Figure 3-1a.

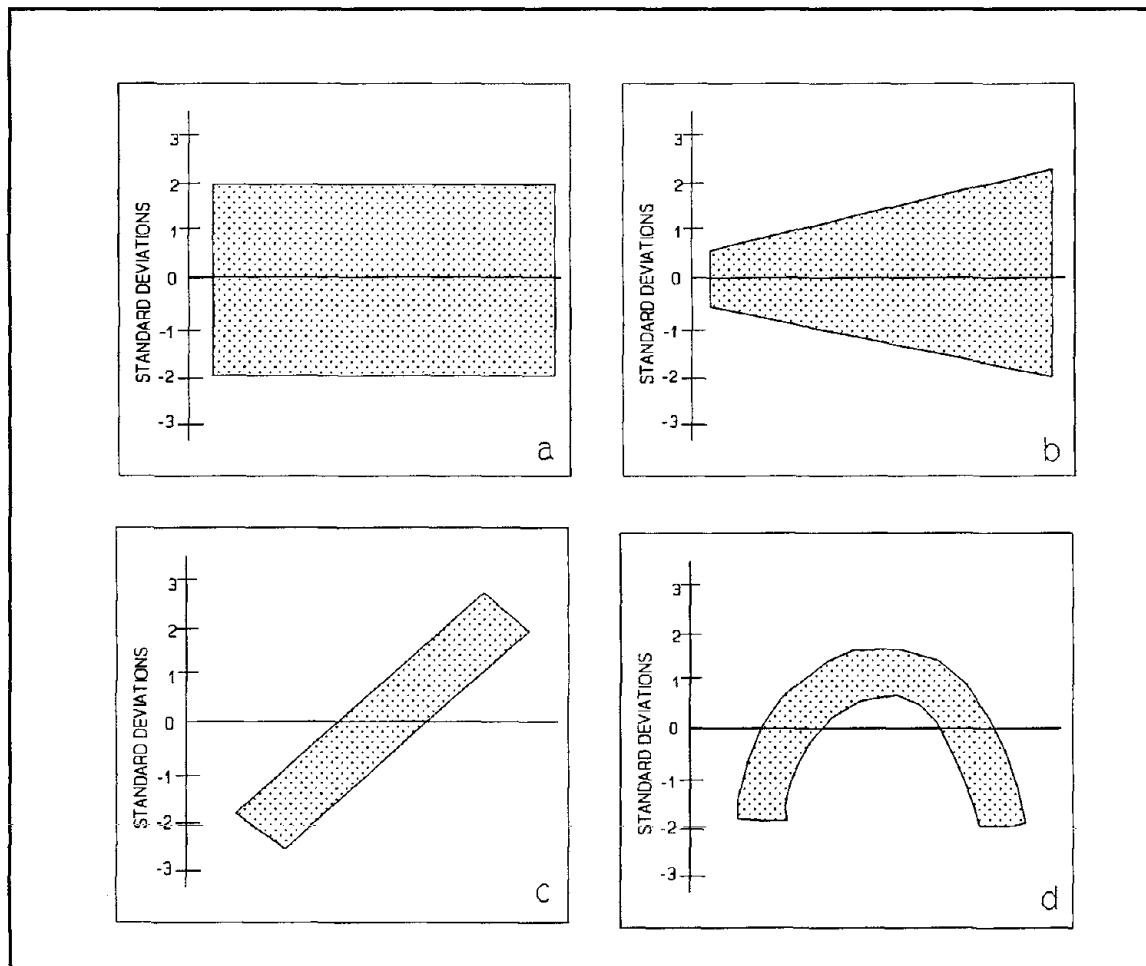


Figure 3-1 Examples of standard residual plots. (a) Satisfactory residual plot gives overall impression of horizontal box centered on zero line. (b) A plot showing nonconstant variance. (c) A plot showing a linear trend suggesting that the residuals are not independent and that another variable is needed in the model. (d) A plot illustrating the need for a transformation or a higher order term to alleviate curvature in the residuals.

Observations having $e_i(s)$ that plot more than 2 to 3 standard deviations above or below the zero line are potential outliers. Figures 3-1b through 3-1d are

examples of unsatisfactory residual plots. The behavior shown in Figure 3-1b suggests that the variance of $e_i(s)$ is not constant (i.e., the residual band widens). Data with a nonconstant variance are usually corrected by transforming Y or by using weighted, least-squares regression analysis (Draper and Smith, 1981). The linear trend shown in Figure 3-1c suggests that the $e_i(s)$ are not independent or that some other X is needed in the model. A residual plot displaying curvature (Figure 3-1d) indicates that a higher order term, a cross-product, or a transformation of Y , or of the $X(s)$, is needed to produce a more linear form.

The performance of MLR models is judged by the coefficient of determination, R^2 :

$$R^2 = [\Sigma(Y^2) - S_e - (\Sigma Y)^2/n] / [\Sigma(Y^2) - (\Sigma Y)^2/n] \quad (3.1.8)$$

where n is the sample size. The value of R^2 ranges from 0 to 1 and measures the proportion of the variability of Y being explained by the $X(s)$. For example, a R^2 of 0.50 means that 50 percent of the variability in Y is being explained by the $X(s)$.

In this study, we used a modified stepwise regression procedure to guide the development of our MLR models. In short, this procedure begins by searching the set of $X(s)$ for the X with the highest correlation with Y and this X enters the model. In the next step, the remaining $X(s)$ are re-examined to find the X that yields the next highest improvement in R^2 and this X is added to the model. The process of examining and adding $X(s)$ to the model continues until no additional X can be found that significantly improves R^2 . At the end of each step, partial t -tests are performed on all $X(s)$ in the current model to verify that each X is still statistically significant. (Sometimes $X(s)$ introduced during earlier steps become nonsignificant at later steps because they are correlated with other $X(s)$ that are just entering the model). Variables that become nonsignificant during later steps are removed from the model prior to beginning the next step.

3.2 Compilation of Case History Data for MLR Analyses

Prior to beginning MLR analysis, 448 horizontal displacement vectors were compiled as the dependent variable, D_H , (m) from 8 earthquakes and the listed lateral spread sites in Table 3-1. Tabulated values of D_H were measured or estimated by the respective investigators using various methods. The values of D_H for Niigata and Noshiro, Japan, and the Jensen Filtration Plant were calculated from pre- and post-earthquake photographs using photogrammetric techniques (Hamada et al., 1986; O'Rourke et al., 1990). These measurements have an accuracy of ± 0.72 , ± 0.17 , and ± 0.47 m, respectively. The values of D_H for the Wildlife Instrument Array and Juvenile Hall were calculated from pre- and post-earthquake ground surveys (Youd, 1973b; Youd and Bartlett, 1988) and have an accuracy of approximately ± 0.02 m. The estimates of D_H at other lateral spread sites were obtained from reports of dislocated or offset buildings, bridge components, fences, canals, etc. The accuracy of D_H at these sites is difficult to determine, but is approximately ± 0.1 to ± 0.5 m.

Because of the large size of these data, the MLR database has been tabulated in ASCII format on the computer disk labeled "Appendix 3" in the file MLR.DAT. This disk and two additional disks, which comprise "Appendix 4", are available from NCEER Information Service, care of Science and Engineering Library, 304 Capen Hall, State University of New York at Buffalo, Buffalo, New York, 14260.

Table 3-2 lists the earthquake, topographical, geological, and soil independent variables that were compiled and tested in our MLR analyses. These data were obtained from seismological reports, topographical maps and surveys, borehole logs, and soil grain-size analyses (Appendix 1, 3, and 4). We used liquefaction susceptibility analysis of SPT data to calculate many of the geological and soil independent variables (Seed and Idriss, 1971; Seed et al., 1983; 1985, NRC 1985,

Liao, 1986). In all, liquefaction susceptibility analysis was performed for 267 boreholes from the lateral spread sites listed in Table 3-1 (Appendix 1 and 4).

TABLE 3-1
EARTHQUAKES AND LATERAL SPREAD SITES USED IN THIS STUDY

1906 San Francisco Earthquake (Youd and Hoose, 1978)

Coyote Creek Bridge near Milpitas, California
Mission Creek Zone in San Francisco, California
Salinas River Bridge near Salinas, California
South of Market Street Zone in San Francisco, California

1964 Alaska Earthquake (Bartlett & Youd, 1992; McCulloch & Bonilla 1970)

Bridges 141.1, 147.4, 147.5, 148.3, Matanuska River, Alaska
Bridges 63.0, 63.5, Portage Creek, Portage, Alaska
Highway Bridge 629, Placer River, Alaska (Ross et al., 1973)
Snow River Bridge 605A, Snow River, Alaska (Ross et al., 1973)
Bridges 3.0, 3.2, 3.3, Resurrection River, Alaska

1964 Niigata, Japan, Earthquake (Hamada et al., 1986)

Numerous lateral spreads in Niigata, Japan

1971 San Fernando Earthquake

Jensen Filtration Plant, San Fernando, CA, (O'Rourke et al., 1990)
Juvenile Hall, San Fernando, CA, (Bennett, 1989; Youd, 1973b)

1979 Imperial Valley Earthquake (Bennett et al., 1984)

Heber Road near El Centro, California (Dobry et al., 1992)
River Park near Brawley, California

1983 Borah Peak Idaho, Earthquake

Whiskey Springs near Mackay, Idaho (Andrus and Youd, 1987)
Pence Ranch near Mackay, Idaho (Andrus et al., 1991)

1983 Nihonkai-Chubu Earthquake (Hamada et al., 1986)

Lateral spreads in the Northern Sector of Noshiro, Japan

1987 Superstition Hills Earthquake (Holzer et al., 1988; 1989)

Wildlife Instrument Array, Brawley, CA, (Youd and Bartlett, 1988)

At many sites, there was more than one borehole drilled within the zone of ground deformation (for example, see Figure 3-2). For these sites, we used an inverse-distance, linearly-weighted average to interpolate all geological and soil independent variables between boreholes. This averaging scheme assigns the largest weight to the borehole located closest to the displacement vector:

$$X_{AVG} = W_1 * X_1 + W_2 * X_2 + \dots + W_n * X_n \quad (3.2.1)$$

where X_{AVG} is the weighted average, X_1, \dots, X_n are the corresponding values of X to be averaged for n boreholes, and W_1, \dots, W_n are the weights. These weights are calculated from:

$$W_i = 1/d_i / \Sigma(1/d_i) \quad (3.2.2)$$

where d_i is the distance from i^{th} borehole to the displacement vector of interest and $\Sigma(1/d_i)$ is summed for n boreholes (Appendix 1, Section A1.4). These weighted averages were calculated for each D_H prior to performing the regression analyses.

3.3 Strategy for Development of MLR Models

Because the earthquakes that generated lateral spreads in Niigata and Noshiro, Japan were seismically similar, we initially ignored the effects that M , R , A , and D have on displacement during preliminary model development. (Niigata and Noshiro incurred 7.5 and 7.7 magnitude earthquakes and were situated approximately 21 and 27 km from the zone of seismic energy release, respectively (Hamada, 1986; Mogi et al., 1964; Hwang and Hammack, 1984). By restricting our initial analyses to these two earthquakes, we were able to develop site-specific MLR models based solely on topographical, geological, and soil factors. Also, the extensive displacement and subsurface data for these two cities provided us with a large MLR database amenable to statistic analyses. (Three hundred and seventy seven (377) of the 448 tabulated displacement vectors are from Niigata and Noshiro). After developing site-specific models for Japan, we added the U.S. data to the analyses and adjusted the site-specific MLR models for a wider range of earthquake, topographical, and soil conditions not present in the Japanese data.

We observed two general types of lateral spread in Niigata: (1) lateral spread towards a free face, and (2) lateral spread down gentle ground slopes where a free face was not present. For example, Figure 3-2 shows the pattern of ground displacement along the banks of the Shinano River near the northern abutment of the Echigo Railway Bridge. The large and erratic displacements near the river obviously resulted from a lack of lateral resistance to deformation created by the incised channel. In contrast, ground deformation occurring north of the railroad embankment was smaller (a maximum of 2 m), more uniform, and directed away from the channel. Lateral spread in this area was not impacted by the channel, but resulted from movement down a gentle gradient that slopes 0.2 percent to the northeast. Our preliminary regression models for Niigata showed that the topographical regression coefficients fitted for free face failures differed significantly from those fitted for ground slope failures. Thus, we developed a separate MLR model for each type of failure. In Section 3.4, we discuss the development of a site-specific, free face model using data exclusively from Niigata. (No free face failures were identified in the study of Noshiro, Japan by Hamada et al., 1986). In Section 3.5, we discuss the development of a site-specific, ground slope model using ground slope failures from both Niigata and Noshiro. In Section 4.0, the U.S. case studies are included in the analyses and the MLR models are adjusted for a wider range of earthquake and site conditions.

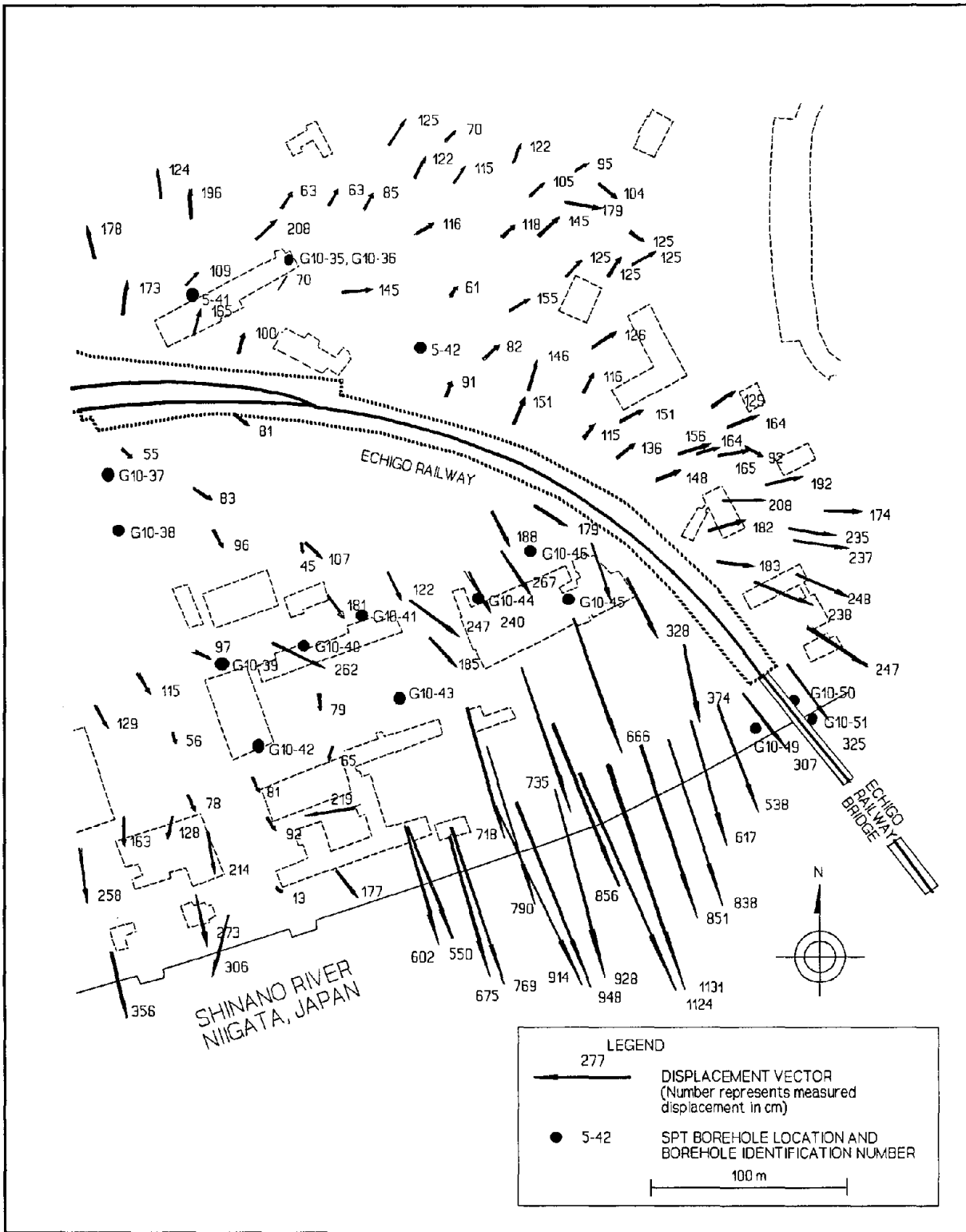


Figure 3-2 A section of working maps developed by Hamada et al. (1986), showing displacement vectors and locations of SPT boreholes from an area along the Shinano River near the Echigo Railway Bridge in Niigata, Japan (source: unpublished ground failure maps courtesy of M. Hamada).

TABLE 3-2
SUMMARY OF INDEPENDENT VARIABLES CONSIDERED IN MLR ANALYSIS
(For more information on these variables, see Section 4 and Appendix 1)

<u>Earthquake</u>	
<u>Variables</u>	<u>Description</u>
M*	Earthquake moment magnitude, M_w .
R*	Nearest horizontal distance to seismic energy source or fault rupture, (km).
A	Peak horizontal ground acceleration, (g).
D	Duration of strong ground motion (>0.05 g), (s).
<u>Topographical</u>	
<u>Variables</u>	<u>Description</u>
S*	Ground slope, (%).
L	Distance to the free face from the point of displacement, (m).
H	Height of free face, (m).
W*	Free face ratio, (%), (i.e., 100 H/L).
<u>Geological</u>	
<u>Variables</u>	<u>Description</u>
T_s	Thickness of liquefied zone(s) (Simplified procedure), (m).
T_L	Thickness of liquefied zone(s) (Liao's 50% probability curve), (m).
T_{10}	Thickness of saturated cohesionless soils with $(N1)_{60} \leq 10$, (m).
T_{15}^*	Thickness of saturated cohesionless soils with $(N1)_{60} \leq 15$, (m).
T_{20}	Thickness of saturated cohesionless soils with $(N1)_{60} \leq 20$, (m).
I_s	Index of Liquefaction Potential (Simplified procedure).
I_L	Index of Liquefaction Potential (Liao's 50% probability curve).
Z_{ub}	Depth to top of liquefied zone (Simplified procedure), (m).
Z_{ul}	Depth to top of liquefied zone (Liao's 50% prob. curve), (m).
Z_{ub}	Depth to bottom of liquefied zone (Simplified procedure), (m).
Z_{bl}	Depth to bottom of liquefied zone (Liao's 50% prob. curve), (m).
Z_s	Depth to the lowest factor of safety (Simplified procedure), (m).
Z_L	Depth to the lowest factor of safety (Liao's 50% prob. curve), (m).
Z_N	Depth to lowest SPT N value in saturated cohesionless soil, (m).
Z_{N160}	Depth to lowest SPT $(N1)_{60}$ value in saturated cohesionless soil, (m).
N	Lowest SPT N value in saturated cohesionless sediments.
$N1_{60}$	Lowest SPT $(N1)_{60}$ value in saturated cohesionless sediments.
J_s	Lowest factor of safety below water table (Simplified procedure).
J_L	Lowest factor of safety below water table (Liao 50% prob. curve).
$N1_{60S}$	$(N1)_{60}$ value corresponding to J_s .
$N1_{60L}$	$(N1)_{60}$ value corresponding to J_L .
K_s	Average factor of safety in T_s .
K_L	Average factor of safety in T_L .
O_s	Average $(N1)_{60}$ in T_s .
O_L	Average factor of safety in T_L .

* Indicates independent variables used in the final MLR model.

TABLE 3-2 (CONTINUED)
SUMMARY OF INDEPENDENT VARIABLES CONSIDERED IN MLR ANALYSIS
 (For more information on these variables, see Section 4 and Appendix 1)

<u>Soil Variables</u>	<u>Description</u>
D50 _S	Average D ₅₀ in T _S , (mm).
D50 _L	Average D ₅₀ in T _L , (mm).
D50 ₁₀	Average D ₅₀ in T ₁₀ , (mm).
D50 ₁₅ *	Average D ₅₀ in T ₁₅ , (mm).
D50 ₂₀	Average D ₅₀ IN T ₂₀ , (mm).
F _S	Average fines content in T _S , (particle size <0.075 mm, in percent).
F _L	Average fines content in T _L , (particle size <0.075 mm, in percent).
F ₁₀	Average fines content in T ₁₀ , (particle size <0.075 mm, in percent).
F ₁₅ *	Average fines content in T ₁₅ , (particle size <0.075 mm, in percent).
F ₂₀	Average fines content in T ₂₀ , (particle size <0.075 mm, in percent).

* Indicates independent variables used in final MLR model.

3.4 Free Face MLR Model for Lateral Spreads in Niigata, Japan

Stepwise regression analyses of lateral spreads in Niigata show that the proximity of the channel is the most important site factor affecting ground displacement for free face failures. Figure 3-3 is a plot of horizontal displacement, D_H, (m), versus the horizontal distance from the channel, L, (m), for several lateral spreads along the Shinano River. This plot suggests that D_H decays logarithmically with increasing L. A regression of this single factor yields the following equation:

$$D_H = 11.6 - 4.38 \text{ LOG } L. \quad (3.4.1)$$

The R² for this model is 31.7 percent. Partial t-tests for the intercept, b₀, and the partial slope for LOG L are significant at the 99.9 percent confidence level (i.e., 99.9% probability that these coefficients are not equal to zero).

In analyzing the ground deformation near the Shinano River, we noted that D_H near the bridge abutments appears to have been impeded by the structures. For example, Figure 3-2 shows that the displacement vectors near the north abutment of the Echigo railroad decreased from approximately 8 m (at a locality 75 m east of the bridge) to 3 m (at 10 m east of the bridge). In order to minimize the variability in D_H resulting from

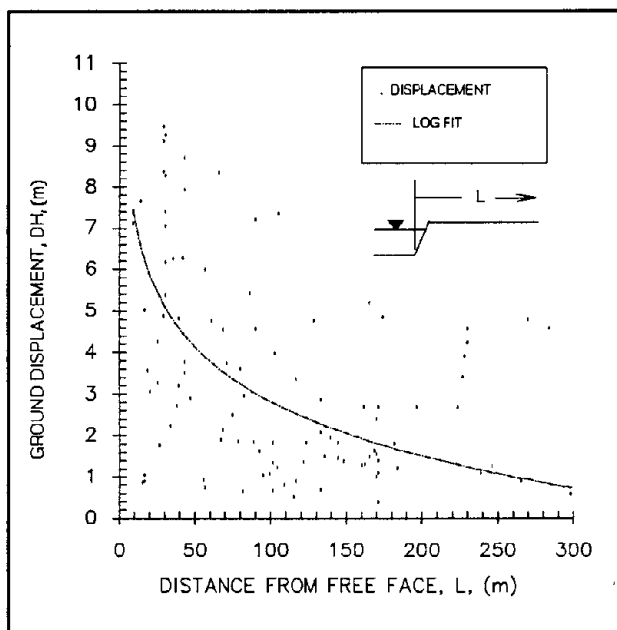


Figure 3-3 Plot of ground displacement, Y, versus distance from the free face, L, for lateral spreads along the Shinano River, Niigata, Japan.

bridge interference, we did not compile displacement vectors found within approximately 50 m of the bridges.

In addition to L , the height of the free face (i.e., the depth of the channel), H , (m), is also correlated with D_H . To normalize L for the effect of H , we combined these two topographic measures into one independent variable called the free face ratio, W , (%) (Figure 3-4):

$$W = 100 H/L. \quad (3.4.2)$$

Although there is considerable scatter due to other geological and soil factors not accounted for in the model, D_H appears to increase in a nonlinear fashion with W (Figure 3-4). To fit this nonlinearity, we tried the following models:

$$D_H = b_1 \sin(H/L) \quad (3.4.3a)$$

$$D_H = b_0 + b_1 \log W \quad (3.4.3b)$$

$$\log D_H = b_0 + b_1 \log W \quad (3.4.3c)$$

Equation 3.4.3a is a plausible model for planar failure surfaces that intersect the free face. This model presupposes that D_H is proportional to the gravitational shear force acting along the base of the mobilized soil block (Figure 3-5). However, for the Niigata data, Equation 3.4.3a yielded poorer predictions compared with Equations 3.4.3b and 3.4.3c (R^2 equals 28.6 percent versus 39.1 and 38.0 percent, respectively).

A fit of model 3.4.3b yielded the highest R^2 value; but a residual plot of $e_i(s)$ versus D_{Hhat} from this model showed evidence of nonconstant variance. Figures 3-2 and 3-3 shows that D_H is more variable near the free face. This extra variability is most likely due to changes in the subsurface geology or is a result of impediments to displacement such as retaining walls, piles, and other buried structures found along the margins of the channel. Because MLR analysis assumes that the variance of e_i is constant throughout the ranges of the independent variables, nonconstant variance is undesirable and may pose problems in estimating the prediction limits for the true value of D_H . A log transformation of the dependent variable, Y , is a standard technique used to reduce nonconstant variance (Draper and Smith, 1981). Also, Hamada et al., 1986 and Youd and Perkins (1987) used log-log transformations similar to Equation 3.4.3c in their MLR models. Thus, we ultimately decided to transform D_H to $\log D_H$ (Figure 3-6) and fitted model 3.4.3c with the following coefficients:

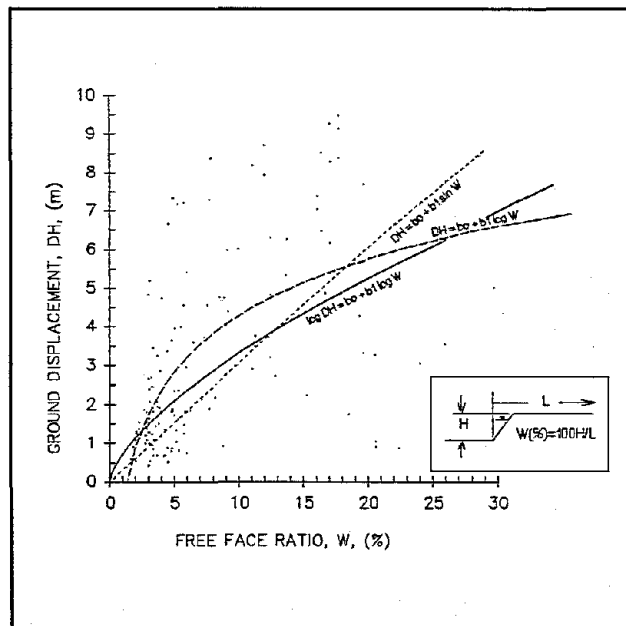


Figure 3-4 Plot of ground displacement, D_H , versus free face ratio, W , for lateral spreads along the Shinano River, Niigata, Japan.

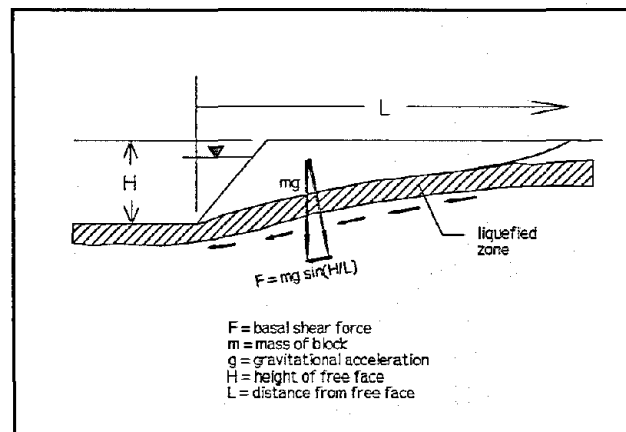


Figure 3-5 Diagram showing that the shear force acting along the base of slide block is proportional to $\sin(H/L)$.

$$\text{LOG } D_H = - 0.138 + 0.660 \text{ LOG } W.$$

(3.4.4)

A residual plot of $e_i(s)$ versus D_{Hhat} for Equation 3.4.4 indicates that the log-log model eliminates the nonconstant variance (Figure 3-7). The intercept and slope for this equation are highly significant. (The intercept is significant at the 97 percent confidence level and the slope for LOG W is significant at the 99.9 percent confidence level.)

In analyzing free face failures near the Shinano River in Niigata, we postulated that the slope of the river bank into or away from the channel may have had an effect on D_H and we tabulated and tested a second variable, S , (%), to represent that possible effect. The value of S was assigned a positive value for cases where the ground sloped toward the channel (Figure 3-8, Case 1) and a negative value for cases where the ground sloped away from the channel (Figure 3-8, Case 2). The inclusion of S in the free face model did not improve R^2 significantly; hence, we concluded that the slope of the floodplain near the Shinano River does not vary enough to have markedly affected D_H . In general, we found this conclusion to be true for other case history sites where free face failures occurred near major river channels.

We also adjusted the free face model for the effects of subsurface geology and soil conditions. Stepwise regression indicated that the cumulative thickness of the liquefied layer, T , (m), is the next variable that should enter the model. Some modelers have used liquefaction analyses based on empirical curves and SPT $(N1)_{60}$ values to estimate T (Seed and Idriss, 1971; Seed et al., 1983, 1985; NRC, 1985; Hamada, 1986; Liao, 1986). However, these techniques require an estimate of the earthquake magnitude, M , and peak ground acceleration, A , as input into the analyses. Thus, T determined from these methods will be correlated with the earthquake factors M and A . To minimize the correlation between earthquake and site factors, we defined and tested three estimates of T that are calculated without performing

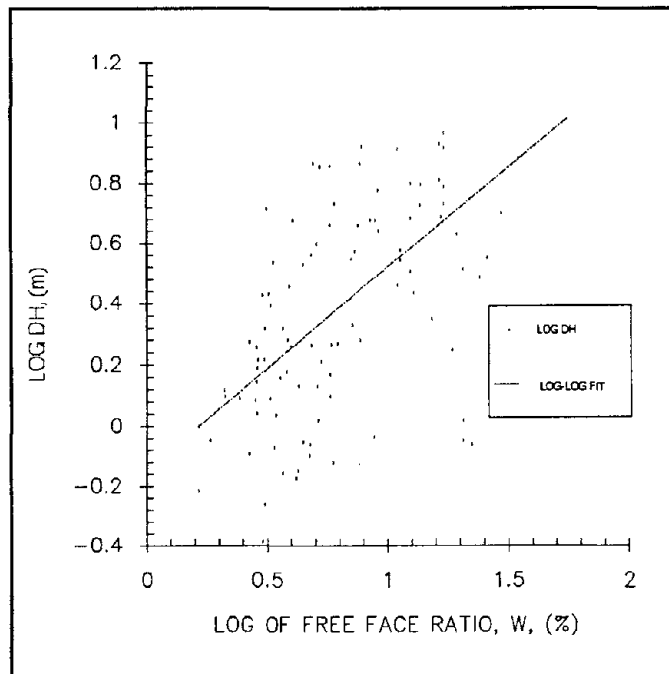


Figure 3-6 Plot of LOG D_H versus LOG W for lateral spread displacements along the Shinano River, Niigata, Japan showing an approximately linear relationship.

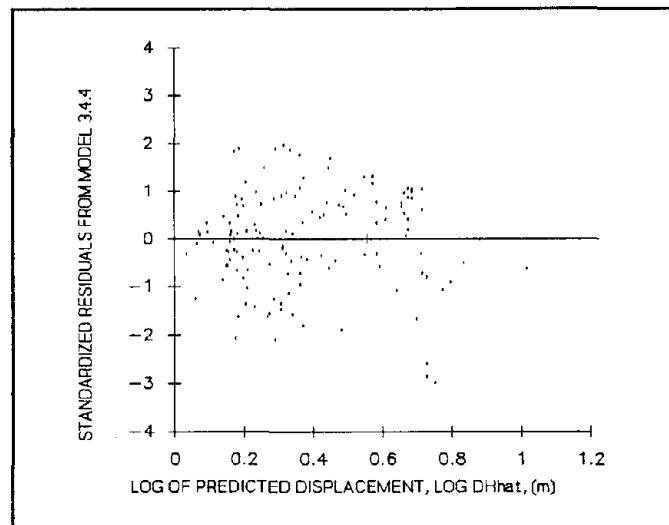


Figure 3-7 Standardized residuals, e_i 's, from model 3.4.4 plotted against LOG D_{Hhat} showing no evidence of nonconstant variance.

liquefaction analyses. We defined T_{10} , T_{15} , and T_{20} as the cumulative thickness, (m), of saturated cohesionless sediments with SPT $(N1)_{60}$ values ≤ 10 , 15, and 20, respectively. Saturated soils with a clay content ≥ 15 percent were not added to these cumulative thickness. Also, because most boreholes included in our study were drilled to a maximum depth of 20 meters, T_{10} , T_{15} , and T_{20} were generally accumulated in the upper 20 m of the soil profile. The substitution of T_{10} , T_{15} , and T_{20} for T into the free face model:

$$\text{LOG } D_H = b_0 + b_1 \text{ LOG } W + b_2 T. \quad (3.4.5)$$

yields R^2 values of 50.9, 62.4, and 63.8 percent, respectively. We ultimately chose to use T_{15} instead of T_{20} in all subsequent models because our case history data suggests that lateral spreads are generally restricted to deposits having $(N1)_{60}$ values ≤ 15 for $M \leq 8.0$ earthquakes. A plot of the $e_s(s)$ from model 3.4.4 versus T_{15} shows an approximately linear relationship between $\text{LOG } D_H$ and T_{15} (Figure 3-9a), thus we formed the model:

$$\text{LOG } D_H = -0.537 + 0.568 \text{ LOG } W + 0.0458 T_{15}. \quad (3.4.6)$$

All regression coefficients for this model are significant at the 99.9 percent confidence level.

After adjusting the free face model for the influence of W and T , stepwise regression indicated that the percentage of fines, F , (particle size ≤ 0.075 mm) of the liquefied layer is the next variable that should enter the free face model. In Figure 3-9b, the $e_s(s)$ from Equation 3.4.6 are plotted against the average fines content in T_{15} . The linear trend implies that horizontal displacement decreases with increasing fines content. The free face model adjusted for F is:

$$\text{LOG } D_H = -0.355 + 0.594 \text{ LOG } W + 0.0369 T_{15} - 0.0102 F_{15} \quad (3.4.7)$$

where:

F_{15} = average fines content in T_{15} , in percent.

The R^2 for this model is 66.0 percent and all regression coefficients are significant at the 99.9 percent confidence level.

The mean grain size, D_{50} , (mm), of the channel deposits along the Shinano River also had a minor influence on displacement. In Figure 3-9c, the $e_s(s)$ from model 3.4.7 are plotted against the average D_{50} in T_{15} . Although showing considerable scatter, this plot suggests that displacement decreases as the average D_{50} value in T_{15} increases. Model 3.4.7 adjusted for D_{50} is:

$$\begin{aligned} \text{LOG } D_H = & 0.301 + 0.563 \text{ LOG } W + 0.0338 T_{15} - 0.0244 F_{15} \\ & - 1.50 D_{50_{15}} \end{aligned} \quad (3.4.8)$$

where:

$D_{50_{15}}$ = average D_{50} in T_{15} , in millimeters.

The R^2 for this model is 70.0 percent and partial t-tests show that intercept is significant at the 90 percent confidence level and all other regression coefficients are significant at the 99.9 percent confidence level.

In addition to $D_{50_{15}}$, the $(N1)_{60}$ value associated with the lowest factor of safety against liquefaction in the liquefied profile, $N1_{60s}$, makes a minor contribution to improving the performance of the free face model. The value of R^2 increased from 70.0 to 72.4 percent as $N1_{60s}$ was included. To determine $N1_{60s}$, a factor of safety against liquefaction, FS , was calculated for each $(N1)_{60}$ value in the profile by applying the "simplified procedure" for liquefaction analysis (Seed

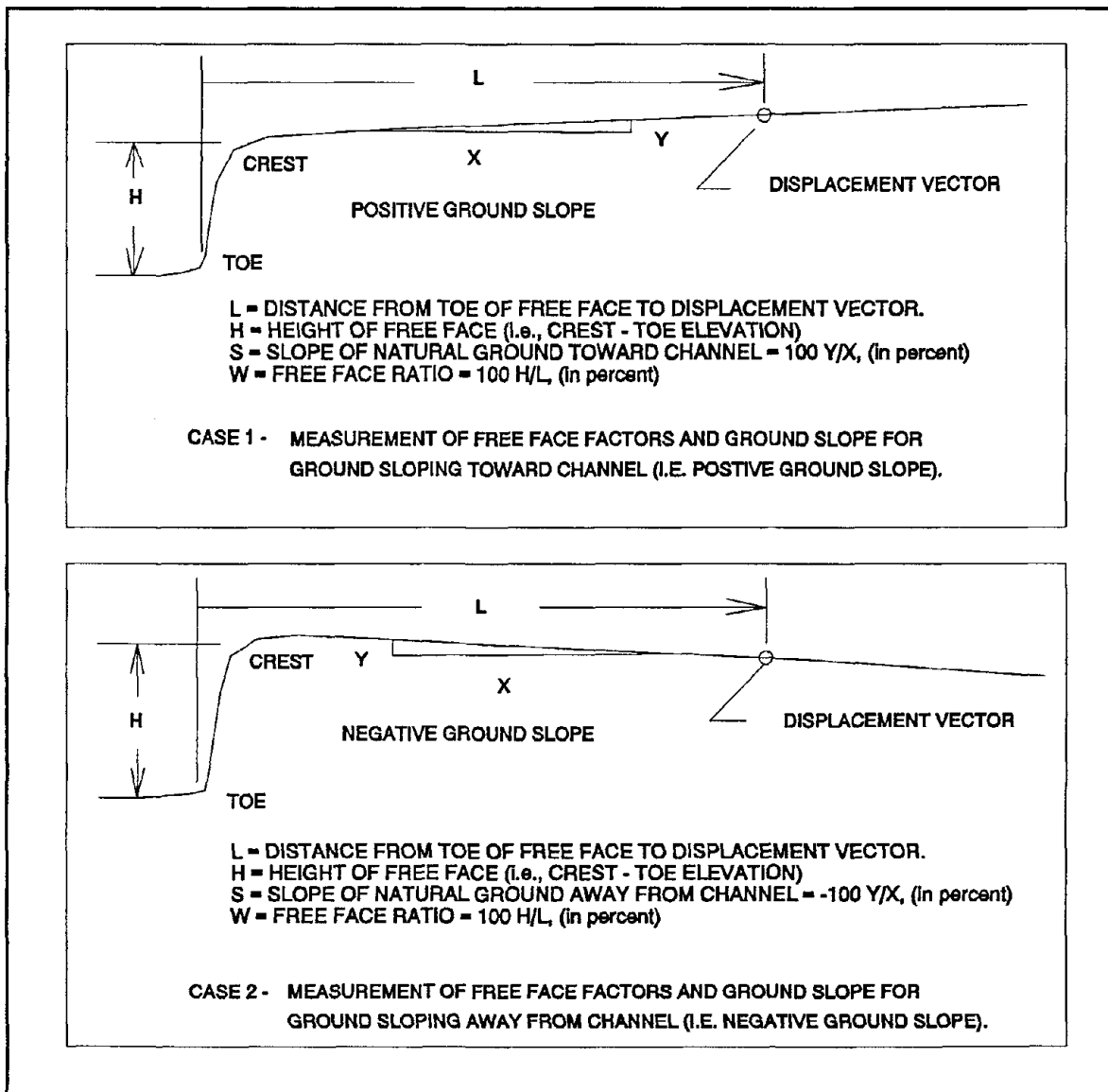


Figure 3-8 Definition of free face factors, L and W , and ground slope, S , for free face failures.

and Idriss, 1971; Seed et al., 1983; 1985; see also Appendix 1):

$$FS = CSRL/CSRQ \quad (3.4.9)$$

where:

CSRL = cyclic stress ratio required for liquefaction

CSRQ = cyclic stress ratio induced in the profile by the earthquake.

The $(N1)_{60}$ value corresponding to the lowest FS in the profile was assigned to $N1_{60s}$. The $e_v(s)$ from Equation 3.4.8 plotted against $N1_{60s}$ indicate that displacement tends to decrease with increasing values of $N1_{60s}$ (Figure 3-9d).

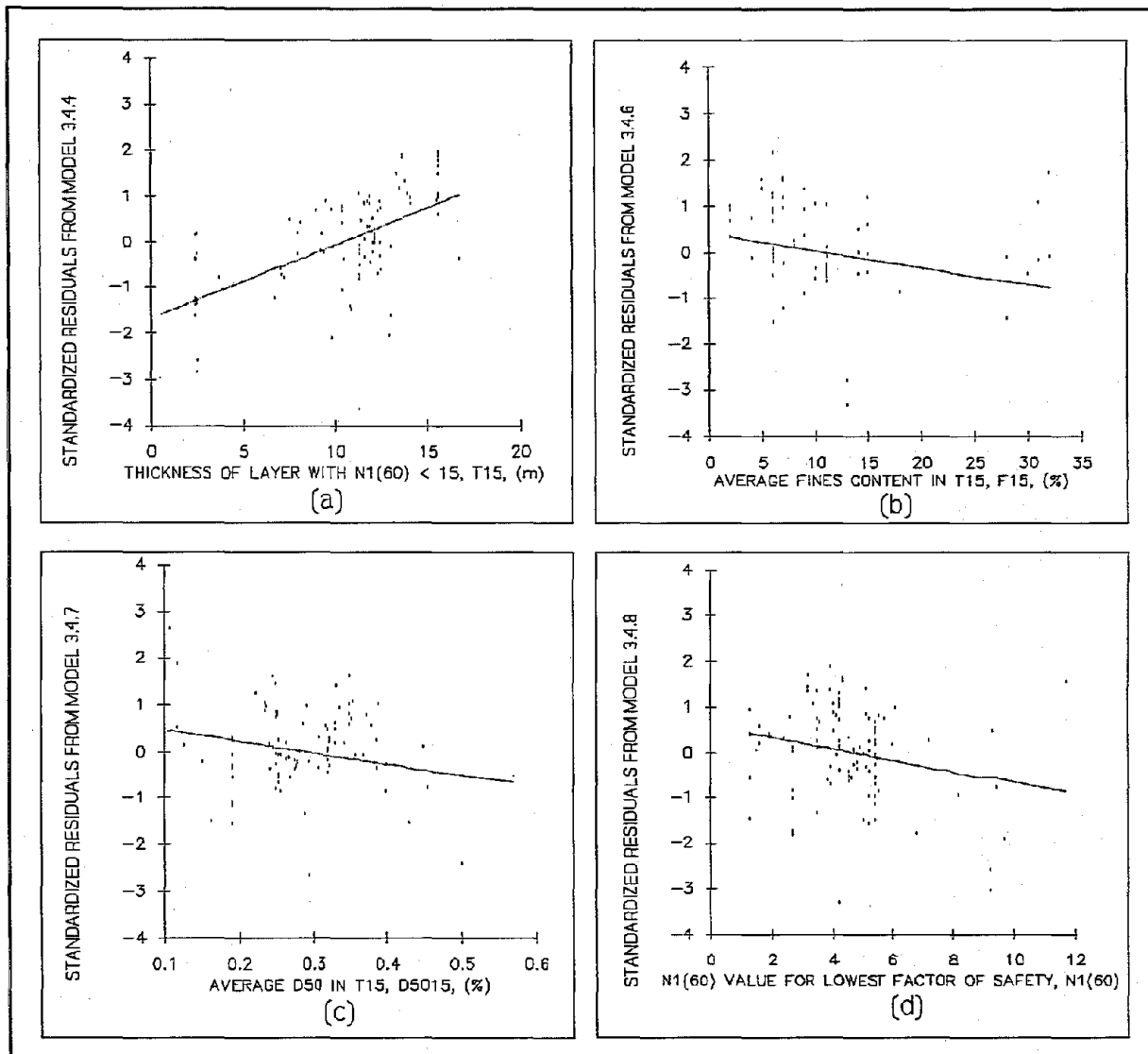


Figure 3-9 (a) Standardized residuals from model 3.4.4 plotted against the thickness of saturated cohesionless sediments with SPT ($N1$)₆₀ values ≤ 15 , T_{15} , showing a linear relationship between T_{15} and e_s . (b) Standardized residuals from model 3.4.6 plotted against the average fines content, F_{15} , in T_{15} showing a linear relationship between F_{15} and e_s . (c) Standardized residuals from model 3.4.7 plotted against the average mean grain size, $D50_{15}$, in T_{15} showing a linear relationship between $D50_{15}$ and e_s . (d) Standardized residuals from model 3.4.8 plotted against the SPT ($N1$)₆₀ value corresponding to the lowest factor of safety in the liquefied profile, $N1_{60s}$, showing a linear relationship between $N1_{60s}$ and e_s .

The addition of $N1_{60s}$ in the free face model yields:

$$\begin{aligned} \text{LOG } D_H = & 0.610 + 0.572 \text{ LOG } W + 0.0247 T_{15} - 0.0278 F_{15} \\ & - 1.61 D50_{15} - 0.0315 N1_{60s} \end{aligned} \quad (3.4.10)$$

The inclusion of other possible geological and soil factors from Table 3-2 in Equation 3.4.10 did not appreciably improve the performance of the model; thus, this equation was adopted as the final model for free face failures in Niigata.

We did obtain a slightly higher R^2 values by including interaction terms in the model (i.e., cross-products of $\text{LOG } W$, T_{15} , F_{15} , $D50_{15}$, and $N1_{60s}$), but the physical

meanings of these interactions were difficult to interpret. Thus, we do not believe that the slight improvement in R^2 warrants the addition of higher order terms and we formulated all of our subsequent models with first order terms only.

All regression coefficients for Equation 3.4.10 are significant at 99 percent confidence level. Appendix 2 contains the MINITAB printout for this model (Minitab, 1989; Ryan et al., 1985). This output lists the regression coefficients, their standard deviations, partial t-tests for significance, an analysis of variance (ANOVA) table, and a list of potential outliers. The standardized residual plots for this model are also given in Appendix 2.

In addition to evaluating R^2 , a plot of D_H versus D_{Hhat} provides a simple way to view the predictive performance of this model (Figure 3-10). The solid "MEASURED = PREDICTED" line represents a perfect prediction line. Observations plotting near this line are closely approximated by the regression model. The dashed line below the "MEASURED = PREDICTED" line represents a 100 percent overprediction bound. Observations plotting below this line are being overpredicted by a factor of two or greater. The dashed line above the "MEASURED = PREDICTED" line is a 50 percent underprediction bound. Observations falling above this line are being underpredicted by a factor of two or greater. In summary, 92 percent (128 out of 139) of the displacements predicted by Equation 3.4.10 fall between these upper and lower prediction bounds.

3.5 Ground Slope Model for Niigata and Noshiro, Japan

Stepwise regression indicated that ground slope, S , is highly correlated with D_H for ground slope failures in Niigata and Noshiro, Japan. In Niigata, lateral spread occurred on very gentle, uniform slopes ($S \leq 1$ percent); whereas, in Noshiro, lateral spread developed on undulating, dune deposits with slopes that are as steep as 5 percent in some locales. Because of the undulating topography found in Noshiro, we used slightly different techniques to measure S for uniform and nonuniform slopes. Figure 3-11, Case 1 shows the technique we used to measure S for the long, uniform slopes that were typical of Niigata. The value of S , (%), for these cases was calculated simply as:

$$s = 100 y/x. \quad (3.5.1)$$

However, in Noshiro, the amount of ground displacement was strongly influenced by undulations in the sand dunes. For example, Figure 3-12 shows that the ground displacement tended to mirror the topography, increasing near the steeper part of the undulating dune and decreasing in more gentle reaches. From the observed

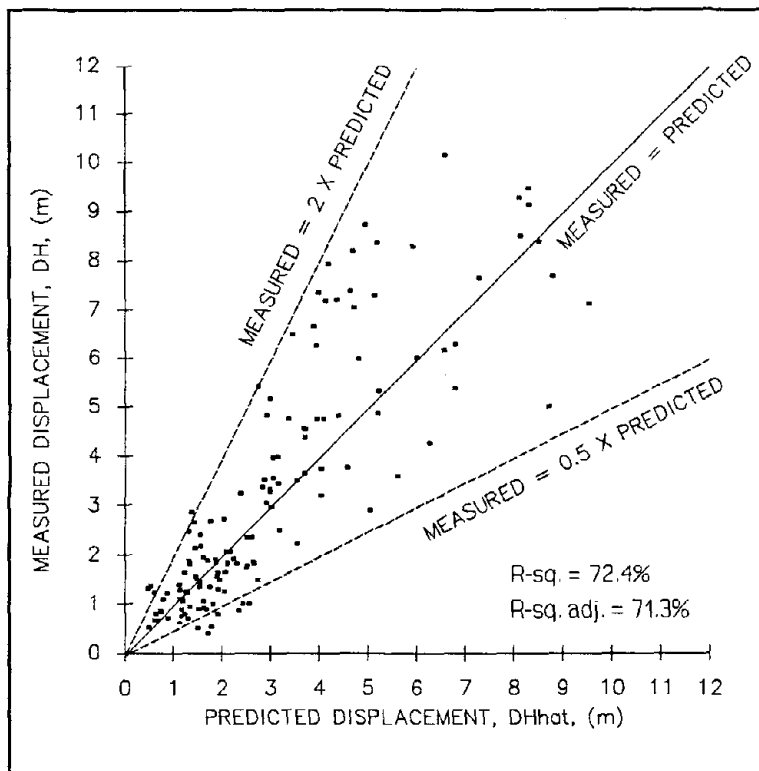


Figure 3-10 Plot of measured displacements, D_H , versus predicted displacements, D_{Hhat} , for Equation 3.4.10, Shinano River, Niigata.

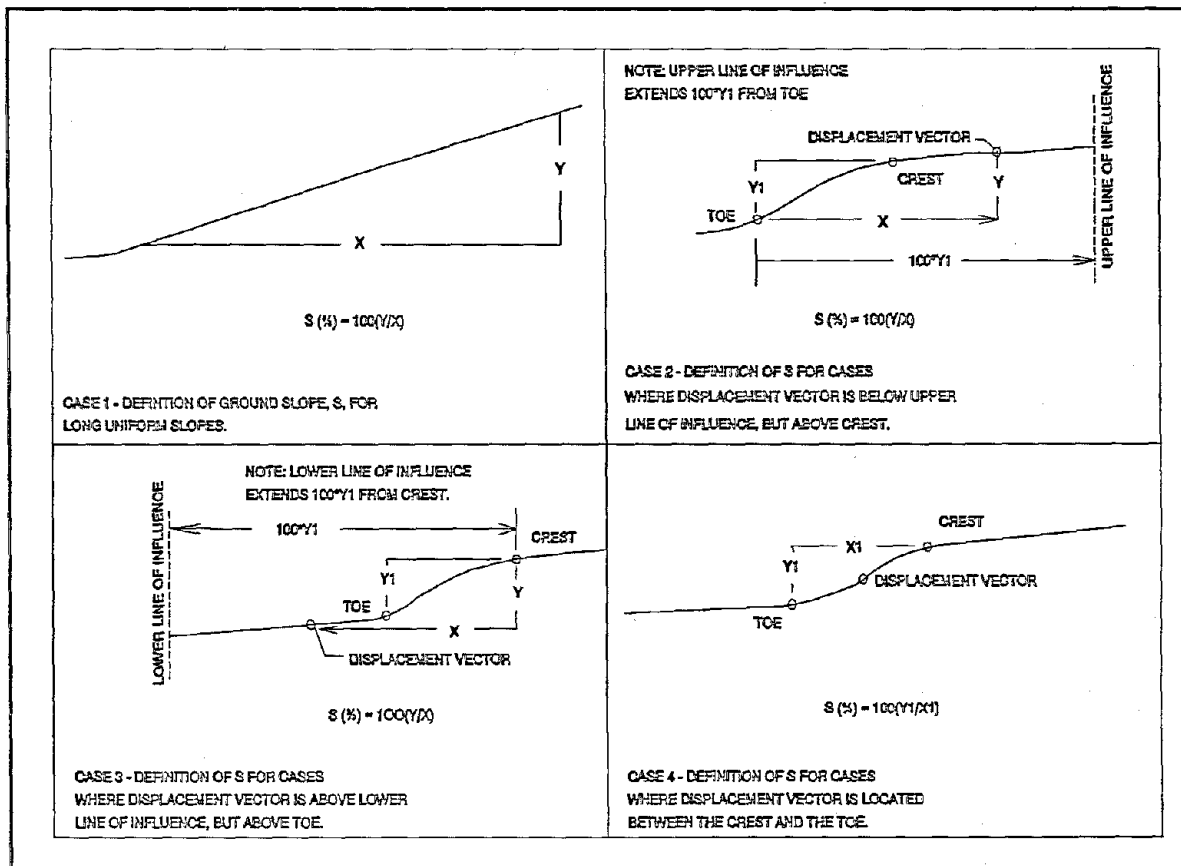


Figure 3-11, Case 1. Definition of ground slope, S, for long uniform slopes. Cases 2 - 4. Definition of S for nonuniform slopes.

displacement pattern, we noted that the zone of increased displacement near the undulations generally extended above and below the toe and crest of the undulations for a maximum horizontal distance of approximately 100 times the height of the undulation. Thus, our measurements of S for displacement vectors falling within this zone were steepened to either the crest or to the toe of the undulations as shown in Figure 3-11, Cases 2 and 3. Figure 3-11, Case 2 shows the definition used to measure S for displacement vectors that occurred above the crest of the undulations, but within $100 Y_1$ of the toe of the undulations. Figure 3-11, Case 3 shows the definition used to measure S for vectors that were located below the toe of the undulations, but within $100 Y_1$ of the crest of the undulations. Figure 3-11, Case 4 shows the definition used to assign S to all vectors located on the face of the undulations. We applied these same techniques to measure S for all undulating slopes found in our study.

As was discovered in developing the free face model, regression analyses of ground slope failures in Niigata and Noshiro indicate that a model comprised of $\text{LOG } D_H$ and $\text{LOG } S$ produces an approximately linear form (Figure 3-13):

$$\text{LOG } D_H = 0.430 + 0.442 \text{ LOG } S. \quad (3.5.2)$$

The R^2 for this model is 42.1 percent. The regression coefficients for this model are significant at the 99.9 percent confidence level.

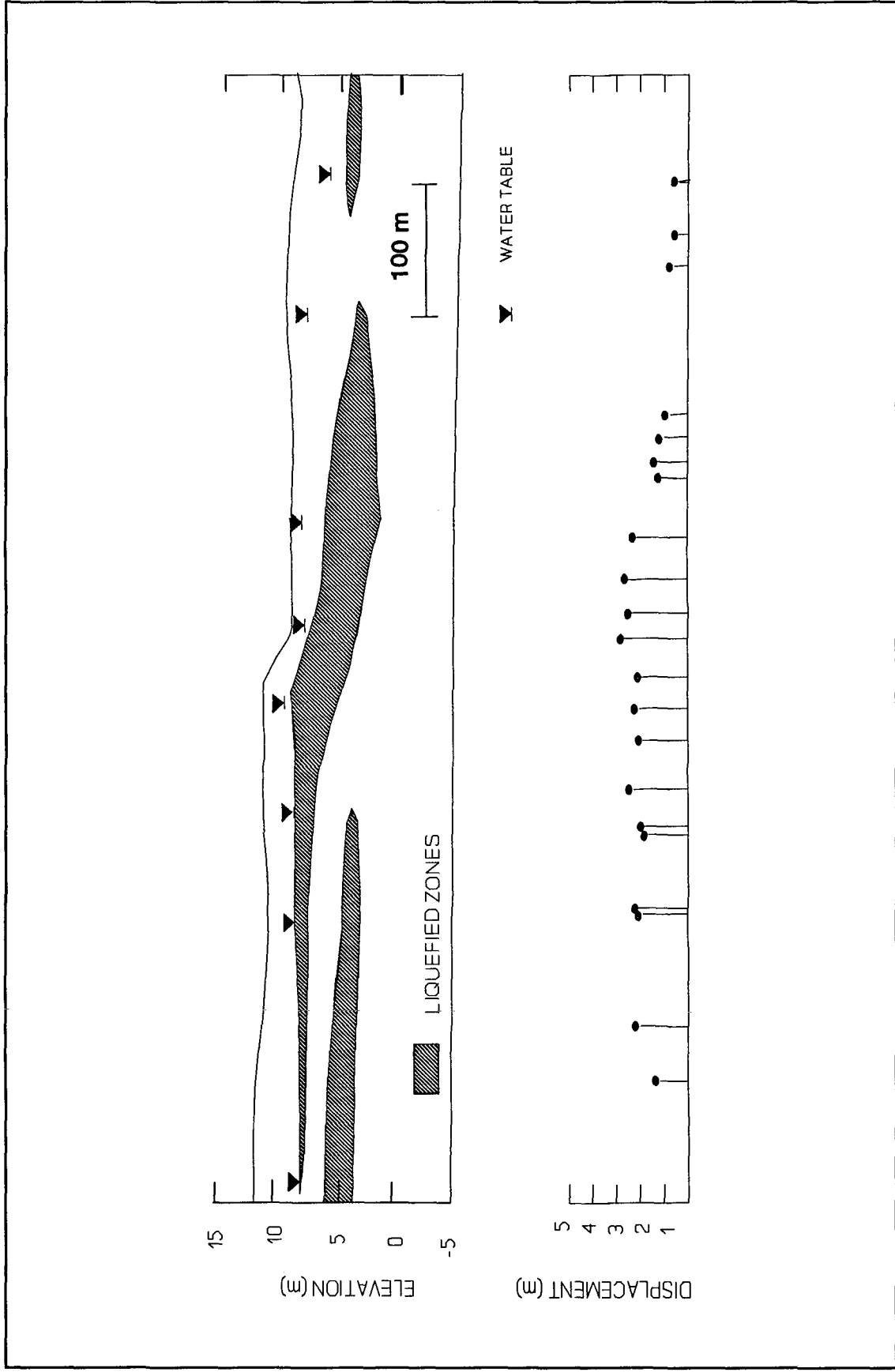


Figure 3-12 Typical topography and ground displacement pattern for ground slope failures in Noshiro, Japan, (after Hamada et al., 1986).

A slightly better fit ($R^2 = 45.6\%$) was obtained by forming the model: $D_H = b_0 + b_1 \text{ LOG } S$, but like the free face model, a plot of $e_i(s)$ versus D_{Hhat} suggested a slight problem with nonconstant variance. Also, because we transformed D_H to $\text{LOG } D_H$ in developing the free face model, it was beneficial to maintain the same functional form in developing the ground slope model. This will allow us to combine both models into a single regression operation as the earthquake factors are brought into the analyses (for further discussion, see the next section).

As was discovered in developing the free face model, the variables T_{15} , $D50_{15}$, and F_{15} also contribute to improving the performance of the ground slope model. Furthermore, like the free face model, standardized residuals from model 3.5.2 plotted against T_{15} , $D50_{15}$, and F_{15} suggest that the relationships between displacement and these variables are approximately linear, thus these factors were also included in the ground slope model:

$$\text{LOG } D_H = 0.698 + 0.378 \text{ LOG } S + 0.0362 T_{15} - 0.0326 F_{15} + 0.929 D50_{15}$$

(3.5.3)

No additional geological and soil factors substantially improved this model, thus it was adopted as the final model for predicting ground slope failures in Niigata and Noshiro. The R^2 for Equation 3.5.3 is 54.2 percent and the intercept and regression coefficients are significant at the 99 percent confidence level (see MINITAB output in Appendix 2). A plot of D_H versus D_{Hhat} for this model shows that 97 percent (224 out of 232) of the predicted displacements fall between the 100 percent overprediction and 50 percent underprediction bounds (Figure 3-14).

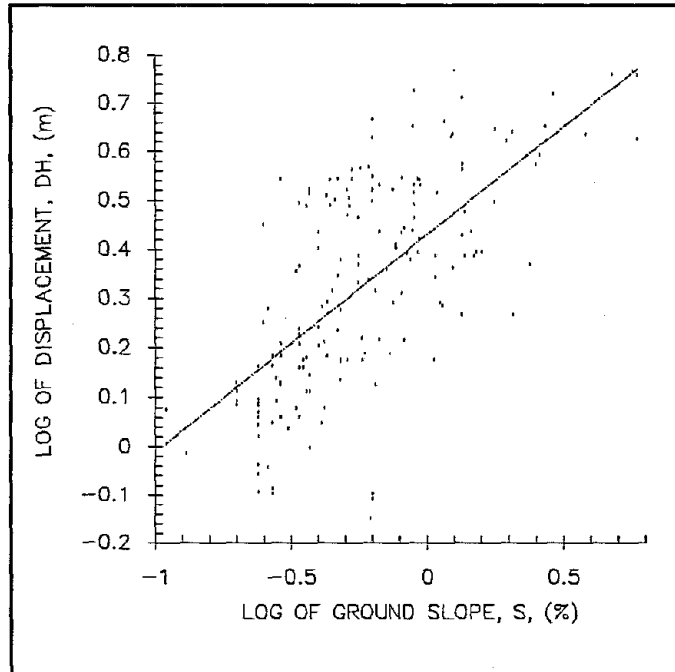


Figure 3-13 Plot of log of displacement, $\text{LOG } D_H$, versus log of ground slope, $\text{LOG } S$, for ground slope failures indicating an approximately linear trend.

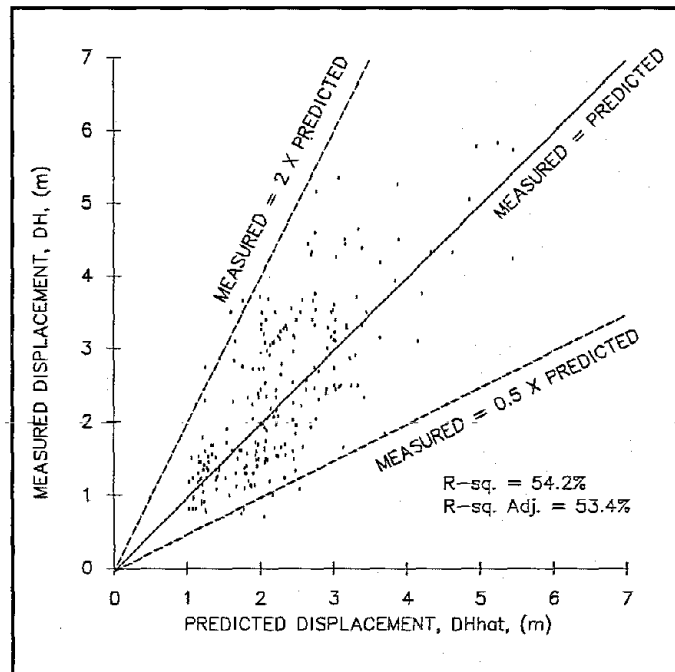


Figure 3-14 Plot of measured displacements, D_H , versus predicted displacements, D_{Hhat} , for Equation 3.5.3, ground slope failures, Niigata and Noshiro.

SECTION 4
COMBINED MLR MODEL FOR JAPANESE AND U.S. CASE HISTORIES

4.1 Earthquake Factors

The site-specific models developed for Niigata and Noshiro, Japan, were adjusted for a wider range of seismic and site conditions by including the U.S. data in the analyses. Youd and Perkins (1987), in developing the LSI model, proposed that displacement is a function of the amplitude, A , and duration, D , of strong ground motion.

$$D_H = f(A, D) \quad (4.1.1)$$

where:

A = peak horizontal ground acceleration (in decimal fraction of g).
 D = time interval between the first horizontal 0.05 g peak to the last 0.05 g peak recorded by a strong motion instrument (in seconds).

Unfortunately, strong motion records were not available for many of the lateral spread sites listed in Table 3-1. For these uninstrumented sites, A and D were estimated from empirical relationships based on earthquake magnitude, M , and the log of the distance to the seismic energy source, $\text{LOG } R$ (Joyner and Boore, 1988; Youd and Perkins, 1987; Krinitzsky and Chang, 1988b; Appendix 1).

In addition to A and D , Youd and Perkins showed that D_H is a function of M and attenuates logarithmically with increasing R .

$$D_H = f(M, \text{LOG } R) \quad (4.1.2)$$

where:

M = moment magnitude, M_w .
 R = horizontal distance from the seismic source (in km).

The moment magnitude, M_w , is commonly used to represent M for these type of analyses because M_w is a better estimate of the amount of seismic energy released by a given earthquake than other measures of earthquake magnitude, especially for $M > 8.0$ events (Kanamori, 1978). Other earthquake magnitude measures such as the local magnitude, M_L , and the surface wave magnitude, M_s , are approximately equivalent to M_w for $6 \leq M \leq 8$ earthquakes (Krinitzsky and Chang, 1988b).

The distance from the seismic source, R , is measured as the horizontal distance from the site in question to the nearest point on a surface projection of the fault rupture zone. Epicentral distances may be adequate estimates of R for $M \leq 6$ earthquakes, but should not be used for larger earthquakes. Earthquakes with $M > 6$ are generally associated with large fault rupture zones that are not adequately characterized by a single point, such as the epicenter. Source zones for strike-slip and normal faults are usually delineated by a band that incorporates surface ruptures associated with recent (i.e., Holocene) faulting events. For these type of faults, which are common in the western U.S., source distances are measured horizontally from the nearest edge of the surface rupture zone to the site in question. For reverse faults, shallow-angle thrusts, and subduction-zone earthquakes, the associated zone of tectonic crustal uplift generally delineates the surface projection of the seismic source. For these type of faults, the source distance is measured from the nearest point of the tectonic uplift zone to the site in question.

Our preliminary regression analyses of the combined U.S. and Japanese data indicated that MLR models based on M and $\text{LOG } R$ yield R^2 values that are about 10 to 15 percent higher than models based on A and D . Thus, we chose to use M and $\text{LOG } R$ in subsequent models. However, we do not wish to imply that M and $\text{LOG } R$ are better measures of seismic energy than instrumentally obtained values of A

and D. Because A and D are more fundamental measures of the seismic energy delivered to a given site than M and LOG R, in general A-D models should yield equivalent, or slightly superior performance, when compared with M-LOG R models. Unfortunately, our MLR database contains many estimated values of A and D, and the poorer quality of these data appears to be hampering our ability to develop satisfactory A-D models.

The LSI model proposed by Youd and Perkins (1987) and the site-specific models developed in the previous section suggest that a more comprehensive MLR model(s) for predicting ground displacement should include, but not be restricted to the following factors:

$$\text{LOG } D_H = f(M, \text{LOG } R, \text{LOG } W, \text{LOG } S, T_{1s}, F_{1s}, D50_{1s}, N1_{60s}). \quad (4.1.3)$$

In developing preliminary MLR models from this function, we divided the MLR database into two databases, one for free face failures and one for ground slope failures and attempted fitting separate regression coefficients for M and LOG R for each type of failure. However, this attempt yielded unsatisfactory results. We concluded that the U.S. database does not contain a sufficient number of ground slope failures to independently adjust the ground slope model for the effects of M and LOG R. To overcome this limitation, we combined the free face and ground slope databases and formulated the MLR model to fit common earthquake regression coefficients for each type of failure. The same model was formulated to fit separate topographical, geological, and soil parameters for free face and ground slope failures:

$$\text{LOG } D_H = f(M, \text{LOG } R, \text{LOG } W_{ff}, T_{1sff}, F_{1sff}, D50_{1sff}, N160_{sff}, \text{LOG } S_{gs}, T_{1sgs}, F_{1sgs}, D50_{1sgs}) \quad (4.1.4)$$

The subscripts ff and gs in Equation 4.1.4 indicate those variables that were assigned to the free face and ground slope components of the model, respectively. Inherent in this formulation is the assumption that M and LOG R influence free face failures in the same way that they influence ground slope failures. This appears to be a reasonable assumption because the amount of seismic energy delivered to a free face and a ground slope failure is the same for a particular seismic event and liquefaction locality. Given that we separately adjust each type of failure for the effects of topographical, geological and soil conditions (i.e., W, S, T, F, D50, and N1₆₀), it seems reasonable to fit common earthquake parameters for free face and ground slope failures.

Based on the function expressed in Equation 4.1.4, we formulated the following MLR model:

$$\text{LOG}(D_H + 0.01) = b_0 + b_{off} + b_1 M + b_2 \text{LOG } R + b_3 \text{LOG } W_{ff} + b_4 T_{1sff} + b_5 F_{1sff} + b_6 D50_{1sff} + b_7 N1_{60sff} + b_8 \text{LOG } S_{gs} + b_9 T_{1sgs} + b_{10} F_{1sgs} + b_{11} D50_{1sgs} \quad (4.1.5)$$

The fitted parameter b_0 is the intercept of the combined free face and ground slope components of the model. The regression coefficient b_{off} is used to adjust b_0 for any difference that may exist between the intercepts of the free face and ground slope components (i.e., the intercept for the free face component of the model is calculated by adding b_0 and b_{off}). Because $\log(0)$ is undefined, we expediently added 0.01 m to all values of D_H prior to performing the regression. This expediency enabled us to calculate $\log(D_H)$ for the zero displacement observations that are included in our MLR database.

A least squares fit of Equation 4.1.5 yields these regression coefficients: $b_0 = -5.085$, $b_{off} = -0.559$, $b_1 = 0.976$, $b_2 = -1.053$, $b_3 = 0.693$, $b_4 = 0.0272$, $b_5 = -0.0328$, $b_6 = -1.124$, $b_7 = -0.0118$, $b_8 = 0.356$, $b_9 = 0.0403$, $b_{10} = -0.0336$, $b_{11} = -1.535$. The R^2 for this equation is 74.9 percent and all regression coefficients, except for b_7 , are significant at the 99 percent confidence level. The fitted value for b_7 is significant at the 92 percent confidence level. Figure 4-1 shows that 89 percent (i.e., 399 out of 448) of the predicted displacement values fall

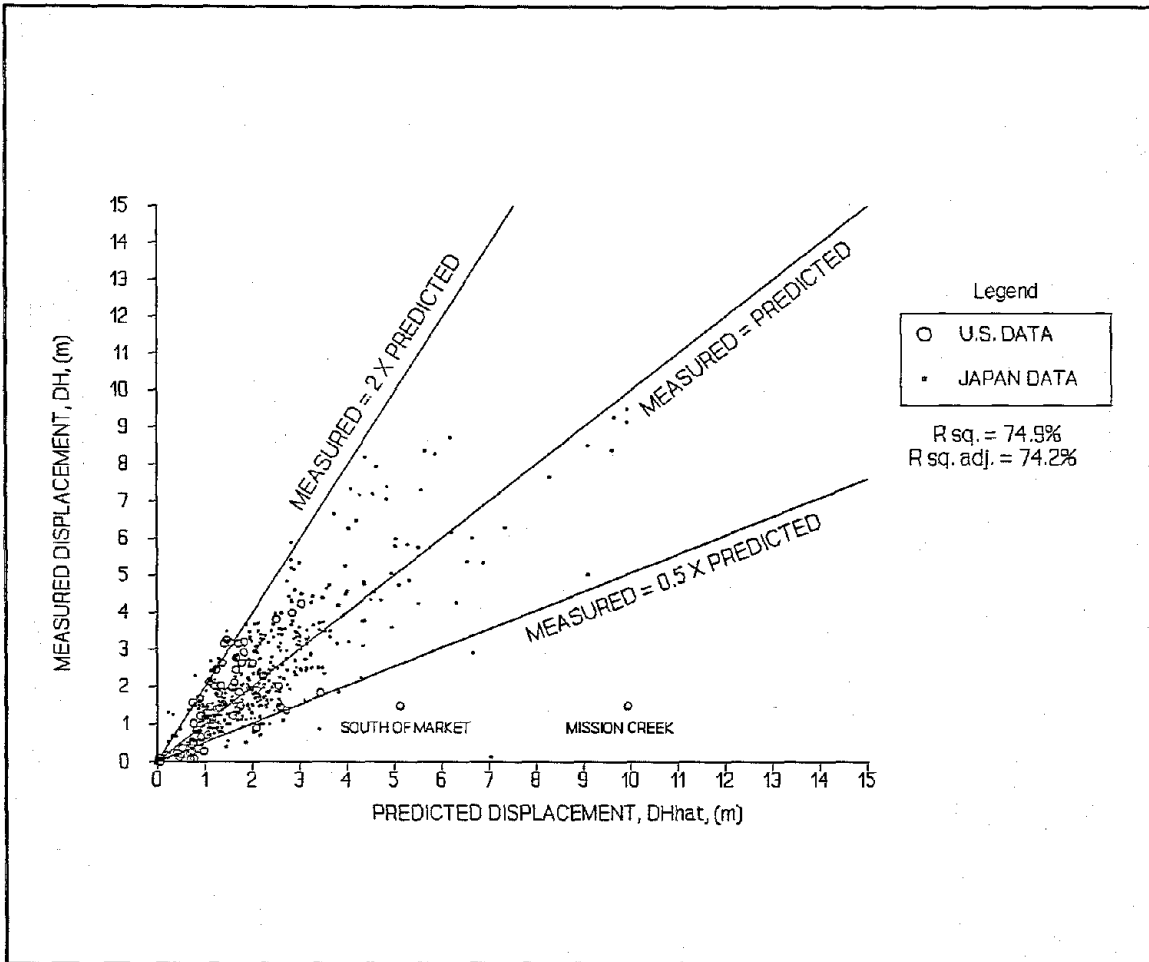


Figure 4-1 Plot of measured displacements, D_H , versus predicted displacements, $D_{\hat{H}}$, for model 4.1.5 using Japanese and U.S. case history data.

between the 100 percent overprediction and 50 percent underprediction bounds. The free face component of Equation 4.1.5 is:

$$\begin{aligned} \text{LOG}(D_H+0.01) = & -5.644 + 0.976 M - 1.053 \text{ LOG } R + 0.693 \text{ LOG } W + 0.0272 T_{15} \\ & - 0.0328 F_{15} - 1.124 D50_{15} - 0.0118 N_{15} \end{aligned} \quad (4.1.5a)$$

and the ground slope component is:

$$\begin{aligned} \text{LOG}(D_H+0.01) = & -5.085 + 0.976 M - 1.053 \text{ LOG } R + 0.356 \text{ LOG } S + 0.0403 T_{15} \\ & - 0.0336 F_{15} - 1.535 D50_{15} \end{aligned} \quad (4.1.5b)$$

Based on our data, Equation 4.1.5 appears to be performing reasonably well for $M = 6.5$ to 7.5 earthquakes and for liquefied sites within a 30 km radius of the seismic source. However, a comparison with data published by Ambraseys (1988) shows that Equation 4.1.5 will tend to overpredict D_H at liquefied sites with $R > 30$ km. In his study, Ambraseys compiled values of M_w and the farthest distance to observed liquefaction effects, R_L , (km), for several earthquakes and bounded these data with the equation:

$$M = 0.18 + 9.2 \times 10^{-8} R_r + 0.90 \text{ LOG } R_r \quad (4.1.6)$$

(See solid, curved bound shown on Figure 4-2). Ambraseys' study suggests that liquefaction (i.e., ground displacement, fissures, sand boils, etc.) are almost always located within this bound and for $R > R_r$, liquefaction effects are usually not observed. We used Equation 4.1.5 to back-calculate the distance, R , corresponding to the inception of lateral spread by using $D_H = 0.05$ m and mean values of W , S , T_{15} , F_{15} , $D50_{15}$, $N_{1_{60s}}$ from our MLR database (Table 4-1). Figure 4-2 shows the results superimposed upon Ambraseys' data and R_r bound. This plot shows that the free face component of Equation 4.1.5 continues to predict ground displacement beyond Ambraseys' R_r bound beginning at $M > 6.25$ and $R > 30$ km and the ground slope component of Equation 4.1.5 does likewise for $M > 7.0$ and $R > 70$ km. Because Equation 4.1.5 does not correctly attenuate D_H with increasing R , we concluded that it should not be applied at sites with $R > 30$ km. This is a serious limitation to the application of Equation 4.1.5, especially for evaluating large earthquakes that typically produce significant lateral spread displacement beyond 30 km. Unfortunately, most of our case history sites are from $R \leq 30$ km; thus, there is very limited information for adjusting Equation 4.1.5 based solely on our compiled data.

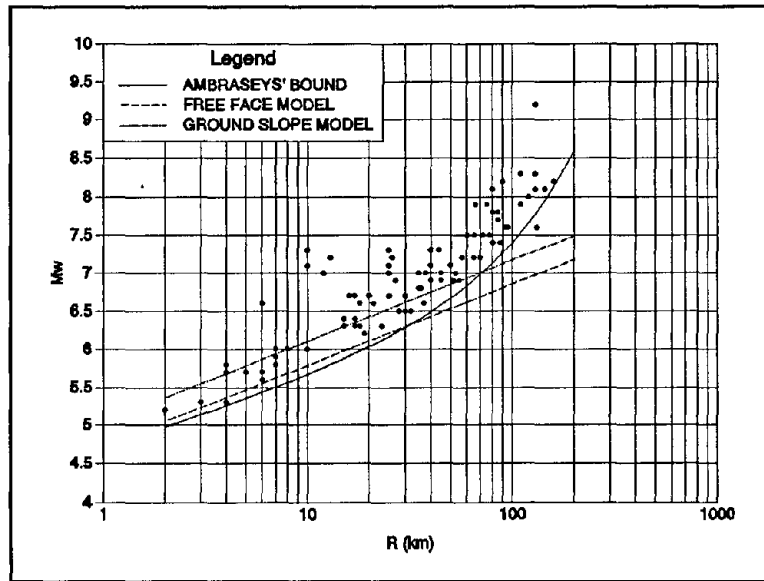


Figure 4-2 Performance of MLR model prior to including Ambraseys' data and adding a R term.

The data from Ambraseys' study, however, offer a means of adjusting Equation 4.1.5 so that it more properly attenuates $\text{LOG } D_H$ as a function of R . To this end, we included 19 observations from Ambraseys' study (Table 4-2) in our analysis to strengthen the MLR database for $R > 30$ km. Because the majority of our case history sites are from earthquakes with $6.4 \leq M \leq 6.6$ and $7.4 \leq M \leq 7.8$, we selected only those observations from Ambraseys' study that fall within these same ranges. Also, prior to incorporating Ambraseys' data into the regression analysis, we needed reasonable estimates of the topographical, geological, and soil conditions at these sites. Because these factors were not compiled by Ambraseys, we decided to use average values of $\text{LOG } W$, $\text{LOG } S$, T_{15} , F_{15} , $D50_{15}$, $N_{1_{60s}}$ from our database to approximate average site conditions at Ambraseys' sites (Table 4-1). In addition, because Ambraseys' sites represent the maximum R to observable liquefaction effects, we assumed that a minimal amount of lateral spread occurred at these localities and assigned $D_H = 0.05$ m to the observations listed in Table 4-2. Also, these observations were randomly assigned to either the free face or ground slope component of our MLR model prior to performing the regression analyses.

The functional form of Ambraseys' equation suggests that, in addition to the earthquake factors, M and $\text{LOG } R$, we need to include a R term in Equation 4.1.5. Therefore, we postulate that:

$$\text{LOG}(D_H + 0.01) = b_0 + b_{0ff} + b_1 M + b_2 \text{LOG } R + b_3 R + b_4 \text{LOG } W_{ff} + b_5 T_{15ff} + b_6 F_{15ff} + b_7 D50_{15ff} + b_8 N_{1_{60sff}} + b_9 \text{LOG}(S)_{ff} + b_{10} T_{15sp} + b_{11} F_{15sp} + b_{12} D50_{15sp} \quad (4.1.7)$$

A regression of this equation yields the following coefficients: $b_0 = -6.086$, $b_{off} = -0.483$, $b_1 = 1.106$, $b_2 = -0.978$, $b_3 = -0.0101$, $b_4 = 0.703$, $b_5 = 0.0269$, $b_6 = -0.0308$, $b_7 = -0.983$, $b_8 = -0.0118$, $b_9 = 0.373$, $b_{10} = 0.0384$, $b_{11} = -0.0304$, $b_{12} = -1.096$. All regression coefficients are significant at the 99 percent confidence level, except for b_8 which is only significant at the 93 percent confidence level, respectively. The R^2 for this equation is 83.6 percent.

Once again we used Equation 4.1.7 to back-calculate R for the inception of lateral spread by inputting $D_H = 0.05$ m and using the average site conditions listed in Table 4-1. Figure 4-3 shows the results compared with Ambraseys' data and R_t bound. The functional form of Equation 4.1.7 mimics Ambraseys' R_t bound quite well and the free face and ground slope components of the model provide a reasonable fit to Ambraseys' data. Thus, we concluded that the functional form of Equation 4.1.7 appears to more correctly attenuate D_H as a function of M and R than Equation 4.1.5.

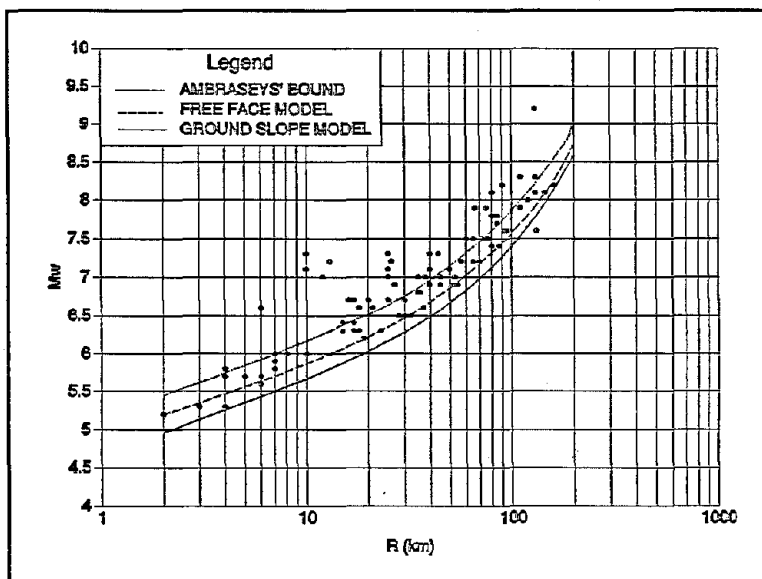


Figure 4-3 Performance of MLR model after including Ambraseys' data and adjusting for R .

A further examination of Equation 4.1.7 shows that $b_5 \approx b_{10}$, and $b_6 \approx b_{11}$, and $b_7 \approx b_{12}$, suggesting that common regression coefficients can be fitted for T_{15FR} and T_{15SP} , and for F_{15FR} and F_{15SP} , and for $D50_{15FR}$ and $D50_{15SP}$. Also, because the regression coefficient for Nl_{60FR} , i.e., b_8 , is significant only at the 93 percent confidence level, it was dropped from the analysis. Hence, we simplified the model to:

$$\text{LOG}(D_H+0.01) = b_0 + b_{off} + b_1 M + b_2 \text{LOG } R + b_3 R + b_4 \text{LOG } W_H + b_5 \text{LOG } S_p + b_6 T_{15} + b_7 F_{15} + b_8 D50_{15} \quad (4.1.8)$$

After fitting Equation 4.1.8, we performed a sensitivity analysis and found that the transformation of T_{15} to $\text{LOG } T_{15}$ and the transformation of F_{15} to $\text{LOG}(100-F_{15})$ yielded predicted displacements that are more credible for small values of T_{15} and F_{15} . Thus, we modified the model to:

$$\text{LOG}(D_H+0.01) = b_0 + b_{off} + b_1 M + b_2 \text{LOG } R + b_3 R + b_4 \text{LOG } W_H + b_5 \text{LOG } S_p + b_6 \text{LOG } T_{15} + b_7 \text{LOG}(100-F_{15}) + b_8 D50_{15} \quad (4.1.9)$$

A least squares fit of Equation 4.1.9 yields the following regression coefficients: $b_0 = -15.787$, $b_{off} = -0.579$, $b_1 = 1.178$, $b_2 = -0.927$, $b_3 = -0.013$, $b_4 = 0.657$, $b_5 = 0.429$, $b_6 = 0.348$, $b_7 = 4.527$, $b_8 = -0.922$. All coefficients are significant at the 99.9 percent confidence level and the R^2 for Equation 4.1.9 is 82.6 percent. Figure 4-4 shows that 90 percent (421 out of 467) of the predicted displacement values, D_{Hhat} , fall between the 100 percent overprediction and 50 percent underprediction bounds. The free face component of Equation 4.1.9 is:

$$\text{LOG}(D_H+0.01) = -16.366 + 1.178 M - 0.927 \text{LOG } R - 0.013 R + 0.657 \text{LOG } W + 0.348 \text{LOG } T_{15} + 4.527 \text{LOG}(100-F_{15}) - 0.922 D50_{15} \quad (4.1.9a)$$

and the ground slope component is:

$$\begin{aligned} \text{LOG}(D_H+0.01) = & -15.787 + 1.178 M - 0.927 \text{ LOG } R - 0.013 R \\ & + 0.429 \text{ LOG } S + 0.348 \text{ LOG } T_{15} + 4.527 \text{ LOG}(100-F_{15}) - 0.922 D50_{15} \end{aligned} \quad (4.1.9b)$$

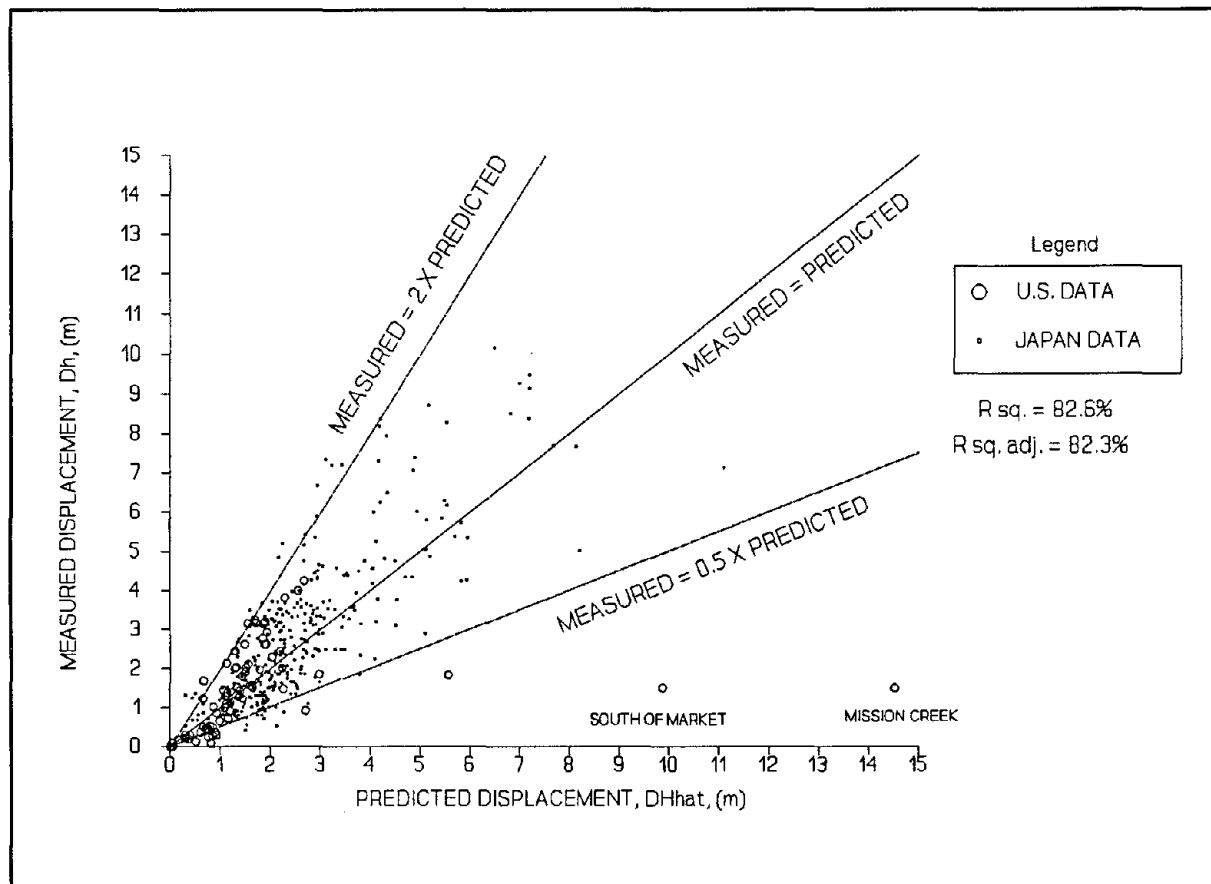


Figure 4-4 Plot of measured displacements, D_H , versus predicted displacements, D_{Hhat} , for Equation 4.1.9 using Japanese, U.S., and Ambraseys' data.

After fitting this model, we re-examined all independent variables listed in Table 3-2 for any linear trends that might greatly improve the performance of the model and found none. Thus, this is our final MLR model.

Although D_{Hhat} is an estimate of the average displacement, D_H , for a set of inputted $X(s)$, it is often desirable for engineering purposes to determine an upper bound or limit to the value of D_H that can be reasonably expected at a given site. Figure 4-4 shows that most values of D_{Hhat} predicted from the model fall below the "MEASURED = 2 X PREDICTED LINE." This suggests that if D_{Hhat} is increased by a factor of 2, then this result provides a conservative estimate of D_H that is not likely to be greatly exceeded. Also, because the relationship between D_H and the $X(s)$ may be strongly nonlinear outside the ranges of the $X(s)$ used in developing the model, extrapolation of Equation 4.1.9 may yield less reliable predictions. In short, it appears that this equation yields good results for $6.0 \leq M \leq 8.0$ earthquakes and at sites underlain by continuous layers of sands and silty sands having $N_{60S} \leq 15$; $0.075 \leq D50_{15} \leq 1.0$ mm, $0 \leq F_{15} \leq 50$ %, $1 \leq T_{15} \leq 15$ m, $Z_{BLS} \leq 20$ m, $1 \leq W \leq 20$ %, and $0.1 \leq S \leq 6$ % (See Table 3-2 for definitions of these factors and Section 5 for a discussion of their

application.) Also, because this model was developed from Japanese and western U.S. data, it is most applicable to regions having high to moderate ground motion attenuation. Extrapolation of the model beyond these conditions may be warranted in some cases, if the inputted factors are reasonably close to these ranges and the extrapolation is deemed to yield conservative results (i.e., overly-predicted estimates of D_H). This model should not be applied to metastable soils (e.g., loess deposits, sensitive clays, and collapsible silts). These metastable soils were not analyzed by this study and may produce large ground displacements, or even flow failure.

TABLE 4-1
AVERAGE SITE CONDITIONS FOR CASE STUDIES TABULATED BY EARTHQUAKE

Earthquake	LOG W_r	LOG S_p	T_{15}	F_{15}^1	$D50_{15}^1$	$N1_{60r}$
1906 San Francisco	1.2981	-0.1549	4.6	18	0.227	6.4
1964 Alaska	1.3832	-1.0969	8.9	32	0.828	9.9
1964 Niigata	0.9244	-0.3188	9.5	10	0.311	4.8
1971 San Fernando	1.1427	0.0899	3.9	50	0.076	8.0
1979 Imperial Valley	0.8244	-0.2518	2.7	27	0.106	4.3
1983 Nihonkai-Chubu	—	0.1847	2.1	1	0.350	—
1987 Superstition Hills	1.3642	—	3.0	33	0.081	4.0
mean	1.1562	-0.2580	5.0	24	0.283	6.2

¹ The combined free face and ground slope data were used to calculate the means for T_{15} , F_{15} , and $D50_{15}$.

TABLE 4-2
OBSERVATIONS FROM AMBRASEYS' STUDY USED TO ADJUST MLR MODELS

M^1	R^1	LOG W_r	LOG S_p	T_{15}^2	F_{15}^2	$D50_{15}^2$	$N1_{60r}$
7.8	80	1.1562	—	5.0	24	0.283	6.2
7.5	77	—	-0.2580	5.0	24	0.283	—
6.5	28	1.1562	—	5.0	24	0.283	6.2
6.4	15	—	-0.2580	5.0	24	0.283	—
7.4	80	1.1562	—	5.0	24	0.283	6.2
6.6	18	—	-0.2580	5.0	24	0.283	—
7.6	92	1.1562	—	5.0	24	0.283	6.2
7.7	85	—	-0.2580	5.0	24	0.283	—
7.5	72	—	-0.2580	5.0	24	0.283	—
6.4	17	—	-0.2580	5.0	24	0.283	—
6.6	37	—	-0.2580	5.0	24	0.283	—
6.6	21	1.1562	—	5.0	24	0.283	6.2
6.5	30	1.1562	—	5.0	24	0.283	6.2
7.5	65	—	-0.2580	5.0	24	0.283	—
6.5	32	1.1562	—	5.0	24	0.283	6.2
7.4	87	1.1562	—	5.0	24	0.283	6.2
7.5	60	—	-0.2580	5.0	24	0.283	—
7.8	85	—	-0.2580	5.0	24	0.283	—
7.6	95	1.1562	—	5.0	24	0.283	6.2

¹ M and $LOG R$ values are from Ambraseys' case studies and values for $LOG W_r$, $LOG S_p$, T_{15} , F_{15} , $D50_{15}$, and $N1_{60}$ are averages from our MLR database (see Table 4-1).

² The same averages for T_{15} , F_{15} , and $D50_{15}$ were used in both the free face and ground slope components of the regression model.

SECTION 5
APPLICATION AND LIMITATIONS OF MLR MODEL

Figures 5-1 to 5-3 are histograms of the independent variables used in developing Equation 4.1.9. These graphs provide a general guide to the range of conditions for which this equation is applicable. This section further discusses the application and limitations of the MLR model.

5.1 Ground Motion Attenuation

Equation 4.1.9 was developed mainly from stiff-soil sites in the western U.S. and from stiff soil sites in Japan that were within 30 km of the seismic source. For these regions and conditions, Equation 4.1.9 should be directly applied to predict lateral spread displacement. For other regions of the world, such as the eastern U.S. where ground motion attenuates more slowly with distance, and for other site conditions, such as liquefiable deposits over soft clay layers where ground motion may be strongly amplified (i.e. soft soil sites), a correction must be applied to Equation 4.1.9 to account for these different seismic and site conditions. The preferred method to adjust the model would be to directly regress D_H on the earthquake factors, M and A . However, because A was measured only at a few of the case history sites, the direct development of a M - A model was not possible with the limited data. We attempted to estimate A from empirical M - R relationships (Appendix 1, Section A1.1.3) and use these estimates to develop a M - A model, but this attempt yielded poorer results than models based on M , $\text{LOG } R$, and R .

Until better case histories are assembled to adequately develop M - A and A - D models, we propose the following procedure to adjust the values of R that are used into Equation 4.1.9 for other regions of the world or for soft soil sites. Figure 5-4 is a plot of A estimated for stiff soil sites in the western U.S. using attenuation relationships and soil amplification factors published by Idriss (Idriss, in press; Idriss, 1990; Equation A1.1.3.2). These accelerations should roughly represent those incurred at our case history sites, which are primarily from stiff soil sites in the western U.S. and Japanese sites found within 30 km of the seismic source. The values of A plotted on this figure were calculated for their respective values of M and R by applying a peak-acceleration attenuation equation developed by Idriss for bedrock sites and then correcting those bedrock accelerations for stiff soil conditions. To adjust the bedrock accelerations to stiff soil conditions, we multiplied the peak bedrock accelerations by a correction factor that was estimated from an acceleration amplification curve for soft soils published by Idriss (1990) (Figure 5-5). The stiff soil acceleration curve was approximated by fitting a series of points that were positioned midway between the non-amplification curve for rock (i.e., 45 degree line) and the high-amplification curve for soft soils (Figure 5-5). The procedure for using the curves shown in Figure 5-4 to correct the R inputted into Equation 4.1.9 for soft soil sites or non-western U.S. or non-Japanese sites is as follows. (1) Using standard procedures, the design earthquake magnitude, M , and peak ground acceleration, A , are determined for the candidate site. (2) That magnitude and acceleration are then plotted on Figure 5-4. (3) From that plotted point, an equivalent source distance, R_{eq} , is interpolated from the R -curves given in Figure 5-4. (4) That R_{eq} is then entered into Equation 4.1.9 instead of the actual R to calculate D_H . For example, during the 1989 Loma Prieta, California earthquake ($M_w = 6.9$), liquefaction and minor lateral spreading occurred on Treasure Island, at a distance of about 80 km from the seismic energy source. Application of that distance in Equation 4.1.9 along with appropriate site properties indicates that an insignificant amount of displacement should have occurred on the island. (This site also falls outside of Ambraseys' R_f bound, suggesting that liquefaction should have not occurred.) However, considerable ground motion amplification was measured at Treasure Island, which was constructed by placing hydraulic fill over thick deposits of soft, San Francisco Bay mud.

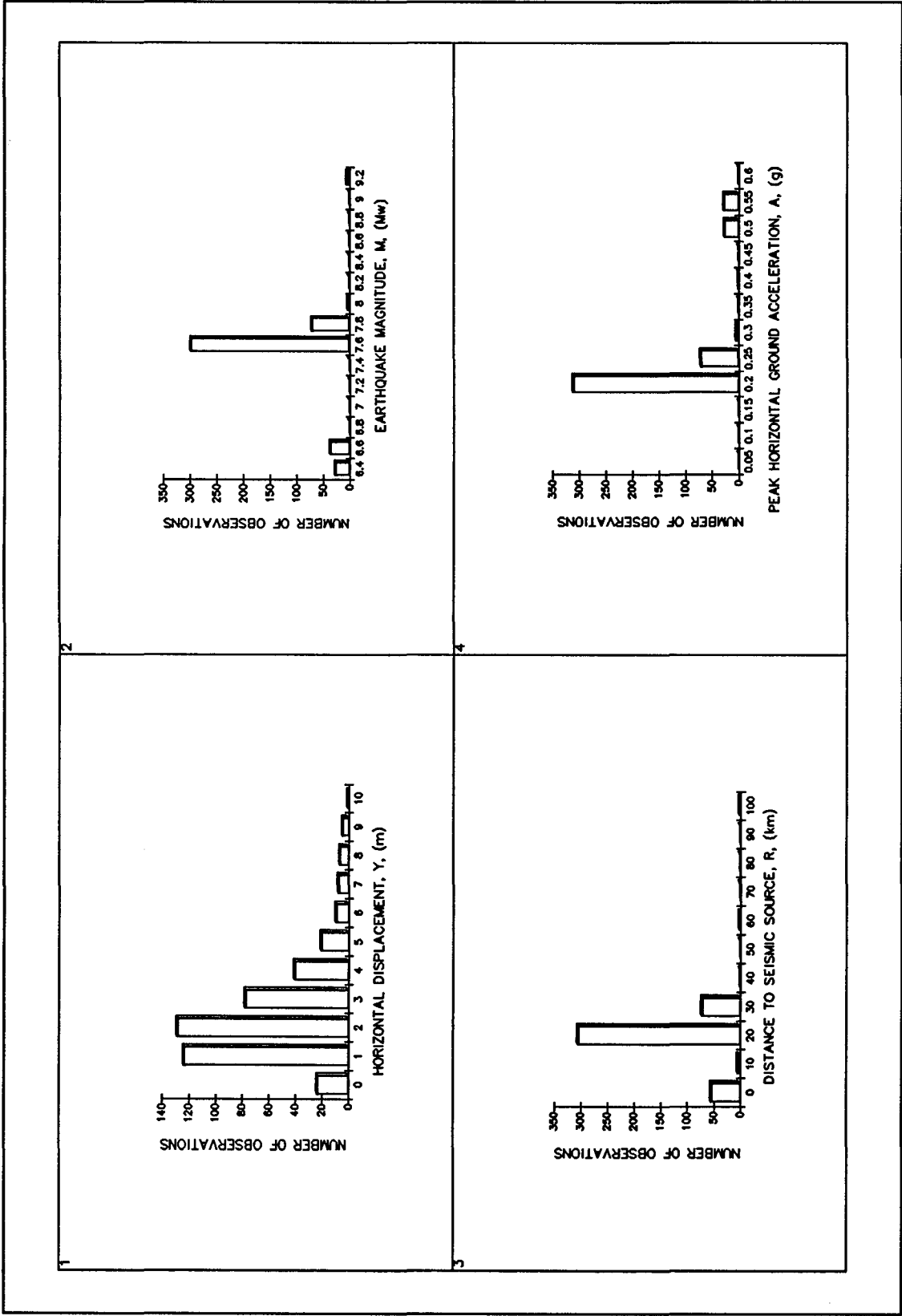


Figure 5-1 Histograms for (1) displacement, D_H , (2) magnitude, M , (3) distance to seismic source, R , (4) peak ground acceleration, A .

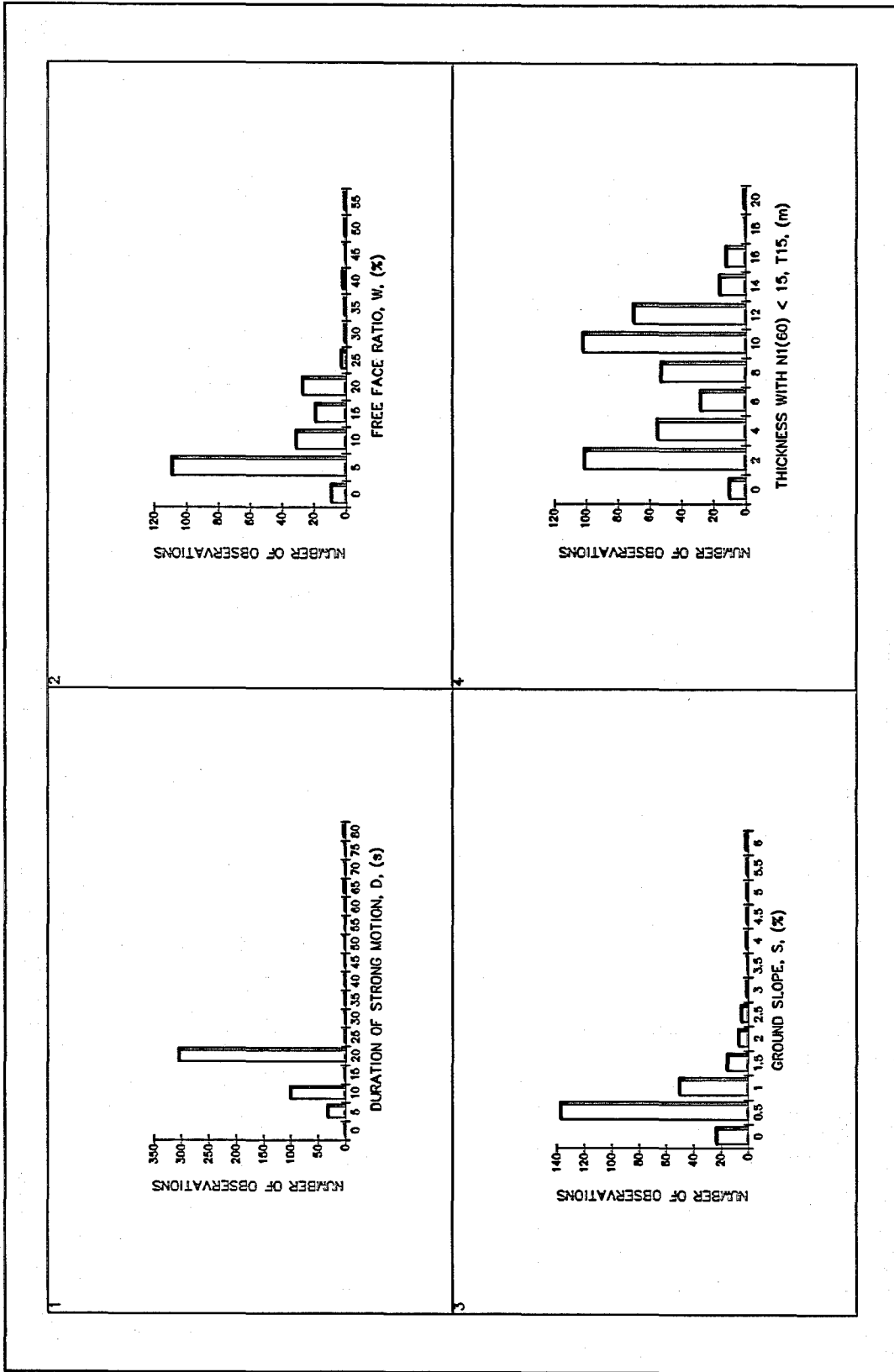


Figure 5-2 Histograms for (1) duration, D, (2) free face ratio, W, (3) ground slope, S, and, (4) thickness with $(NI)_{60} < 15$, T_{15} .

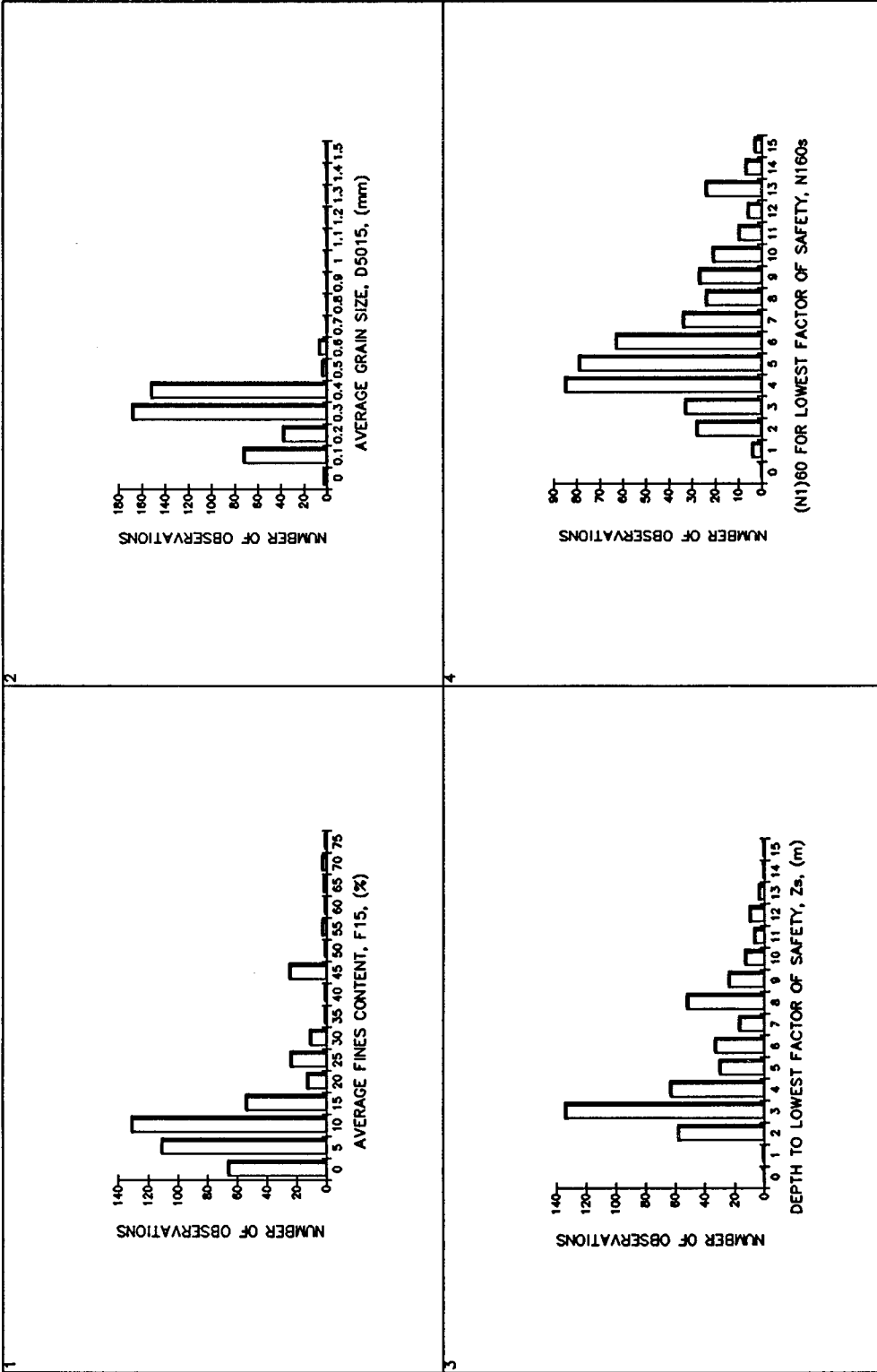


Figure 5-3 Histograms for (1) fines content, F_{15} , (2) mean grain size, D_{50gr} , (3) depth to low FS, Z_s , (4) lowest M_{160s} .

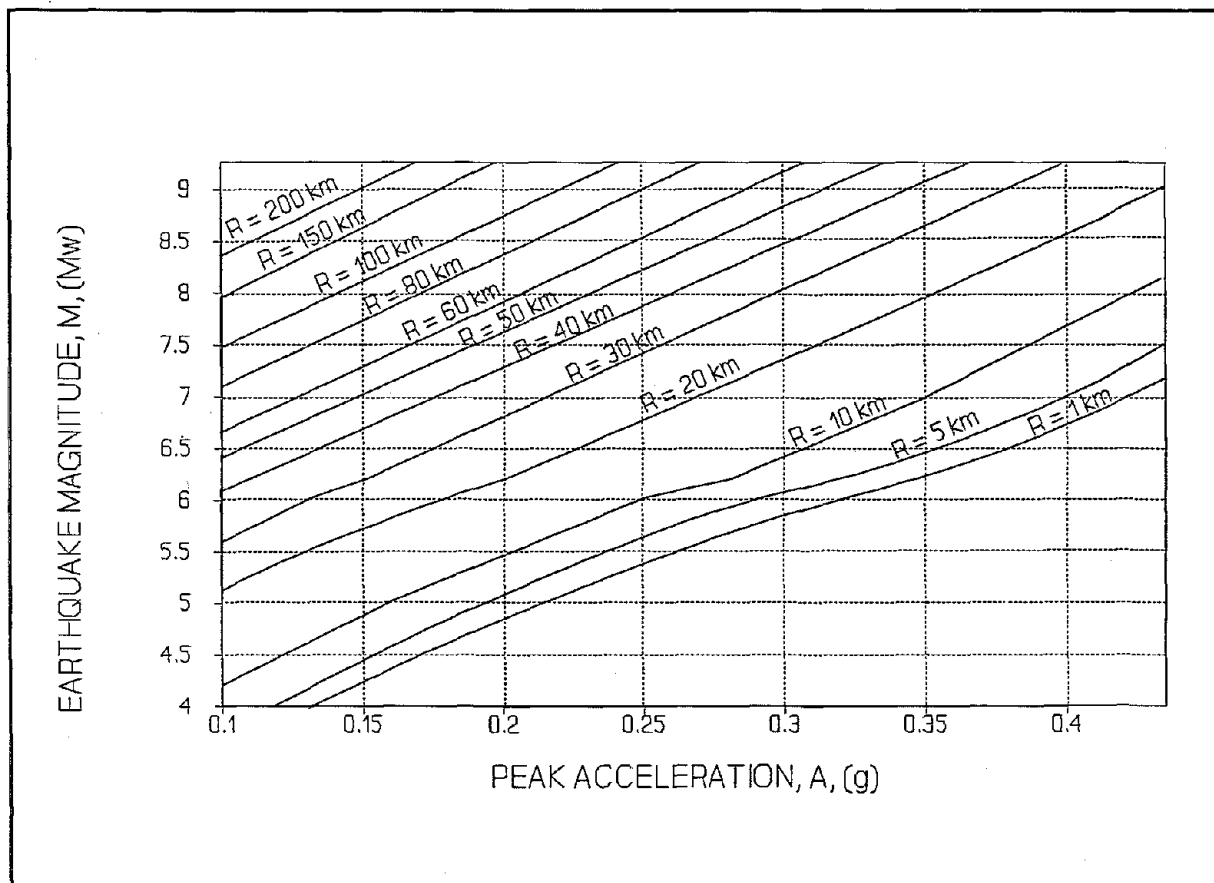


Figure 5-4 Graph for Determining Equivalent Source Distance, R_{eq} , from Magnitude and Peak Acceleration.

Although maximum bedrock accelerations measured just a few hundred meters away on nearby Yerba Buena Island were roughly 0.07 g, and accelerations measured on nearby stiff soil sites were generally about 0.10 g, the instrumented value of A on Treasure Island was 0.16 g. Thus, this measured A was more than twice the bedrock acceleration and was also significantly higher than that expected for stiff soil sites at that distance. However, if $M = 6.9$ and $A = 0.16$ is plotted on Figure 5-4, the resulting R_{eq} is about 50 km (compared to the actual source distance of 80 km). Entering a R_{eq} of 50 km into Equation 4.1.9 with the appropriate soil properties predicts that a few tenths of a meter of lateral spread displacement should occur near the free face edges of the island. This prediction roughly corresponds with that measured on Treasure Island after the earthquake.

5.2 Earthquake Magnitude

The bulk of our data are from $6 \leq M \leq 8$ earthquakes and extrapolation of Equation 4.1.9 beyond this range increases the uncertainty in the predicted displacements (Figure 5-1). However, because lateral spread displacement appears to decrease markedly for $M < 6$ earthquakes, extrapolation of Equation 4.1.9 to $M < 6$ earthquakes appears to yield predicted displacements, which with conservative allowance for the greater uncertainty, appear to be usable for engineering analyses. Extrapolation of the equation to earthquakes with $M > 8$ also appears to give reasonable predictions for fine to coarse grain sands and silty sands based on the limited data available from extremely large earthquakes. (Seven

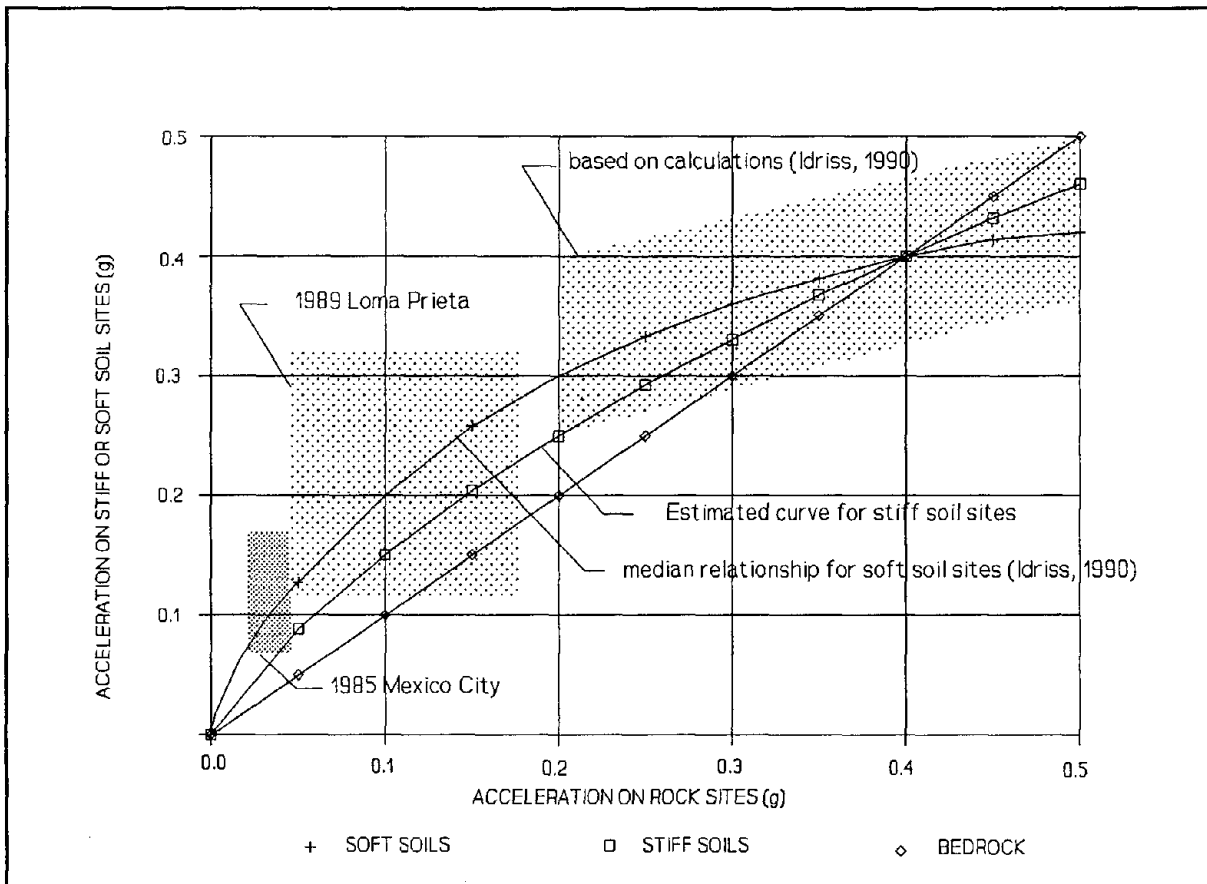


Figure 5-5 Approximate Curve for Estimating A for Stiff Soil Sites (Modified from Idriss, 1990).

observations from the 1964 Alaska earthquake ($M = 9.2$) were fitted and an examination of the $e_r(s)$ for these data shows no unusual residual behavior (see $e_r(s)$ versus M plot in Appendix 2 for Equation 4.1.9.) Nonetheless, the addition of more case studies for $M > 8$ earthquakes would strengthen the MLR database and improve its reliability for extremely large events.

5.3 Distance to the Fault Rupture or Zone of Seismic Energy Release

Equation 4.1.9 appears to attenuate D_H with increasing R in a manner that is consistent with our case history data and with Ambraseys' R_f bound. On the other hand, if the inputted R is allowed to decrease to a distance that is approaching zero, the predicted displacements from Equation 4.1.9 can become quite large, especially for $M > 7.5$. Based on a sensitivity analysis, in which we allowed M to vary from 6.5 to 9.5 and using the average site conditions given in Table 4-1, we noted that $D_{I_{hat}}$ becomes unreasonably large (e.g., larger than 5 to 10 m) when the inputted R is allowed to decrease below the values listed in Table 5-1. Because Equation 4.1.9 appears to yield predicted displacements that are larger than those normally expected for lateral spread and because only a few case histories are available for lateral spreads located very near the seismic source, extrapolation of Equation 4.1.9 to distances less than those listed in Table 5-1 may yield unreliable estimates of D_H .

TABLE 5-1
MINIMUM VALUES OF R FOR VARIOUS EARTHQUAKE MAGNITUDES

M	R (km)
6.5	0.25
7.0	1
7.5	5
8.0	10
8.5	25
9.0	50

5.4 Free Face Ratio and Ground Slope

Most of the free face failures analyzed by this study are for $W \leq 20$ percent and caution should be used when extrapolating the MLR model beyond this value. However, some extrapolation may be warranted at sites where the liquefiable sediments are not deemed to be prone to slumping or flow failure. For example, an important problem for engineers is the estimation of the potential lateral spread displacement near bridge crossings where W typically exceeds 20 percent. In this study, six observations having $20 < W \leq 55$ percent were fitted and Equation 4.1.9a appears to yield credible predictions for this range. Nonetheless, field observations of free face failures along river channels reveals that the displacement may have a significant vertical component due to rotation of slump blocks. Also, gravitational shear forces near the free face may be large enough to induce flow failure in highly susceptible soils. If slumping or flow failure is a potential concern, Equation 4.1.9 is not applicable and more sophisticated 2-D models, such as dynamic, finite-element analyses should be used (Prevost, 1981; Finn and Yogendrakumar, 1989).

In formulating Equation 4.1.9a, we attempted a MLR model that included both W and S as topographical factors, but our analyses suggested that the inclusion of S does not significantly improve the performance of the free face model. Thus, we concluded that the slope of the river banks, either into or away from the channel, does not vary enough to have markedly affect displacement when compared with the influence exerted by W . However, most of the free face failures in our database had values of $S < 0.5$ percent. If additional conservatism is desired at sites where $S > 0.5$ percent, the results from the ground slope component, (i.e., Equation 4.1.9b) could be added to the results of the free face component, (i.e., Equation 4.1.9a); but in most cases, we do not believe that this degree of conservatism is required.

In applying Equation 4.1.9 to sites which are farther removed from the free face, questions may arise about whether to apply Equation 4.1.9a or Equation 4.1.9b. In highly liquefiable sediments, like those found in Niigata, movement of the river banks towards the channel initiated at a maximum distance of 100 times the height of the channel (i.e., $100 H$). Thus, in highly susceptible soils, the free face appears to influence D_H for values of $W \geq 1$ percent. (Note that $100 H$ is equal to a W value of 1 percent). However, we do not recommend the exclusive use of the Equation 4.1.9a at all sites with $W \geq 1$ percent. Figure 3-4 shows that at some places in Niigata, free face failure was not initiated until W was about 5 percent. Thus, for sites with $1 \leq W \leq 5$ percent, it is possible that D_H may be also influenced by S , and the ground slope model may be just as applicable as the free face model. For ambiguous cases, we suggest estimating D_H from both Equation 4.1.9a and 4.1.9b and applying the larger value for design purposes. As previously mentioned, if the designer believes that both the free face and ground slope will contribute to produce displacement, then both components of Equation 4.1.9 could be added to produce a conservative estimate of D_H .

For the ground slope failures evaluated herein, S ranged from about 0.1 percent to 6 percent. Extrapolation of Equation 4.1.9b beyond this range may lead to uncertain predictions. For $S < 0.1$ percent, chaotic displacements due to ground oscillation are likely to exceed those from lateral spreading and Equation 4.1.9b may give uncertain estimates of D_H for flat ground conditions. Also, ground slopes that exceed 6 percent may cause flow failure in highly susceptible soils and consequently produce large displacements. Equation 4.1.9b is not valid for estimating D_H for such conditions.

5.5 Gravelly Soils

During preliminary analyses, we noted that our MLR models performed poorly at predicting lateral spread displacements measured at gravelly sites from the 1964 Alaska and 1983 Borah Peak, Idaho earthquakes. Due to the high number of outliers for gravelly sites, it appears that gravel has a different displacement behavior than sand and silty sand. For example, Figure 5-6 shows the $e_i(s)$ plotted against $D50_{15}$ for one of our preliminary MLR models. Four of 6 observations with $D50_{15}$ values > 2 mm are potential outliers. These outliers are from alluvial gravels that underwent lateral spread at Whiskey Spring and Pence Ranch during the 1983 Borah Peak, Idaho, earthquake (Andrus and Youd, 1987).

Because our data contains only a few examples of lateral spread at gravelly sites, we did not have an adequate number of observations to properly fit the displacement behavior of gravelly sediments. Thus, we removed observations with $D50_{15} > 2$ mm from the MLR database prior to fitting Equation 4.1.9. (Case histories at Whiskey Springs, Idaho; Pence Ranch, Idaho; and some gravelly sites in Alaska were removed). Figure 5-6 also shows that there are very few observations for $1 < D50_{15} \leq 2$ mm. Consequently, for verified predictions, we restrict the use of Equation 4.1.9 to saturated cohesionless sediments with $D50_{15}$ values ≤ 1 mm.

5.6 Fines Content and Layered Profiles

In addition to $D50_{15}$, there are limits on the range of the average fines content, F_{15} , for which Equation 4.1.9 has been verified. Figure 5-3 shows that most of F_{15} values in the MLR database are from soils with F_{15} values ≤ 50 percent; thus, we limit the use of Equation 4.1.9 to this range. Also, because F_{15} is strongly correlated with $D50_{15}$, there are limits on the allowable range for the combination of these factors. Figure 5-7 is a plot of F_{15} versus $D50_{15}$ for the 267 boreholes included in this study. This plot shows the envelope of F_{15} and $D50_{15}$ values for which Equation 4.1.9 has been verified. Extrapolation of the model to soils with textures beyond these limits introduces extra uncertainty into the predicted displacement.

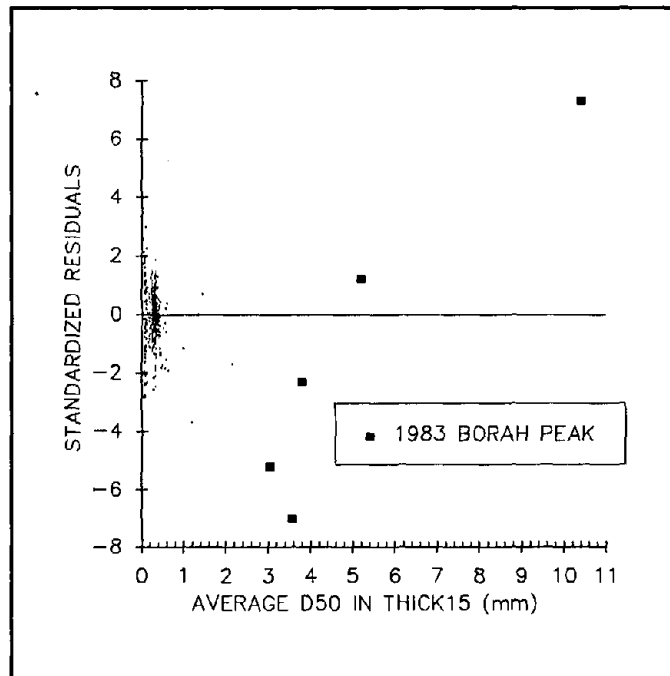


Figure 5-6 Standardized residuals, $e_i(s)$, plotted against the average mean grain size, $D50_{15}$, in T_{15} , showing outliers in gravelly soils.

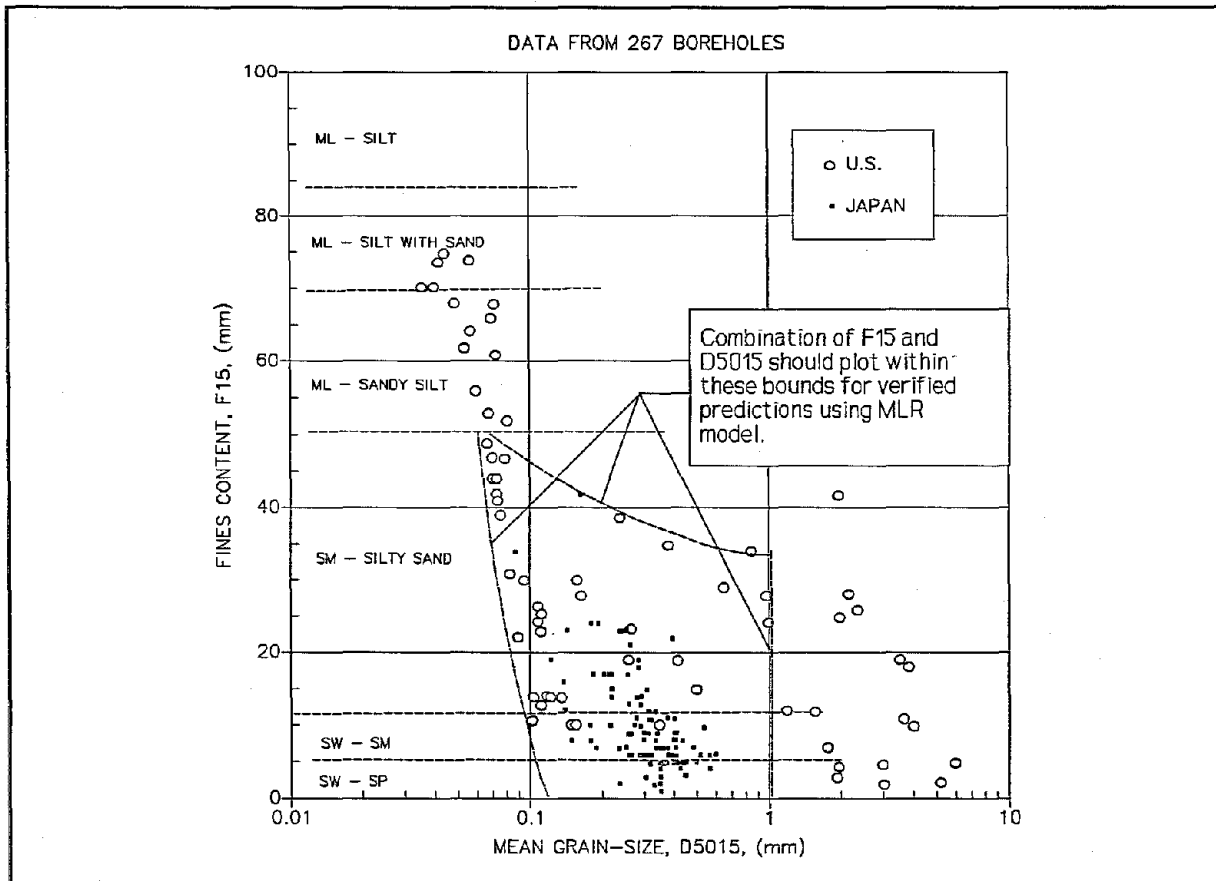


Figure 5-7 Plot of ranges of F₁₅ versus D_{50,15} for which Equation 4.1.9 has been verified (data from 267 boreholes).

Equation 4.1.9 suggests that fines content has a major influence on lateral spread displacement. All other factors remaining constant, predicted displacements diminish rapidly with increasing fines content. For example, lateral spread at Juvenile Hall during the 1971 San Fernando Valley, California earthquake illustrates the marked affect that the inputted fines content has on predicted values of displacement. Lateral spread at Juvenile Hall ranged from 0.5 to 1.68 m and occurred on a gentle ground slope ($S = 1.2\%$) (Bennett et al., 1989; Youd, 1973b). Liquefaction appears to have occurred primarily in a sandy silt (ML) layer that is interbedded with thinner, silty sand (SM) layers. The T_{15} layer at Juvenile Hall has an average fines content of about 59 percent and an average mean grain size of 0.06 mm. Equation 4.1.9 predicts a maximum displacement of about 0.7 m for Juvenile Hall, which underestimates the maximum observed value by a factor slightly greater than 2 (Figure 5-8). However, further examination of the borehole data and watertable elevations taken soon after the earthquake suggests that a relatively thin, continuous silty sand (SM) layer may have liquefied just below the watertable. If this SM layer is analyzed separately, and not averaged with the thicker, underlying ML layer, the inputted factors are: $T_{15} = 0.6$ m, $F_{15} = 41\%$, $D_{50,15} = 0.131$ mm and Equation 4.1.9b predicts an average displacement of about 1.8 m for this soil, which is in good agreement with the observed displacement. Thus, in analyzing a layered system with two potentially liquefiable layers that have distinctly different textures, averaging F_{15} and $D_{50,15}$ throughout the entire T_{15} layer may produce smaller predicted displacements than if the individual layers are analyzed separately. This is especially true if the thickest layer has a high fines content. Hence, for

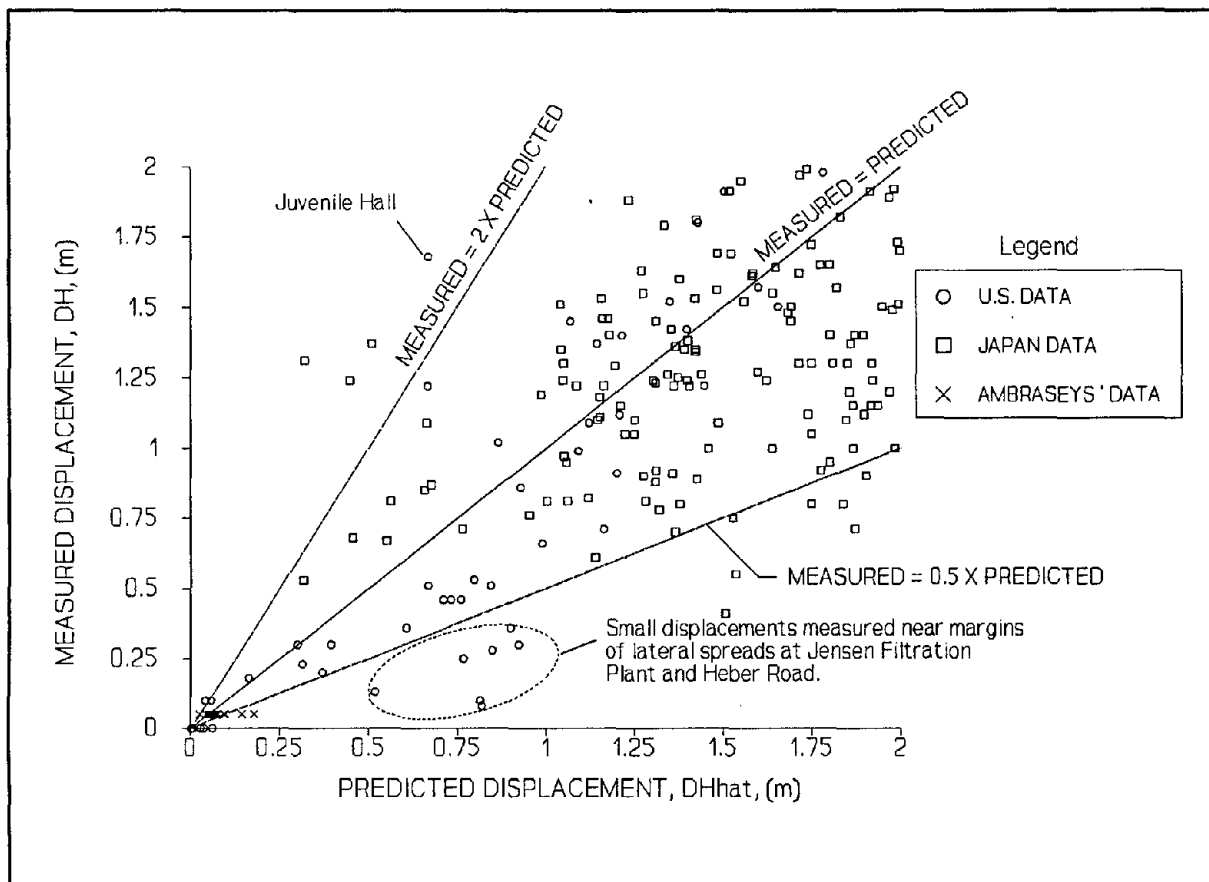


Figure 5-8 Plot of measured displacements versus displacements predicted by Equation 4.1.9 for displacements that are less than 2 meters.

conservative design in layered profiles, we recommend that distinctly different T_{15} layers be analyzed separately by calculating T_{15} , F_{15} , and $D50_{15}$ for each distinct soil type. The total predicted displacement may then be conservatively estimated as the sum of the displacements predicted for the individual layers. However, to divide the profile into individual layers, there must be a distinct textural difference between the layers.

Also, Figure 5-8 shows that a small number of Japanese observations are underpredicted by a factor greater than 2. The poorer quality of the subsurface data available for these observation or errors in the measured displacements at these locales (Section 3.2) may be the reason for the slight underprediction of these smaller displacements.

5.7 Soils with $(N1)_{60}$ Values Greater than 15

In almost all cases reviewed herein, significant ground displacement was restricted to saturated cohesionless soils having $(N1)_{60}$ values ≤ 15 . This finding does not appear to be coincidental, nor does it appear to represent a deficiency in our MLR database. The case studies reviewed herein do include boreholes where all $(N1)_{60}$ values in the profile exceed 15 (e.g., boreholes from Juvenile Hall, Heber Road, Niigata, and Noshiro, Japan), but these boreholes were generally located near the margins of the lateral spreads where no appreciable amount of displacement was reported. Thus, in general, cohesionless materials with $(N1)_{60}$ values > 15 appear to be resistant to lateral spread displacement for

M < 8 earthquakes and we limit the application of Equation 4.1.9 to saturated, cohesionless soils having $(N1)_{60}$ values ≤ 15 .

However, it is possible during the 1964 Alaska earthquake that fluvial deposits with $(N1)_{60}$ values > 15 underwent lateral spread. During this extremely large and long-lived earthquake (M = 9.2), gravelly, channel deposits ($15 \leq (N1)_{60} \leq 20$) displaced a maximum of 1 m at the Resurrection River and Placer Rivers (Bartlett and Youd, 1992). However, the quality of the subsurface data for these Alaskan sites is poor. The penetration tests at the Resurrection River were performed with a non-standard hammer and have questionable validity. Also, N values recorded in gravelly soils generally tend to be higher when compared with finer grained sediments of comparable relative densities. Thus, we found no conclusive evidence of significant displacement in sediments with $(N1)_{60}$ values > 15 for M > 8 earthquakes.

5.8 Thickness and Depth of the Liquefiable Layer

Prior to applying Equation 4.1.9, however, standard liquefaction analyses (Seed and Idriss, 1971; Seed et al., 1983; 1985; NRC, 1985) should be performed to verify that liquefaction is expected in the layer for the inputted earthquake factors (Figure 5-9). Based on the compiled case history data, it appears that lateral spread occurs in relatively thick, T_{15} layers (T_{15} values for our database average 5.5 m (Table 4-1)). In general, T_{15} is thicker than 1 m at locales that underwent a significant amount of lateral spread. In a few instances, however, small displacements occurred along the margins of some lateral spreads where the thickness of the T_{15} layer appears to be less than 1 m. Thus, for conservative design, we suggest that continuous, T_{15} layers having a thickness less than 1 m be considered as potential candidates for lateral spread. However, because our MLR database contains only a few cases of $T_{15} < 1$ m, Equation 4.1.9 may yield less reliable results for these conditions. Equation 4.1.9 should not be applied at sites having thin, noncontinuous, T_{15} layers. The researched database is deficient for such conditions.

Our liquefaction analyses also suggest that the depth to the top of the liquefied layer, Z_{T15} , is usually found within the upper 10 m of the profile and that the depth to the bottom of the liquefied layer, Z_{B15} , is usually found within the upper 20 m of profile at sites that underwent a significant amount of lateral spread. These same analyses also suggest that the depth to the lowest factor of safety against liquefaction, Z_s , generally occurs in the upper 15 m of the profile.

5.9 Residual Strength and SPT N Measures

Many analytical and numerical models use residual strength as a key input parameter for estimating liquefaction-induced ground displacement. Seed et al. (1988) have proposed an empirical curve relating residual strength with SPT $(N1)_{60}$ values. In this study, we also postulated that lateral spread is a function of residual strength and devised several SPT N and $(N1)_{60}$ variables to represent residual strength in our preliminary MLR models. We tested models that included the lowest N, lowest $(N1)_{60}$, average N, and average $(N1)_{60}$ values in the liquefied profile. Of these measures, $N1_{60s}$ (defined in Table 3-2) yielded the best results when included in the free face model developed for Niigata and Noshiro, Japan. (R^2 values for the models increased from 2 to 9 percent depending upon which other independent variables were present.) However, as the U.S. data were added to the analyses, $N1_{60s}$ made only a slight contribution to improving R^2 (R^2 increased only 0.1 percent when $N1_{60s}$ was present in the final model). Thus, this variable was dropped from the final model.

Given that lateral displacement is correlated with residual strength and that residual strength is a function of the lowest and average SPT N and $(N1)_{60}$ values in the liquefied profile, we offer the following explanations to why our SPT N

and $(N1)_{60}$ variables appear to be only modestly correlated with displacement. First, there probably is a certain amount of variability in the SPT N and $(N1)_{60}$ values tabulated in our MLR database due to the different types of hammers that were employed at the various case history sites. Second, perhaps the lowest and average N and $(N1)_{60}$ values in the MLR database do not vary enough to show a strong correlation with displacement. Tabulated values of $N1_{60s}$ range from 1.3 to 14.7, and have a mean of 6.1 (Figure 5-3). Approximately 75 percent of the compiled $N1_{60s}$ values are ≤ 8 , and 90 percent are ≤ 10 . Third, and most importantly, it appears that residual strength, and ground displacement are not solely a function of the lowest or average N and $(N1)_{60}$ values in the liquefied profile, but are strongly influenced by other subsurface and soil factors, such as the fines content, thickness, and mean-grain size of the liquefied layer. This study indicates that F_{15} , T_{15} , and $D50_{15}$ are strongly to moderately correlated with displacement. Also, T_{15} correlates reasonably well with $N1_{60s}$ ($R = -0.59$) suggesting that thick, T_{15} layers tend to have lower $N1_{60s}$ values. Hence, we suggest that relatively thick, clean, fine-grained, T_{15} layers appear to produce lower residual strengths and are consequently subjected to a larger amount of ground displacement.

5.10 Boundary Effects

Because the regression coefficients for Equation 4.1.9 are heavily dependent upon Japanese case studies, where liquefaction was widespread and lateral boundary effects were relatively minor, our model may overpredict ground displacements occurring near the margins of smaller lateral spreads. Figure 5-8 shows that a few of the U.S. and Japan observations are overpredicted by a factor greater than 2. Overpredicted observations at the Jensen Filtration Plant and Heber Road were measured at the head or along the side margins of the lateral spreads where ground was apparently inhibited by the nearby lateral boundary. We suspect that changes in the subsurface geology played a large role in limiting liquefaction and ground displacement at these locales. Also, errors the estimates of D_H for these smaller displacements may have contributed to the underpredictions (Section 3.2).

Equation 4.1.9 also significantly overestimates ground displacement measured at Mission Creek and the South of Market Zone following the 1906 San Francisco earthquake (Figure 4-4). At these sites approximately 1.5 m of lateral spread occurred on gentle slopes of 0.6 to 0.8 percent, respectively (Youd and Hoose, 1978; O'Rourke et al., 1991). Equation 4.1.9 predicts approximately 7.5 m of displacement for the South of Market Zone and 12 m for the Mission Creek Zone. We believe that this overestimation is largely due to: (1) the poor quality of available subsurface data at these two sites, and (2) local boundary effects. The penetration tests at Mission Creek and South of Market were performed with a non-standard hammer and no grain-size distribution data are available (O'Rourke et al., 1991). We converted the non-standard penetration resistances to SPT N values and used estimated soil properties for our liquefaction analyses, but these estimates are suspect. Also, ground displacement at these sites were inhibited by lateral boundary effects. The ground failure at Mission Creek formed in a narrow, sinuous, old, creek channel which caused the lateral spread to change directions at several junctures along its path (O'Rourke et al., 1991). These directional changes undoubtedly impeded the ground displacement.

5.11 Flow Chart for the Application of Equation 4.1.9

Figure 5-9 summarizes the suggested procedure for applying the MLR model. In summary, Equation 4.1.9 yields the best results for $6.0 \leq M \leq 8.0$ earthquakes and at sites underlain by continuous layers of sands and silty sands having $N1_{60s} \leq 15$; $0.075 \leq D50_{15} \leq 1.0$ mm, $0 \leq F_{15} \leq 50$ %, $1 \leq T_{15} \leq 15$ m, $1 \leq W \leq 20$ %, and $0.1 \leq S \leq 6$ %. Also, the depth to the bottom of the liquefied layer, Z_{BLS} , should be found within the upper 20 m of the profile. In addition, because this model was developed from western U.S. and Japanese sites founded primarily on stiff soils,

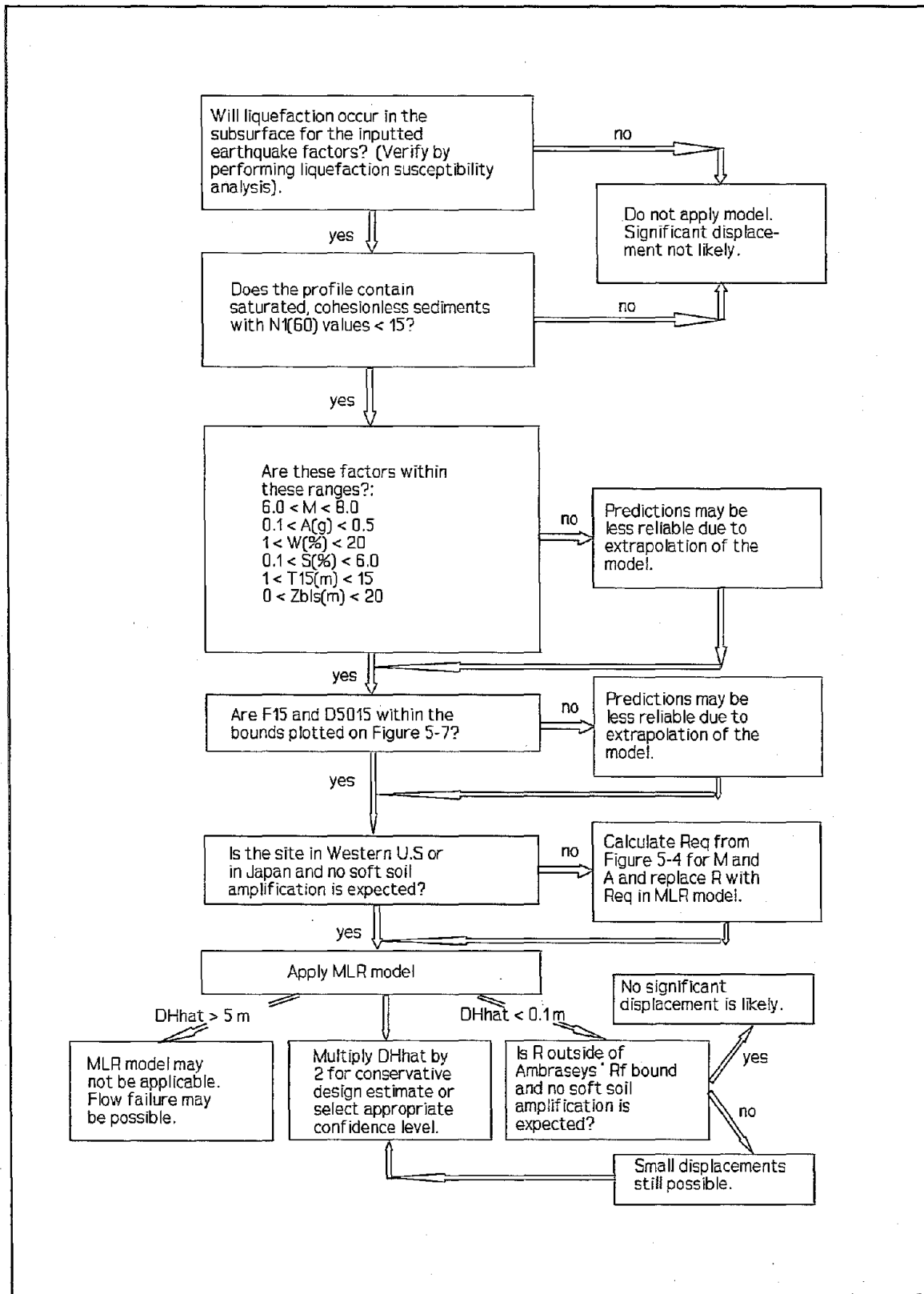


Figure 5-9 Flow chart for the application of Equation 4.1.9

it is most applicable to these soil conditions and to seismic regions having high to moderate ground motion attenuation. However, Figure 5-4 may be used to adjust the value of R used in the model so that it can be applied to other regions with different seismic attenuation or to sites where significant soft soil amplification is expected.

5.12 Calculation of the Upper Prediction Limit for Displacement

Although D_{Hhat} is an estimate of the mean displacement for a given set of $X(s)$, it is often desirable to determine an upper bound or limit to the amount of displacement that can be reasonably expected at a given site. Figure 4-4 shows that almost all values of D_{Hhat} calculated from Equation 4.1.9 fall below the "MEASURED = 2 X PREDICTED LINE." This suggests that if D_{Hhat} is multiplied by a factor of 2, then that result will provide a conservative estimate of D_H that is not likely to be exceeded. However, MLR models offer a more rigorous, probabilistic approach to calculating the upper prediction limit or bound for the true response. For example, a 90 percent prediction limit forms the bound where it is expected that 90 percent of the observed displacements will be less than the bound and 10 percent will exceed the bound. The predicted value,

$$D_{Hhat} = b_0 + b_1 X_1 + \dots + b_p X_p, \quad (5.12.1)$$

is a best-fit estimate of

$$E(D_H) = B_0 + B_1 X_1 + \dots + B_p X_p \quad (5.12.2)$$

where:

$E(D_H)$ is the mean or expected value of D_H .

The variance of D_{Hhat} , i.e., $V(D_{Hhat})$, is calculated from:

$$V(b_0) + X_{12} V(b_1) + \dots + X_p^2 V(b_p) + 2X_1 \text{ covar}(b_0, b_1) + \dots + 2X_{p-1} X_p \text{ covar}(b_{p-1}, b_p) \quad (5.12.3)$$

where: "covar" is the covariance.

This expression is solved in matrix notation as follows (Draper and Smith, 1981):

$$V(D_{Hhat}) = \sigma^2 (X_0' C X_0) \quad (5.12.4)$$

where:

σ = standard deviation of D_H and is estimated by the standard deviation of the regression model, s . The s for Equation 4.1.9 is 0.207 (i.e., $s = (\text{MS error})^{1/2}$ from the Analysis of Variance Table for Equation 4.1.9, see Appendix 2).

The matrix, X_0 , contains the site-specific values of the $X(s)$ used to calculate D_{Hhat} :

$$X_0' = [1, X_1, \dots, X_p] \quad (5.12.5)$$

and the C matrix is the variance-covariance matrix:

$$\begin{matrix} C_{00} & C_{01} & \dots & C_{0p} \\ C_{10} & C_{11} & \dots & C_{1p} \\ \dots & \dots & \dots & \dots \\ C_{p0} & C_{p1} & \dots & C_{pp} \end{matrix} \quad (5.12.6)$$

The C matrix is calculated from the matrix operation:

$$(X'X)^{-1} \quad (5.12.7)$$

where:

X is the matrix comprised of the set of $X(s)$ used in fitting the regression model.

The C matrix for Equation 4.1.9 has been tabulated in the file C.DAT on the computer disk labelled Appendix 3 which is available from NCEER.

The $1-\alpha$ upper prediction limit for the true displacement is given by (Draper and Smith, 1981):

$$D_{Hhat} + t_{(n-p-1, 1-\alpha)} * s * (1 + X_0' * C * X_0)^{1/2}. \quad (5.12.8)$$

where:

α is selected by the evaluator and is called the significance level.

For example to calculate the 90 percent upper prediction limit for the true displacement, then $1-\alpha$ equals 0.90 and α equals 0.10. The critical t -value for the selected $1-\alpha$ value is determined from the t distribution for $n-p-1$ degrees of freedom (Table 5-2). Equation 4.1.9 has 457 degrees of freedom, ($n = 467$, $p = 10$). Because t -values are not usually tabulated for 457 degrees of freedom, the critical t -values corresponding to 400 degrees of freedom have been listed in Table 5-2. (The use of t_{400} critical values has very little impact on the final answer because t_{457} is closely approximated by t_{400} .)

As an example of the application of Equation 4.1.9 and Equation 5.12.8, we will calculate the 90 percent upper prediction limit for true value of D_H at borehole 5-42, in Niigata (see Figure 3-2). Because this is a ground slope failure, we will apply Equation 4.1.9b and the following values of the $X(s)$ to form the X_0 matrix: (1, 0, $M = 7.5$, $\text{LOG } R = 1.32$, $R = 21$, $\text{LOG } W_{\pi} = 0$, $\text{LOG } S_p = -0.699$, $\text{LOG } T_{15} = 0.477$, $\text{LOG}(100-F_{15}) = 1.978$, $D50_{15} = 0.433$). The predicted value for $\text{LOG}(D_H + 0.01)$ from Equation 4.1.9 is -0.03275 and:

$$D_{Hhat} = 10^{-0.03275} - 0.01 = 0.917 \text{ m}. \quad (5.12.9)$$

To calculate the 90 percent upper predict limit for D_H , we first form the X_0' matrix:

$$X_0' = [1, 0, 7.5, 1.32, 21, 0, -0.699, 0.477, 1.978, 0.433] \quad (5.12.10)$$

The first two elements in this matrix, $\{1, 0\}$, are called dummy variables (Draper and Smith, 1981). The first element, $\{1\}$, indicates that b_0 applies to the ground slope component of the model, and the second element, $\{0\}$, indicates that $b_{0\pi}$ does not apply. Next, we perform the matrix operation $X_0' C X_0$:

$$X_0' C X_0 = 0.0213. \quad (5.12.11)$$

The 90 percent upper prediction limit is calculated from equation 5.12.8:

$$\text{LOG}(D_{H90}) = -0.03275 + 1.284 * 0.207 * (1+0.0213)^{1/2} = 0.236 \quad (5.12.12)$$

or

$$D_{H90} = 10^{0.236} - 0.01 = 1.712 \text{ m}. \quad (5.12.13)$$

Thus, we conclude that we are 90 percent confident (i.e., 90 percent probability) that the true value of D_H at borehole 5-42 will not exceed 1.712 m.

Similarly, we can calculate the 90 percent upper prediction limit for true value of D_H at borehole G10-39 (Figure 3-2). Because this is a free face failure, we apply Equation 4.1.9a and the following values of $X(s)$ to form the X_0 matrix: (1, 1, $M = 7.5$, $\text{LOG } R = 1.32$, $R = 21$, $\text{LOG } W_{\pi} = 0.477$, $\text{LOG } S_p = 0$, $\text{LOG } T_{15} = 1.114$,

$\text{LOG}(100-F_{15}) = 1.982$, $D50_{15} = 0.400$. The predicted value of $\text{LOG}(D_H + 0.01)$ from Equation 4.1.9a is 0.27241 and:

$$D_{Hiat} = 10^{0.27241} - 0.01 = 1.862 \text{ m.} \quad (5.12.14)$$

The X_0' matrix is:

$$X_0' = [1, 1, 7.5, 1.32, 21, 0.477, 0, 1.114, 1.982, 0.400] \quad (5.12.15)$$

The dummy variables for the first two elements in this matrix, {1,1}, indicates that both b_0 and $b0_H$ apply to the free face component of the model. The value of $X_0'CX_0$ equals 0.0151, and the 90 percent upper prediction limit is:

$$\text{LOG}(D_{H90}) = 0.27241 + 1.284 * 0.207 * (1+0.0151)^{1/2} = 0.540 \quad (5.12.16)$$

or

$$D_{H90} = 10^{0.540} - 0.01 = 3.459 \text{ m.} \quad (5.12.17)$$

Thus, we are 90 percent confident that the true value of D_H at borehole 5-42 will not exceed 3.459 m.

Other upper prediction limits, besides the 90% upper prediction limit used in the above example, can be calculated by simply selecting the desired confidence level from Table 5-2 and using that value in Equation 5.12.8 for $t_{(n-p-1), 1-\alpha}$.

TABLE 5-2
CRITICAL t VALUES FOR CONFIDENCE LIMITS
(based on 400 degrees of freedom, after Ostle and Malone, 1988)

Confidence level (1- α) in percent						
<u>75%</u>	<u>80%</u>	<u>85%</u>	<u>90%</u>	<u>95%</u>	<u>97.5%</u>	<u>99.5%</u>
0.676	0.843	1.038	1.284	1.649	1.966	2.588

5.13 Comparison of Equation 4.1.9 with Other Empirical Models

We applied the LSI model proposed by Youd and Perkins (1987) and the slope-thickness model of Hamada et al. (1986) to our compiled data and compared the performance of these models with Equation 4.1.9 (Figure 5-10). The LSI model (Equation 2.7.1.3) conservatively bounds almost all of the U.S. data, but underestimates many of the displacement vectors measured in Niigata and Noshiro, Japan. There are a few plausible reasons for this underprediction of the Japanese data by the LSI. First, the LSI was primarily developed from U.S. case studies where subsurface conditions were generally less favorable to widespread liquefaction. Thus, the LSI does not adequately reflect the high liquefaction susceptibility of the soils found in Niigata and Noshiro, Japan. Second, the location of the seismic source for the 1964 Niigata and 1983 Nihonkai-Chubu earthquakes is not well known. Both of these subduction zone earthquakes occurred in the Japan Sea where the faulting is not well understood. We estimate that R was approximately 21 and 27 km, respectively from Niigata and Noshiro cities, based on studies of crustal warping in the Japan Sea (Mogi et al., 1964; Hwang and Hammack, 1984). However, if R was indeed closer than our estimates, then the LSI would bound much more of the Japanese data.

The thickness-slope model proposed by Hamada et al. (Equation 2.7.2.8) performs adequately for Niigata and Noshiro, Japan, but tends to overpredict many of the displacements measured at U.S. sites (Figure 5-10). The R^2 for this model is 35.1 percent and 73 percent (329 of 448) of the predicted observations fall between the upper and lower prediction bounds. (To be consistent with the techniques used by Hamada et al. in developing this model, we modified our liquefaction analysis program to calculate the thickness of the liquefied layer, H , using the liquefaction susceptibility curves outlined by the Japanese Code of Bridge Design (Section 2.7.2). We also measured θ in a manner that was consistent with the definition proposed by Hamada et al. (Figures 2-2a and 2-2b.)) There are a few possible reasons why the Japanese model tends to perform poorly at many U.S. sites. First, the earthquakes that generated lateral spread in the U.S. were significantly different from those that struck Niigata and Noshiro. Niigata and Noshiro experienced very similar earthquakes ($M = 7.5$ and 7.7 , respectively) and the seismic sources were located approximately the same distance from the two cities (approximately 21 and 27 km, respectively). In contrast, the U.S. case studies include earthquakes that range from $6.6 \leq M \leq 9.2$, and lateral spread sites that were located at varying distances from the seismic source ($0.2 \leq R \leq 100$ km). Second, the liquefied sediments in Niigata and Noshiro tend to be relatively clean compared to many U.S. sediments that are more silty. Third, our techniques of measuring H and θ may not be entirely consistent with those used by the Japanese investigators in reducing their data.

Based on the performance of Equation 4.1.9 as shown in Figure 5-10, we conclude that our attempt to formulate a more comprehensive MLR model for predicting lateral spread displacement has been successful. Because our model is derived from and adjusted for a wider range of seismic, site, and soil conditions than the previously proposed empirical models, it is more general and will yield better results if properly applied.

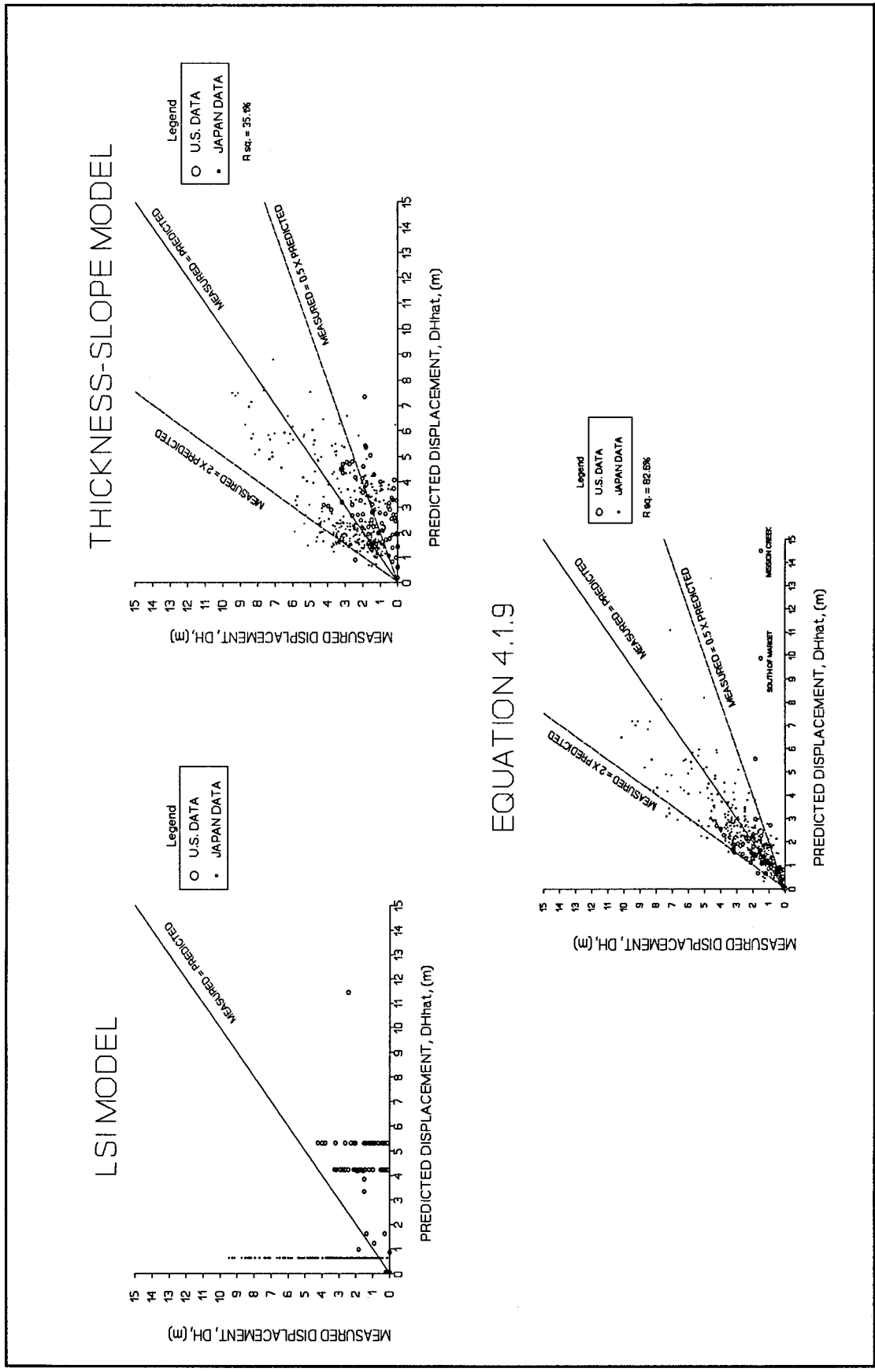


Figure 5-10 Comparison of D_h versus $D_{\hat{h}}$ for LSI model, Hamada et al. thickness-slope model, and Equation 4.1.9 showing improved performance of Equation 4.1.9.

5-18

SECTION 6 CONCLUSIONS

Considerable progress has been made since the 1964 Alaska and 1964 Niigata earthquakes in understanding liquefaction and predicting its occurrence. However, only limited progress has been made in developing practical models for estimating the liquefaction-induced, horizontal ground displacement. The thickness-slope model proposed by Hamada et al. (1986) emphasizes certain site factors, such as slope and thickness of the liquefiable layer, but it does not directly address the effects that earthquake and soil factors have on displacement. In contrast, the LSI model (Youd and Perkins, 1987) is based on earthquake factors, but it is not adjusted for the influence of topographical and soil factors. In this study, we used an extensive database derived from Japanese and U.S. lateral spread sites to formulate a more comprehensive empirical model for predicting lateral spread displacement. Because our model was developed from a wider range of seismic and site conditions than previously proposed models, it is more general and will yield better results. In summary, Equation 4.1.9 yields the best predictions and is applicable for magnitude 6 to 8 earthquakes and at sites underlain by relatively thick ($T_{15} > 1$ m), continuous, shallow ($Z_{BLS} < 20$ m) layers of liquefiable sand and silty sand ($F_{15} < 50\%$) having SPT $(N1)_{60}$ values ≤ 15 .

In developing our model, we observed two general types of failures: (1) lateral spread toward a free face (i.e., river channel or some other abrupt topographical depression), and (2) lateral spread down gentle ground slopes. Our regression analyses indicate that the topographical parameters fitted for free face failures differ significantly from those fitted for ground slope failures, thus we formulated our final MLR model with separate components for each type of failure. These analyses also indicate that ground displacement is strongly influenced by the height and proximity of the free face and that this influence decays logarithmically with increasing distance. In contrast to free face failures, ground slope failures generally produces smaller, more uniform displacements and typically occur on slopes that are less than 6 percent. Displacement produced by ground slope failure is strongly correlated with the steepness of the ground slope and generally occurs in the direction of the maximum topographical gradient.

In addition to these topographical factors, the thickness, silt content and mean grain-size of the liquefied layer are strongly to moderately correlated with displacement. Our study suggests that significant lateral spread is almost always restricted to saturated cohesionless sediments having $(N1)_{60}$ values ≤ 15 for $M < 8$ earthquakes. We also found that lateral spread is generally restricted to liquefiable sediments that are thicker than 1 m and found in the upper 15 to 20 m of the soil profile. Our analyses also indicates that horizontal displacement tends to markedly decrease as the percentage of fines and mean grain-size of the liquefied sediment increase.

Because our MLR models performed poorly at predicting displacement for soils with D_{50} values > 2 mm, we concluded that gravelly sediments behave differently than fine-grained sediments in some nonlinear fashion that our model does not accommodate. Also, silty sediments appear to displace much less than clean, sandy sediments. More research and case histories are needed to better understand and model the dynamic displacement behavior of gravels and silts. In addition, because our model is heavily dependent on Japanese case histories, where liquefaction was widespread and boundary effects were small, it may tend to overpredict displacements occurring near the margins of failures. More detailed subsurface investigations are needed from locales where liquefaction and lateral spread are influenced by lateral boundaries. Finally, as more case studies become available from past and future earthquakes, the performance of this model should be re-evaluated and the model parameters adjusted as necessary.

SECTION 7
REFERENCES

- Ambraseys, N. N., 1988, "Engineering Seismology," Earthquake Engineering and Structural Dynamics, Volume 17, pp. 1-105.
- Andersen, K. H., 1983, "Report, Foundation Analyses for Gravity Platforms Stability, Soil Stiffness and Settlements," Lecture presented at the NIF Course, "Fundamentberegninger for Gravitasjonsplattformer," Fagerness 5.7.12.1983, December, 1983, Norwegian Geotechnical Institute, Oslo, Norway.
- Andrus, R. D., and Youd, T. L., 1987, "Subsurface Investigation of Liquefaction-Induced Lateral Spread Thousand Springs Valley, Idaho," U. S. Army Corp of Engineers, Miscellaneous Paper GL-87-8, 106 p.
- Andrus, R. D., and Youd, T. L., 1989, "Penetration Tests in Liquefiable Gravels," Proceedings of the 12th International Conference on Soil Mechanics and Foundation Engineering, A. A. Balkema, Publishers, Vol. 1, pp. 679-682.
- Andrus, R. D., Stokoe, K. H., and Roesset, J. M., 1991, in press, "Liquefaction of Gravelly Soil at Pence Ranch During the 1983 Borah Peak, Idaho Earthquake," Preprint of Proceedings of the Fifth International Conference on Soil Dynamics and Earthquake Engineering, Karlsruhe, Germany, Sept. 1991.
- Bartlett, S. F., 1992, "Empirical Analysis of Horizontal Ground Displacement Generated by Liquefaction-Induced Lateral Spread," Doctoral Dissertation, Department of Civil Engineering, Brigham Young University, Provo, Utah, Technical Report CEG-92-01, 129 p.
- Bartlett, S. F., and Youd, T. L., 1989a, "Compilation of Case Histories of Ground Failure Displacement Associated with Soil Liquefaction," Brigham Young University Civil Engineering Department Report No. CEG 89-01.
- Bartlett, S. F., and Youd, T. L., 1989b, "Case Studies of Liquefaction-Induced Ground Failures," Address to the Symposium on Earthquake-Induced Landslides, Joint Meetings of the Cordilleran and Rocky Mountain Sections, Geological Society of America, Spokane, Washington, May 8-11, 1989.
- Bartlett, S. F., and Youd, T. L., 1990, "Evaluation of Ground Failure Displacement Associated with Soil Liquefaction: Compilation of Case Histories," Miscellaneous Paper S-73-1, Department of the Army, U.S. Army Corps of Engineers, Washington, D.C., 84 p.
- Bartlett, S. F., and Youd, T. L., 1992, "Case Histories of Lateral Spreads Caused by the 1964 Alaska Earthquake," Case Studies of Liquefaction and Lifeline Performance During Past Earthquakes, Volume 2, United States Case Studies, Technical Report NCEER-92-0002, National Center for Earthquake Engineering Research (NCEER), State University of New York at Buffalo, Red Jacket Quadrangle, Buffalo, NY, 127 p.
- Bennett, M. J., 1988, "Liquefaction Analysis of the San Fernando Valley Juvenile Hall, California," U. S. Geological Survey Open File Report 81-502, 83 p.
- Bennett, M. J., 1989, "Liquefaction Analysis of the 1971 Ground Failure at the San Fernando Valley Juvenile Hall, California," Bulletin of the Association of Engineering Geologists, Vol. XXVI, No. 2, pp. 209-226.
- Bennett, M. J., Youd, T. L., Harp, E. L., and Wieczorck, G. F., 1981, "Subsurface Investigation of Liquefaction, Imperial Valley Earthquake, California, Oct. 15, 1979," U.S. Geological Survey Open File Report 81-502, 83 p.

Bennett, M. J., McLaughlin, P. V., Sarimento, J. S., and Youd, T. L., 1984, "Geotechnical Investigation of Liquefaction Sites, Imperial Valley, California, U. S. Geological Survey Open File Report 84-252, 103 p.

Bouckovalas, G., Whitman, R. V., Marr, W. A., 1984, "Permanent Displacement of Sand with Cyclic Loading," Journal of Geotechnical Engineering, ASCE, Vol. 110(11), pp. 1606-1623.

Byrne, P. M., 1990, "LIQDISP; A Computer Program to Predict Liquefaction Induced Displacements of Slopes," Soil Mechanics Series No. 147, Department of Civil Engineering, University of British Columbia, September, 1990.

Campbell, K. W., 1985, "Strong Motion Attenuation Relations: A Ten-Year Perspective," Earthquake Spectra, Vol. 1, No. 4, pp. 759-804.

Casagrande, A., 1936, "Characteristics of Cohesionless Soils Affecting the Stability of Slopes and Earth Fills," Journal of the Boston Society of Civil Engineers, Jan. 1936, Reprinted in Contributions to Soil Mechanics 1925 to 1940, Boston Society of Civil Engineers, Oct. 1940, pp. 257-276.

Castro, G., 1969, "Liquefaction of Sands" Harvard Soil Mechanics, Serial No. 81, 112 p.

Castro, G., 1975, "Liquefaction and Cyclic Mobility of Saturated Sands," Journal of the Geotechnical Engineering Division, ASCE, Vol. 101, No. GT6, pp. 551-569.

Castro, G., and Poulos, S. J., 1977, "Factors Affecting Liquefaction and Cyclic Mobility," Journal of the Geotechnical Engineering Division, ASCE, 103(GT6), pp. 501-506.

Castro, G., Poulos, S. J., France, J. W. and Enos, J. L., 1982, "Liquefaction Induced by Cyclic Loading." Report to National Science Foundation, Geotechnical Engineers, Inc., Winchester, Massachusetts.

Chen, A. T. F., 1988, "On Seismically Induced Pore Pressure and Settlement," Earthquake Engineering and Soil Dynamics II, Recent Advances in Ground-Motion, ASCE Publication No. 20, pp. 482-492.

Crouse, C. B., and Turner, B. E., 1980, "Processing and Analysis Japanese Accelerograms and Comparisons with U.S. Strong Motion Data," Proceedings, 7th World Conference on Earthquake Engineering, Istanbul, Turkey, Vol. 2, p. 419-426.

Dikmen, S. U. and Ghaboussi, J., 1984, "Effective Stress Analysis of Seismic Response and Liquefaction Theory," Journal of the Geotechnical Engineering Division, ASCE, Vol. 110, No. 5, Proceedings Paper 18790, pp. 628-644.

Dobry, R., Stokoe, K. H., Ladd, R. S, and Youd T. L., 1982, "Liquefaction Susceptibility from S-Wave Velocity," Preprint 81-544, ASCE Nation Convention, St. Louis, Missouri, October, 1981, ASCE, New York, New York.

Dobry, R., Ladd, R. S., Yokel F. Y., Chung, R. M., and Powell, D., 1982, "Prediction of Pore Water Pressure Buildup and Liquefaction of Sands During Earthquakes by the Cyclic Strain Methods," Building Science Series 138, National Bureau of Standards, U.S. Department of Commerce, U.S. Government Printing Office, Washington, D.C.

Dobry, R. and Baziar, M. H., 1990, "Permanent Ground Deformations Due to Lateral Spreading During Earthquakes", Conference Proceedings, Third Japan-U.S. Workshop on Earthquake Resistant Design of Lifeline Facilities and Countermeasures for Soil Liquefaction, December 17-19, San Francisco, CA, Sponsored by Nation Center for Earthquake Engineering Research, State University of New York at Buffalo, Red Jacket Quadrangle, Buffalo, NY, pp. 209-223.

Dobry, R., Bazier, M. H., O'Rourke, T. D., Roth, B. L., and Youd T. L., "Liquefaction and Ground Failure in the Imperial Valley, Southern California during the 1979, 1981, and 1987 Earthquakes," Case Studies of Liquefaction and Lifeline Performance during Past Earthquakes: National Center for Earthquake Engineering Research Technical Report NCEER-92-0002, Vol. 2, pp. 4-1 to 4-85.

Draper, N. R., and Smith, H., 1981, Applied Regression Analysis, Second Edition, John Wiley and Sons, New York, New York, 709 p.

Dyvik, R., Dobry, R., Thomas G. E., and Pierce, W. G., 1984, "Influence of Consolidation Shear Stresses and Relative Density on Threshold Strain and Pore Pressure During Cyclic Straining of Saturated Sands," Miscellaneous Paper GL-84-15, Department of the Army, U.S. Army Corps of Engineers, Washington, D.C.

Finn, W. D. L., Lee, W. K. and Martin, G. R., 1976, "An Effective Stress Model for Liquefaction," Journal of the Geotechnical Engineering Division, ASCE, Vol. 103, No. GT6, Proceeding Paper 13008, pp. 517-533.

Finn, W. D. L., 1980, "Seismic Deformations in an Underwater Slope," Report to Earth Technology Corporation.

Finn, W. D. L., 1982, "Computation of Seismically Induced Settlements in Sands," Preliminary Report to U.S. Army Corps of Engineers, Waterways Experiment Station, Vicksburg Mississippi.

Finn, W. D. L., 1984, "Progress Reports," U.S. Army Corps of Engineers Office of Standardization, London.

Finn, W. D. L., 1985a, "Dynamic Analysis of EPR Gravity Platform," Report to Exxon Production Research Company.

Finn, W. D. L., 1985b, "Permanent Deformations in Lornex Tailings Dam, Preliminary Feasibility Study," Report to Klohn Leonoff Consultants Ltd.

Finn, W. D. L., 1988, "Dynamic Analysis in Geotechnical Engineering," Earthquake Engineering and Soil Dynamics II, Recent Advances in Ground-Motion Evaluation, ASCE Publication No. 20, pp. 523-591.

Finn, W. D. L., 1990, "Analysis of Post-Liquefaction Deformations in Soil Structures," H. Bolton Seed, Vol. 2 Memorial Symposium Proceedings, May, 1990, Editor J. Michael Duncan, BiTech Publishers, Ltd., Vancouver, B.C., Canada, pp. 291-311.

Finn, W. D. L., and Yogendrakumar, M., 1989, "TARA-3FL: Program for Analysis of Liquefaction Induced Flow Deformations, Department of Civil Engineering, University of British Columbia, Vancouver, B. C., Canada.

Franklin, A. G., and Chang, F. K., 1977, "Permanent Displacements of Earth Embankments by Newmark Sliding Block Analysis," Earthquake Resistance of Earth and Rock-Fill Dams, Report 5, Misc. Paper No. S-71-17, U.S. Army Engr. Waterways Experiment Station, Vicksburg, Mississippi.

Goodman, R. E., Seed, H. B., 1966, "Earthquake-Induced Displacements in Sand Embankments," Journal of the Soil Mechanics and Foundations Division, ASCE 92(SM2), pp. 125-146.

Hamada, M., 1992, "Large Ground Deformations and Their Effects on Lifelines: 1964 Niigata Earthquake," Case Studies of Liquefaction and Lifeline Performance During Past Earthquakes, Vol. 1, Japanese Case Studies, National Center for Earthquake Engineering Research, State University of New York at Buffalo, New York, Technical Report NCEER-92-0001, 123 p.

Hamada, M., Yasuda, S., Isoyama, R., and Emoto, K., 1986, "Study on Liquefaction Induced Permanent Ground Displacements," Published by the Association for the Development of Earthquake Prediction in Japan, p. 87.

Hamada, M., Towhata, I., Yasuda, S., Isoyama, R., 1987, "Study of Permanent Ground Displacement Induced by Seismic Liquefaction," Computers and Geotechnics, Vol. 4, No. 4, Elsevier Applied Science Publishers, pp. 197-220.

Hamada, M., Yasuda, S., Wakamatsu, K., 1988, "Case Study on Liquefaction-Induced Ground Failures during Earthquakes in Japan," Proceedings, First Japan-U.S. Workshop on Liquefaction, Large Ground Deformation and Their Effects on Lifeline Facilities, pp. 3-21.

Hardman, S. L., and Youd, T. L., 1987, Mapping the Extent and Thickness of Liquefiable Soil Layers at Engineering Sites, U. S. Army Corp of Engineers, Miscellaneous Paper S-73-1, 161 p.

Hirono T., 1968, "Seismometrical Features," General Report on the Niigata Earthquake of 1964, Published by Tokyo Electrical Engineering College Press, 2-2 Nishiki-cho, Kanda, Chiyoda-ku, Tokyo Japan, pp. 47-62.

Holzer, T. L., Youd, T. L., Bennett, M. J., 1988, "In Situ Measurement of Pore-Pressure Build-Up During Liquefaction," 20th Joint UJNR Panel on Wind and Seismic Effects, 17 p.

Holzer, T. L., Youd, T. L., Hanks, T. C., 1989, "Dynamics of Liquefaction During the 1987 Superstition Hills, California, Earthquake," Science, Vol. 244, pp. 56-59.

Hwang, Li-San and Hammack, J., 1984, "The Japan Sea Control Region Tsunami of May 26, 1983," National Academy Press, Washington D. C., 33 p.

Idriss, I. M., 1985, "Evaluating Seismic Risk in Engineering Practice," Proceedings of the Eleventh International Conference on Soil Mechanics and Foundation Engineering, A. A. Balkema Publishers, Rotterdam, Netherlands.

Idriss, I. M., 1990, "Response of Soft Soil Sites During Earthquakes," Proceedings, H. Bolton Seed Memorial Symposium, Vol 2, BiTech Publishers, LTD, Vancouver, B.C., Canada, pp. 273-290.

Idriss, I. M., in press, "Procedures for Selecting Earthquake Ground Motions at Rock Sites," A Report to the National Institute of Standards and Technology, U.S. Department of Commerce, Gaithersburg, Maryland.

Idriss, I. M., Seed, H. B., 1968, "Seismic Response of Horizontal Soil Layers," Journal of the Soil Mechanics and Foundations Division, ASCE, Vol. 94, No. SM4, pp. 1003-1031.

Ishihara, K., 1985, "Stability of Natural Deposits During Earthquakes," Proceedings of the Eleventh International Conference on Soil Mechanics and Foundation Engineering, Vol. 1, pp. 321-376.

Ishihara, K. and Towhata, I., 1982, "Dynamic Response Analysis of Level Ground Based on the Effective Stress Method," in Soil Mechanics - Transient and Cyclic Loads, Edited by G. N. Pande and O. C. Zienkiewicz, John Wiley and Sons, Ltd., New York, pp 133-172.

Iwasaki, T., Tatusoka F., Tokida, K., and Yasuda S., 1978, "A Practical Method for Assessing Soil Liquefaction Potential Base on Case Studies at Various Sites in Japan," Proceedings of the Fifth Japan Earthquake Engineering Symposium, (in Japanese).

Joyner, W. B., and Boore, D.M., 1981, "Peak Horizontal Acceleration and Velocity from Strong Motion Records Including Records from the 1979 Imperial Valley, California Earthquake," Bulletin of the Seismological Society of America, Vol 71, No. 6, pp. 2011-2038.

Joyner, W. B., and Boore, D. M., 1988, "Measurement, Characterization and Prediction of Strong Ground Motion," Earthquake Engineering and Soil Dynamics II, Recent Advances in Ground Motion Evaluation, ASCE, No. 20, pp. 43-102.

Kachadoorian, R., 1968, "Effects of the Earthquake of March 27, 1964, on the Alaska Highway System," U. S. Geological Survey Professional Paper 545-C, 66 p.

Kanamori, H., 1978, "Quantification of Earthquakes," Nature, Vol. 271, pp. 411-414.

Kawasumi, H., 1968, "Introduction to Niigata Earthquake of 1964," General Report on the Niigata Earthquake of 1964, Published by Tokyo Electrical Engineering College Press, 2-2 Nishiki-cho, Kanda, Chiyoda-ku, Tokyo Japan, pp. 1-6.

Kokusho, T., Yoshida, Y., Esashi, Y., 1983, "Evaluation of Seismic Stability of Dense Sand Layer (Part 2), Evaluation Method by Standard Penetration Test," Report 383026, Central Research Institute for Electric Power Industry, Tokyo Japan.

Krinitzsky, E. L., Chang, F. K., 1988a, "Intensity-Related Earthquake Ground Motions," Bulletin of the Association of Engineering Geologists, Vol. XXV, No. 4, pp. 425-435.

Krinitzsky, E. L., Chang, F. K., 1988b, "Magnitude-Related Earthquake Ground Motions," Bulletin of the Association of Engineering Geologists, Vol. XXV, No. 4, pp. 399-423.

Ledbetter, R., 1983, "Current Methodologies for Assessing Seismically Induced Settlements in Soil," U. S. Nuclear Regulatory Commission Publication NRC Fin E7002, 54 p.

Liao, S. S. C., 1986, "Statistical Modeling of Earthquake-Induced Liquefaction," Ph.D. Dissertation, Department of Civil Engineering, Massachusetts Institute of Technology, 470 p.

Mabey, M. A., 1992, "Prediction of Displacements Due to Liquefaction Induced Lateral Spreading," Doctoral Dissertation, Department of Civil Engineering, Brigham Young University, Provo, Utah, Technical Report CEG-92-02.

Makdisi, F. I., Seed, H. B., 1978, "Simplified Procedure for Estimating Dam and Embankment Earthquake-Induced Deformations," Journal of the Geotechnical Engineering Division, ASCE 104(GT7), pp. 849-867.

Maley, R. P., and Cloud, W. K., 1971, "Preliminary Strong-Motion Results from the San Fernando Earthquake of February 9, 1971," The San Fernando, California Earthquake of February 9, 1971, United States Geological Survey Professional Paper 733, U.S.G.S., Denver, CO, pp. 163-176.

Marcuson, W. F., Hynes, M. E. and Franklin A. G., 1990, "Evaluation and Use of Residual Strength in Seismic Safety Analysis of Embankments," Earthquake Spectra, Vol. 6, No. 3, August, 1990, pp. 529-572.

Marr, W. A., Christian, J. T., 1981, "Permanent Displacements Due to Cyclic Wave Loading," Journal of the Geotechnical Engineering Division, ASCE, Vol. 107(GT8), pp. 1129-1149.

Marr, W. A., Urzua, A., Bouckovalas, G., 1982, "A Numerical Model to Predict Permanent Displacement from Cyclic Loading of Foundations," Proceedings of the Third International Conference on the Behavior of Offshore Structures, Vol. 1, McGraw Hill/Hemisphere Publishing Company, New York, New York, pp. 297-312.

Martin, G. R., Finn, W. D. L., Seed, H. B., 1975, "Fundamentals of Liquefaction Under Cyclic Loading," Soil Mechanics Series Report No. 23, Department of Civil Engineering, University of British Columbia, Vancouver; also Proc. Paper 11284, Journal of Geotechnical Engineering Division, ASCE, Vol. 101, No. GT5, pp. 324-438.

Martin, P. P. and Seed, H. B., 1978, "MASH - A Computer Program for the Nonlinear Analysis of Vertically Propagating Shear Waves in Horizontally Layered Soil Deposits," EERC Report No. UCB/EERC-78/23, University of California, Berkeley California.

McCulloch, D. S., Bonilla, M. G., 1970, "Effects of the Earthquake of March 27, 1964, on the Alaska railroad," U. S. Geological Survey Professional Paper 545-D, 161 p.

MINITAB, 1989, "Minitab Statistical Software, Release 7", Minitab Inc., 3081 Enterprise Drive, State College, PA 16801.

Mogi, A., Kawamura, B., and Iwabuchi, Y., 1964, "Submarine Crustal Movement Due to the Niigata Earthquake in 1964," Journal of Geodetic Society of Japan, Vol. 10, No. 3-4, 1964, pp. 180-186.

National Research Council (NRC), 1985, Liquefaction of Soils During Earthquakes, National Academy Press, Washington D. C., 240 p.

Newmark, N. M., 1965, "Effects of Earthquakes on Dams and Embankments," Geotechnique, 15(2), pp. 139-160.

Ostle, B., Malone, L. C., 1988, Statistics in Research, Iowa State University Press, Ames, Iowa.

O'Rourke, T. D., Roth, B. L., and Hamada, M., 1990, in press, "Large Ground Deformations and Their Effects on Lifeline Facilities: 1971 San Fernando Earthquake," Technical Report, National Center for Earthquake Engineering Research, State University of New York at Buffalo, Red Jacket Quadrangle, Buffalo, N.Y., 14261, 71 p.

O'Rourke, T. D., Beaujon, P. A., and Scawthorn, C. R., 1991, in press, "Large Ground Deformations and Their Effects on Lifelines Facilities: 1906 San Francisco Earthquake," Technical Report, National Center for Earthquake Engineering Research, State University of New York at Buffalo, Red Jacket Quadrangle, Buffalo, N.Y., 14261, 65 p.

Page, R. A., Boore, D. M., Joyner, W. B., Coulter, H. W., 1972, "Ground Motion Values for Use in Seismic Design of the Trans-Alaska Pipeline System," U. S. Geological Survey Circular 672, 16 p.

Poulos, S. J., 1971, "The Stress-Strain Curves of Soils," unpublished paper, available from Geotechnical Engineers, Inc., Winchester, Massachusetts.

Poulos, S. J., Castro, G., and France, J. W., 1985, "Liquefaction Evaluation Procedure," Journal of the Geotechnical Engineering Division, ASCE, GT6, pp. 772-792.

Prevost, J. H., 1981, "DYNA-FLOW: A Nonlinear Transient Finite Element Analysis Program," Report No. 81-SM-1, Department of Civil Engineering, Princeton University, Princeton, N.J.

Ramberg, W. and Osgood, W. R., 1943, "Description of Stress-Strain Curves by Three Parameters", National Advisory Committee Aeronautics Technical Note 902, Washington D.C.

Robertson, P. K., Campanella, R. G., and Wightman, A., 1983, "SPT-CPT Correlations," Journal of Geotechnical Engineering, Vol. 109, pp. 1449-1459.

Ross, G. A., Seed, H. B., and Migliaccio, R. R., 1969, "Bridge Foundation Behavior in Alaska Earthquake," Journal of the Soil Mechanics and Foundations Division, ASCE, Vol. 95, No. SM4. pp. 1007-1036.

Ross, G. A., Seed, H. B., and Migliaccio, R. R., 1973, "Performance of Highway Bridge Foundations," The Great Alaska Earthquake of 1964, Engineering Volume, National Academy of Sciences, Washington D. C., pp. 190-242.

Ryan, B. F., Joiner, B. L., and Ryan, T. A. Jr., 1985, "Minitab Handbook Second Edition," PWS-Kent Publishing Company, Boston, MA, 385 p.

Sarma, S. K., 1979, "Response and Stability of Earth Dams During Strong Earthquakes," Miscellaneous Paper GL-79-13, U.S. Army Corps of Engineers, Waterways Experiment Station, Vicksburg, Mississippi.

Scott, R. F., 1973, "The Calculation of Horizontal Accelerations from Seismoscope Records," Bulletin of Seismological Society of America, Vol. 63, No. 5, Oct. 1973, pp. 1637-1661.

Seed, H. B., 1979, "Soil Liquefaction and Cyclic Mobility Evaluation for Level Ground during Earthquakes," Journal of the Geotechnical Engineering Division, ASCE, Vol. 105, No. GT2, pp. 201-255.

Seed, H. B., 1983, "Earthquake-Resistant Design of Earth Dams," in Seismic Design of Embankments and Caverns, Terry R. Howard, Editor, ASCE, pp. 41-64.

Seed, H. B., 1987, "Design Problems in Soil Liquefaction," Journal of Geotechnical Engineering, Vol. 113, No. 8, pp. 827-845.

Seed, H. B. and Lee K. L., 1966, "Liquefaction of Saturated Sands During Cyclic Loading," Journal of the Soil Mechanics and Foundations Division, ASCE 92(SM6) pp. 105-134.

Seed, H. B. and Idriss, I. M., 1967, "Analysis of Soil Liquefaction: Niigata Earthquake," Journal of the Soil Mechanics and Foundation Division, SM 3, May 1967, ASCE, pp. 83-108.

Seed, H. B. and Idriss, I. M., 1970, "Soil Moduli and Damping Factors for Dynamic Response Analyses," Report No. EERC 70-10, Earthquake Engineering Research Center, University of California, Berkeley.

Seed, H. B., and Idriss, I. M., 1971, "Simplified Procedure for Evaluation of Soil Liquefaction Potential," Journal of Soil Mechanics and Foundations Division, ASCE, Vol. 97, No. SM9, pp. 1249-1273.

Seed, H. B., Lee, K. L., Idriss, I. M., Makdisi, F., 1973, "Analysis of the Slides in the San Fernando Dams During the Earthquake of Feb. 9, 1971," Report No. EERC 73-2, Earthquake Engineering Research Center, University of California, Berkeley.

Seed, H. B., Idriss, K. L., Lee, K. L., Makdisi, F. I., 1975, "Dynamic Analysis of the Slide in the Lower San Fernando Dam During the Earthquake of February 9, 1971," Journal of the Geotechnical Engineering Division, ASCE, Vol. 101(GT9), pp. 889-911.

Seed, H. B., Martin P. P. and Lysmer J., 1976, "Pore Pressure Changes During Soil Liquefaction," Journal of the Geotechnical Engineering Division, ASCE, 102(GT4), pp. 323-346.

Seed, H. B. and Idriss, I. M., 1982, Ground Motions and Soil Liquefaction During Earthquakes, Earthquake Engineering Research Institute Monograph, 134 p.

Seed, H. B., Idriss, I. M., Arrango, I., 1983, "Evaluation of Liquefaction Potential Using Field Performance Data," Journal of Geotechnical Engineering, ASCE, Vol. 109(3), pp. 458-482.

Seed, H. B., Tokimatsu, K., Harder, L. F., and Chung, R. M., 1984, "The Influence of SPT Procedures in Soil Liquefaction Resistance Evaluations," Report No. UBC/EERC-84/15, Earthquake Engineering Research Center, University of California, Berkeley California.

Seed, H. B., Tokimatsu, L. F., Harder, L. F., and Riley, M. C., 1985, "Influence on SPT Procedures in Soil Liquefaction Resistance Evaluations." Journal of Geotechnical Engineering, ASCE, Vol. 3, No. 12, pp. 1425-1446.

Seed, H. B., and De Alba, P., 1986, "Use of SPT and CPT Tests for Evaluating the Liquefaction Resistance of Sands," Use of In-Situ Tests in Geotechnical Engineering, ASCE, Geotechnical Special Publication No. 6, pp. 281-302.

Seed, H. B., Wong, R. T., Idriss, I. M., Tokimatsu, K., 1986b, "Moduli and damping Factors for Dynamic Analyses of Cohesionless Soils," Journal of the Geotechnical Engineering Division, ASCE, Vol. 112, No. 11, pp. 1016-1032.

Seed H. B., Seed R. B., Harder, L. F., Jr., and Jong, H. L., 1988, "Re-Evaluation of the Slide in the Lower San Fernando Dam in the Earthquake of February 9, 1971," Report No. UCB/EERC-88/04, University of California, Berkeley, California.

Seed H. B., Harder, L. F., 1990, "SPT-Based Analysis of Cyclic Pore Pressure Generation and Undrained Residual Strength," H. Bolton Seed, Memorial Symposium Proceedings, Vol. 2, BiTech Publishers LTD, Vancouver, B.C., Canada.

Shibata, T., 1981, "Relations Between N-Value and Liquefaction Potential of Sand Deposits," Proceedings of the Sixteenth Annual Convention of Japanese Society of Soil Mechanics and Foundation Engineering, pp. 621-624.

Taniguchi, E., 1983, "Prediction of Earthquake Induced Deformation of Earth Dams," Soils and Foundations, Vol. 23(4), pp. 126-132.

Streeter, V. L., Wylie, E. B. and Richart, F. E., 1973, "Soil Motion Computations by Characteristics Methods," ASCE National Structural Engineering Meeting, San Francisco, California, Preprint No. 1952.

Terzaghi, K., and Peck, R. B., 1948, Soil Mechanics in Engineering Practice, New York, John Wiley and Sons, 566 p.

Tohno, I., and Shamoto, Y., 1985, "Liquefaction Damage to the Ground During the 1983 Nihonkai-Chubu (Japan Sea) Earthquake in Akita Prefecture, Tohoku, Japan," Natural Disaster Science, Vol. 7, No. 2, pp. 67-93.

Tokimatsu, K., Yoshimi, Y., 1983, "Empirical Correlation of Soil Liquefaction Based on SPT N-Value and Fines Content," Soils and Foundations, Japanese Society of Soil Mechanics and Foundation Engineering, Vol. 23(4), pp. 56-74.

Tokimatsu, D., Seed, H. B., 1987, "Evaluation of Settlements in Sands due to Earthquake Shaking," Journal of Geotechnical Engineering, ASCE, Vol. 113, No. 8, pp. 861-878.

Towhata, I., Tokida, K., Tamari Y., Matsumoto H., and Yamada, K., 1990, "Prediction of Permanent Lateral Displacement of Liquefied Ground by Means of Variational Principle," Conference Proceedings, Third Japan-U.S. Workshop on Earthquake Resistant Design of Lifeline Facilities and Countermeasures for Soil Liquefaction, December 17-19, San Francisco, CA, Sponsored by Nation Center for Earthquake Engineering Research, State University of New York at Buffalo, Red Jacket Quadrangle, Buffalo, NY, pp. 237-251.

Utermohle, G. E., 1962, "Amended Copy, Foundation Study Report, Snow River Bridge #605, Project Number F 031-1(6), Anchorage District, Alaska Department of Transportation, Anchorage, Alaska, 28 p.

Utermohle, G. E., 1963, "Foundation Study Report, Knik and Matanuska River Bridges, Bridge Numbers 1121, 1122, 1123, 1124, Project Number F 042-1(7), Anchorage District," Alaska Department of Transportation, Anchorage, Alaska, 37 p.

Utermohle, G. E., 1965, "Foundation Investigation, Twenty Mile River, Bridge No. 634, Project No. ERFO-36(1), Anchorage District," Alaska Department of Transportation, Anchorage, Alaska, 5 p.

Utermohle, G. E., 1965, "Foundation Investigation, Portage River No. 1 (#630) and Portage River No. 2 (#631), Project No. ERFO-20(1), Anchorage District," Alaska Department of Transportation, Anchorage, Alaska, 8 p.

Utermohle, G. E., 1965, "Foundation Investigation, Placer River #1 and Placer River Main Crossing, Bridges #627 and 629, Project No. ERFO-20(1), Anchorage District," Alaska Department of Transportation, Anchorage, Alaska, 9 p.

VanMarcke, E. H., Lai, S. P., 1980, Strong Motion Duration and RMS Amplitude of Earthquake Records," Bulletin of the Seismological Society of America, Vol. 70, No. 4, pp. 1293-1307.

Whitman R. V., and Liao, S., 1985, "Seismic Design of Gravity Retaining Walls," Miscellaneous Paper GL-85-1, U.S. Army Corps of Engineers, Waterways Experiment Station, Vicksburg, Mississippi.

Yasuda, S., Nagase, H., Kiku, H., Uchida, Y., 1990, "A Simplified Procedure for the Analysis of the Permanent Ground Displacement," Conference Proceedings, Third Japan-U.S. Workshop on Earthquake Resistant Design of Lifeline Facilities and Countermeasures for Soil Liquefaction, December 17-19, San Francisco, CA, Sponsored by Nation Center for Earthquake Engineering Research, State University of New York at Buffalo, Red Jacket Quadrangle, Buffalo, NY, pp. 225-236.

Yegian, M. K., Marciano, E. A., and Ghahraman, V. G., 1988, "Integrated Seismic Risk Analysis for Earth Dams," Report No. 88-15, Northeastern Univ., Boston, Mass.

Yegian, M. K., Marciano, E. A., and Ghahraman, V. G., 1991, "Earthquake-Induced Permanent Deformation Probabilistic Approach," Journal of Geotechnical Engineering, Vol. 117, No. 1, pp. 35-50.

Youd, T. L., 1972, "Compaction of Sands by Repeated Shear Straining," Journal of the Soil Mechanics and Foundations Division, ASCE, SM 7, pp. 709-725.

Youd, T. L., 1973a, "Liquefaction, Flow, and Associated Ground Failure," U. S. Geological Survey Circular 688, 12 p.

Youd, T. L., 1973b, "Ground Movements in Van Norman Lake Vicinity During San Fernando Earthquake," The San Fernando, California Earthquake of February 9, 1971, Vol. 3, U.S. Department of Commerce, National Oceanic and Atmospheric Administration, Washington D.C., 1973, pp. 197-206.

Youd, T. L., 1977, "Packing Changes and Liquefaction Susceptibility," Journal of the Geotechnical Engineering Division, ASCE, Vol. 103, No. GT8, pp. 918-922.

Youd, T. L., 1978, "Major Cause of Earthquake Damage is Ground Failure," Civil Engineering, ASCE, April 1978, pp. 47-51.

Youd T. L., 1984, "Geologic Effects - Liquefaction and Associated Ground Failure," Proceedings of the Geologic and Hydrologic Hazards Training Program, Open File Report 84-760, U.S. Geological Survey, Menlo Park California, pp. 210-232.

Youd, T. L., 1985, Brigham Young University Civil Engineering Department Memorandum, Dec. 26, 1985.

Youd, T. L., 1989, "Ground Failure Damage to Buildings during Earthquakes," Foundation Engineering: Current Principles and Practices, Vol. 1, Proceeding of the Congress sponsored by the Geotechnical Engineering Division of ASCE, Evanston, Illinois, June 25-29, 1989, pp. 758-770.

Youd, T. L., and Hoose, S. N., 1976, "Liquefaction During 1906 San Francisco Earthquake," Journal of the Geotechnical Engineering Division, Vol. 102, No. GT5, pp. 425-439.

Youd, T. L., and Hoose, S. N., 1978, "Historic Ground Failures in Northern California Triggered by Earthquakes," U. S. Geological Survey Professional Paper 993, 177 p.

Youd, T. L., and Perkins, D. M., 1978, "Mapping Liquefaction-Induced Ground Failure Potential," Journal of the Geotechnical Engineering Division, ASCE, Vol. 104, No. GT4, April, 1978, pp. 433-446.

Youd, T. L., and Bennett, M. J., 1981, "Liquefaction Studies Following 1979 Imperial Valley Earthquake," ASCE Preprint 81-544, Session No. 24, 1981, ASCE National Convention.

Youd, T. L., and Bennett, M. J., 1983, "Liquefaction Sites, Imperial Valley, California," Journal of Geotechnical Engineering, Vol. 109, No. 3, pp. 440-457.

Youd, T. L., Harp, E. L., Keefer, D. K., and Wilson, R. C., 1985, "The Borah Peak, Idaho Earthquake of October 28, 1983," Earthquake Spectra, Vol. 2, No. 1, pp. 71-89.

Youd, T. L., and Perkins, D. M., 1987, "Mapping of Liquefaction Severity Index," Journal of Geotechnical Engineering, Vol. 113, No. 11, pp. 1374-1392.

Youd, T. L., and Bartlett, S. F., 1988, "U.S. Case Histories of Liquefaction-Induced Ground Displacement," Proceeding, First Japan -U.S. Workshop on Liquefaction, Large Ground Deformation and Their Effects on Lifeline Facilities, pp. 22-31.

APPENDIX 1
DISCUSSION OF INDEPENDENT VARIABLES USED IN MLR ANALYSES

This appendix discusses the procedures used to measure the independent variables compiled by this study. All variables tested in our MLR analyses are tabulated in ASCII format on the computer disk labeled Appendix 3 in the file named "MLR.DAT." This disk and two additional disks, which comprise "Appendix 4", are available from NCEER Information Service, care of Science and Engineering Library, 304 Capen Hall, State University of New York at Buffalo, Buffalo, New York, 14260. The independent variables included in our final MLR model are also discussed in the body of this report. This appendix provides additional information about all independent variables compiled and tested by this study (see Table 3-2). It also discusses the borehole summary sheets, SPT data, and liquefaction analyses contained in Appendix 4. Finally, an example of the weighted average, which was used to assign geological and soil independent variables to individual displacement vectors, is given in Section A1.5.

The liquefaction analyses summary sheets are found in Appendix 4 for the 267 SPT boreholes compiled by this study. These summary sheets tabulate the earthquake, topographical, geological, and soil measurements for each borehole and give the results of liquefaction analyses that were done according to the "simplified procedure" (Seed and Idriss, 1971; Seed et al., 1983; 1985, NRC, 1985) and Liao's 50 percent probability of liquefaction curve (Liao, 1986). Each summary sheet lists the methods used to measure the independent variables and documents the source(s) of the information. An example summary sheet is shown in Table A1-1. These summary sheets are grouped by earthquake on the computer disks labelled Appendix 4. Table A1-2 lists the files names for the earthquakes and lateral spreads found in Appendix 4.

A1.1 Earthquake Independent Variables

Table A1-3 lists the earthquake independent variables that are tabulated in Appendix 3 in MLR.DAT.

A1.1.1 Earthquake Magnitude

Earthquake magnitude is a measure of the amount of seismic energy released by an earthquake. Large magnitude earthquakes are capable of producing large and widespread ground failure in moderately to highly liquefiable soils that are located near the seismic source. In contrast, lateral spread displacement tends to be smaller and more limited for moderate to smaller earthquakes. Because the moment magnitude, M_w , is defined in terms of energy, it is generally a better estimate of the amount of seismic energy released by a given event than other earthquake magnitude measures. The moment magnitude is calculated from the seismic moment, M_0 (Kanamori, 1978):

$$M_w = (\log M_0 / 1.5) - 10.7 \quad (A1.1.1.1)$$

where:

M_0 = seismic moment (dyne*cm).

M_0 is based on elastic dislocation theory and is a function of the amount of tectonic deformation at the seismic source and the rigidity of the earth's crust:

$$M_0 = u S D \quad (A1.1.1.2)$$

where:

u = rigidity of the ruptured material

S = surface area of the fault

D = average displacement of the fault.

TABLE A1-1
EXAMPLE SUMMARY SHEET SHOWING CASE HISTORY
INFORMATION AND LIQUEFACTION ANALYSES
(Summary sheets are found in Appendix 4)

SUMMARY SHEET OF CASE HISTORY INFORMATION AND LIQUEFACTION ANALYSES

BOREHOLE ID. NO.: 13
 BORING: M-4

EARTHQUAKE: 1964, ALASKA
 SITE NAME: RAILROAD BRIDGE MP 147.1
 LOCATION: MATANUSKA RIVER, ALASKA

SOURCE OF HORIZONTAL DISPLACEMENT DATA

METHOD: DISPLACEMENT OF BRIDGE PIER
 DOCUMENTATION: McCULLOCH AND BONILLA, 1970

EARTHQUAKE MEASUREMENTS

METHOD: M_w
 DOCUMENTATION: KANAMORI, 1978
 SCALED FROM 0 CONTOUR, p. D7 McCULLOCH AND BONILLA, 1970
 SCALED FROM p. D7 McCULLOCH & BONILLA, 1970
 MAG.-DIST. (INCREASED 2.33 X) JOYNER AND BOORE, 1988
 MAGNITUDE-DISTANCE RELATION KRINITZSKY AND CHANG, 1988

GEOLOGICAL AND TOPOGRAPHICAL MEASUREMENTS

METHOD: MODERN CHANNEL DEPOSITS
 DOCUMENTATION: McCULLOCH & BONILLA, 1970
 AT OR NEAR SURFACE, p. D158 McCULLOCH AND BONILLA, 1970
 TOPOGRAPHICAL SURVEY BARTLETT AND YOOD, 1991
 1958 PROFILE BY ALASKA RR BARTLETT AND YOOD, 1991
 NOT ESTIMATED NOT REPORTED

AGE OF SEDIMENTS (yrs): RECENT
 DEPTH TO GROUNDWATER (m): 0.0
 SOURCE OF SLOPE DATA
 SOURCE OF FREE FACE DATA
 AREA OF FAILURE (sq. m):

STANDARD PENETRATION AND SOIL MEASUREMENTS

METHOD: SPT
 DOCUMENTATION: UTERMÖHLE, 1963
 DONUT ROPE AND PULLEY
 SIEVE ANALYSIS UTERMÖHLE, 1963
 SIEVE ANALYSIS UTERMÖHLE, 1963
 AVG FINES IN T10, F10, (%): 0 AVG D50 IN T10, D5010, (%): 10.85
 AVG FINES IN T15, F15, (%): 16 AVG D50 IN T15, D5015, (%): 3.615
 AVG FINES IN T20, F20, (%): 14 AVG D50 IN T20, D5020, (%): 3.871

SPLIT SPOON 2" O.D.
 HAMMER ENERGY RATIO: 45
 SOURCE OF % FINES DATA
 SOURCE OF D50 DATA
 THICKNESS N₁₍₆₀₎ < 10, T10, (m): 0.0
 THICKNESS N₁₍₆₀₎ < 15, T15, (m): 13.3
 THICKNESS N₁₍₆₀₎ < 20, T20, (m): 15.8

LOWEST N IN PROFILE, N: 11.0
 LOWEST N₁₍₆₀₎ IN PROFILE, N160: 10.4

DEPTH TO LOWEST N, Z_N, (m): 4.6
 DEPTH TO LOWEST N₁₍₆₀₎, Z_{N160}, (m): 10.7

LIQUEFACTION ANALYSIS (SIMPLIFIED PROCEDURE)

LIQUEFACTION POTENTIAL, I_S: 6.32
 ACCUMULATIVE THICKNESS OF LIQUEFIED ZONE, T_S, (m): 16.0
 DEPTH TO TOP OF LIQUEFIED ZONE, Z_{TLS}, (m): 0.0
 DEPTH TO BOTTOM OF LIQUEFIED ZONE, Z_{BLS}, (m): 19.8
 AVG. FACTOR OF SAFETY IN LIQUEFIED ZONE, K_S: 0.60
 AVG. N₁₍₆₀₎ IN LIQUEFIED ZONE, O_S: 13.6
 LOWEST FACTOR OF SAFETY, J_S: 0.35
 LOWEST FACTOR OF SAFETY N₁₍₆₀₎, N160_S: 10.8
 DEPTH TO LOWEST FACTOR OF SAFETY, Z_S, (m): 3.0
 AVG. FINES IN LIQUEFIED ZONE, F_S, (%): 14
 AVG. CLAY IN LIQUEFIED ZONE (%): 2
 AVG. D50 IN LIQUEFIED ZONE, D50_S, (mm): 3.732

LIQUEFACTION ANALYSIS (LIAO'S 50% PROBABILITY CURVE)

LIQUEFACTION POTENTIAL, I_L: 6.04
 ACCUMULATIVE THICKNESS OF LIQUEFIED ZONE, T_L, (m): 17.5
 DEPTH TO TOP OF LIQUEFIED ZONE, Z_{TLL}, (m): 0.1
 DEPTH TO BOTTOM OF LIQUEFIED ZONE, Z_{BLL}, (m): 26.8
 AVG. FACTOR OF SAFETY IN LIQUEFIED ZONE, K_L: 0.64
 AVG. N₁₍₆₀₎ IN LIQUEFIED ZONE, O_L: 11.5
 LOWEST FACTOR OF SAFETY, J_L: 0.45
 LOWEST FACTOR OF SAFETY N₁₍₆₀₎, N160_L: 10.8
 DEPTH TO LOWEST FACTOR OF SAFETY, Z_L, (m): 3.0
 AVG. FINES IN LIQUEFIED ZONE, F_L, (%): 20
 AVG. CLAY IN LIQUEFIED ZONE (%): 3
 AVG. D50 IN LIQUEFIED ZONE, D50_L, (mm): 3.366

TABLE A1-2

NAMES OF DATA FILES FOUND IN APPENDIX 4

<u>File Name</u>	<u>Earthquake and Case History Name</u>
SANFRAN.DAT	1906 San Francisco Earthquake Coyote Creek Bridge Mission Creek Zone Salinas River Bridge South of Market Street Zone
ALASKA.DAT	1964 Alaska Earthquake Bridges 141.1, 147.4, 147.5, 148.3, Matanuska R. Bridges 63.0, 63.5, Portage Creek Highway Bridge 629, Placer River Snow River Bridge 605A, Snow River Bridges 3.0, 3.2, 3.3, Resurrection River
NIIGATA.DAT	1964 Niigata, Japan Earthquake Many lateral spreads in Niigata, Japan
SANFERN.DAT	1971 San Fernando Earthquake Jensen Filtration Plant, San Fernando, Ca. Juvenile Hall, San Fernando, Ca.
IMPERIAL.DAT	1979 Imperial Valley Earthquake Heber Road near El Centro, California River Park near Brawley, California
BORAH.DAT	1983 Borah Peak, Idaho Earthquake Whiskey Springs near Mackay, Idaho Pence Ranch near Mackay, Idaho
NIHONKAI.DAT	1983 Nihonkai-Chubu Earthquake Many lateral spreads in Noshiro, Japan
SUPER.DAT	1987 Superstition Hills Earthquake Wildlife Instrument Array, near Brawley, Ca.

TABLE A1-3

SUMMARY OF EARTHQUAKE INDEPENDENT VARIABLES USED IN MLR

Earthquake Variables	Description
M*	Earthquake moment magnitude, M_w .
R*	Nearest horizontal distance to seismic energy source or fault rupture, (km).
A	Peak horizontal ground acceleration, (g).
D	Duration of strong ground motion (>0.05 g), (s).

* Indicates independent variables used in final MLR models.

In this study, we tabulated values of M_w as the variable M . For some of the smaller earthquakes included in this study, M_w was not reported by the original researchers, and the surface wave magnitude, M_s , or the local magnitude, M_L , was used to represent M instead of M_w (see documentation of earthquake magnitude in Appendix 4). Nonetheless, M_s and M_L are comparable to M_w , especially for smaller magnitude earthquakes (Kanamori, 1978).

A1.1.2 Distance to Seismic Energy Source or Fault Rupture

During large earthquakes, severe and damaging lateral spread occurs close to the seismic energy source. The amount of liquefaction-induced ground displacement tends to diminish logarithmically with increasing distance from the seismic source (Youd and Perkins, 1978, 1987). For this study, the distance to the seismic energy source or fault rupture, R , was tabulated the horizontal distance (km) from the site in question to the nearest point on a surface projection of the fault rupture zone (see Section 4.1).

A1.1.3 Peak Ground Acceleration

The peak horizontal ground acceleration, A , (g), is often used to characterize the intensity of strong ground motion. Earthquake shaking must have a sufficient amplitude to generate excess pore pressure and initiate liquefaction. Once the soil has liquefied, the resulting ground displacement also increases with increasing values of A . For sites where a strong ground motion accelerometer was nearby, we recorded the instrumented value of A ; for sites without a strong motion record, a magnitude-distance, empirical relationship was used to estimate A (Joyner and Boore, 1988):

$$\log A = a + b(M-6) + c(M-6)^2 + d(\log r) + kr + s \quad (A1.1.3.1)$$

where:

A = the larger value of the two horizontal components of peak horizontal acceleration measured on rock or stiff soil sites (g)

M = moment magnitude

a = 0.49

b = 0.23

c = 0.0

h = 8.0

d = -1.0

k = -0.0027

s = 0.0

r = $(r_o^2 + h^2)^{1/2}$

The value of r_0 in Equation A1.1.3.1 is the shortest horizontal distance, (km), from the recording site to the surface projection of the fault rupture. The summary sheets found in Appendix 4 document those sites having instrumented values of A and those sites where A was estimated from Equation A1.1.3.1.

We also attempted formulating a M-A model by using A values estimated from Equation A1.1.3.2 for our non-instrumented sites (Idriss, in press) and modifying those bedrock estimates of A for stiff soil conditions by using Figure 5-5. For this analysis, we applied a faulting factor, F , of 0.5; but, we also found that A is not very sensitive to the selected value of F . The attempt to formulate M-A models using A estimated from either Equation A1.1.3.1 or from Equation A1.1.3.2 and modified for stiff soil conditions using Figure 5-5 yielded poorer correlations than models based directly on M , $\log R$, and R (see Sections 4.1 and 5.1).

$$\ln(A) = [a_0 + \exp(a_1 + a_2 M)] + \frac{[E_0 - \exp(E_1 + E_2 M)] \ln(R+20) + 0.2 F}{\ln(R+20) + 0.2 F} \quad (\text{A1.1.3.2})$$

where:

- A = peak bedrock horizontal acceleration (g)
- M = moment magnitude, M_w
- R = closest distance to source in km; however for $M \leq 6$ the hypocentral distance is used.
- F = style of faulting factor; $F = 0$ for strike slip fault; $F = 1$ for a reverse fault and $F = 0.5$ for an oblique source.
- $a_0 = -0.150$ for $M \leq 6$ and -0.050 for $M > 6$
- $a_1 = 2.262$ for $M \leq 6$ and 3.477 for $M > 6$
- $a_2 = -0.083$ for $M \leq 6$ and -0.284 for $M > 6$
- $E_0 = 0$ for both $M \leq 6$ and $M > 6$
- $E_1 = 1.602$ for $M \leq 6$ and 0.286 for $M > 6$
- $E_2 = -0.142$ for $M \leq 6$ and -0.286 for $M > 6$

A1.1.4 Duration of Strong Ground Motion

Long-lived strong ground motion tends to increase the extent of liquefaction in the soil and prolongs the time that the mobilized soil mass is subjected to downslope translation by earthquake and gravitational forces. Page et al. (1972) used the bracketed interval, (s), between the first 0.05 g peak to the last 0.05 g peak to measure the duration of strong ground motion, D . For this study, we used the same definition of D at lateral spread sites where strong ground motion records were available. For noninstrumented sites, we used an empirical relationship developed by Krinitzsky and Chang (1988b) to estimate D :

$$\log D = -2.36 + 0.43 M + 0.30 \log (r/10) \quad (\text{A1.1.4.1})$$

where:

- D = the bracketed interval, (s), defined by Page et al.
- M = earthquake magnitude
- r = epicentral distance, (km).

Equation A1.1.4.1 was applied to hard and soft soil sites for earthquakes with a focal depth > 19 km. Equation A1.1.4.1 was also applied to hard soil sites for earthquakes with a focal depth ≤ 19 km. For soft soil sites and for earthquakes with a focal depth ≤ 19 km, the following equation was used (Krinitzsky and Chang, 1988b):

$$\log D = -2.06 + 0.43 M + 0.60 \log (r/10). \quad (\text{A1.1.4.2})$$

where:
D, M, r are defined above.

The summary sheets in Appendix 4 document the methods used to estimate D.

A1.2 Topographical Independent Variables

The topographical variables listed in Table A1-4 are compiled in MLR.DAT in Appendix 3.

TABLE A1-4
SUMMARY OF TOPOGRAPHICAL INDEPENDENT VARIABLES USED IN MLR

<u>Topographical Variables</u>	<u>Description</u>
--------------------------------	--------------------

S*	Ground slope, (%).
L	Distance to the free face from the point of displacement, (m).
H	Height of free face, (m).
W*	Free face ratio, (%), (i.e., 100H/L).

* Indicates independent variables used in final MLR models.

A1.2.1 Ground Slope

Figure 3-11, in Section 3.5, shows the techniques we used to measure ground slope, S, for all ground slope failures. The technique shown in Figure 3-11, Case 1, was used to measure S for all uniform slopes:

$$S (\%) = 100 Y/X \quad (A1.2.1.1)$$

where:

Y = the change in vertical elevation

X = the horizontal distance of the slope.

In gently undulating topography, like that found in Noshiro, Japan, many slopes were undulating and required a slightly modified method of measuring S (see Figure 3-11, Cases 2 and 3).

In the case of free face failures, S was used to measure the slope of the floodplain into or away from the channel. The value of S was recorded as a positive value for ground sloping toward the free face (Section 3.4, Figure 3-8, Case 1) and was recorded as negative value for ground sloping away from the free face (Figure 3-8, Case 2). However, our regression analyses showed that S was not significant when included in the free face model, thus S was omitted from the free face component of our final MLR model.

A1.2.2 Distance to and Height of Free Face

A free face is any abrupt topographical depression such as an escarpment, river channel, canal, or road cut. Lateral spread displacement markedly increased with the proximity of the free face (see Section 3.4). In modeling the influence of the free face, Hamada et al. (1986) artificially steepened their estimate of the ground slope, θ , to the base of the free face (Figure 2-2b). We decided not to steepen our estimate of S to the base of the free face, but used the free face ratio, W, to represent the effects of the free face in our MLR models. To calculate W, we tabulated the height of the free face, H, (m), and the distance from the displacement vector to the free face, L, (m). In order to normalize L

with respect to H, we formed the free face ratio, W, (%), where: $W = 100H/L$ (see Section 3.4). If a free face was not present (e.g., ground slope failures), the values H and L are set equal to zero in MLR.DAT found in Appendix 3.

A1.3 Geological and Soil Independent Variables

In post-earthquake liquefaction investigations, the thickness and depth of the liquefied zone(s) cannot be determined by direct observation. Thus, empirical analyses are commonly used to detect layers in the subsurface that are susceptible to liquefaction. Layer(s) that are shown to be susceptible by these analyses are often assumed to be the same layer(s) that liquefied during the earthquake. In this study, two techniques were used to estimate the thickness of and depth to the liquefied layer: (1) the so called "simplified procedure of liquefaction analysis" by Seed and Idriss, 1971; Seed et al. 1983, 1985, 1986a, and (2) Liao's 50 percent probability of liquefaction curve (Liao, 1986).

Table A1-5 lists the geological independent variables compiled in Appendix 3 and 4. Variables that are subscripted with a "S" were determined from the simplified procedure curves; variables subscripted with a "L" were determined from Liao's 50% probability of liquefaction curve. A liquefaction analysis program was written in dBase III to perform the liquefaction analyses. The dBase program was used to calculate all subsurface measures listed in Tables A1-5 and A1-6. The results of these analyses are found in Appendix 4. The program constructs a continuous SPT N and soil profile for each SPT log by linearly interpolating (at 0.1 m increments) between measured values of N, D_{50} , and the percentage of fines and clay in subsurface sample (Figure A1-1). However, linear interpolation is not done across a soil boundary. The soil parameters for the last, or deepest sample in a given layer are kept constant to until the next layer is encountered. Likewise, the soil parameters for the first sample in the underlying layer are transferred upward to the layer boundary, forming a discontinuity in the interpolated profile at the layer boundary. The computer program also accumulates the thickness of cohesionless sediments below the water-table that have $(N1)_{60}$ values ≤ 10 , ≤ 15 , and ≤ 20 . These thickness measures, (m), are tabulated as the independent variables T_{10} , T_{15} , and T_{20} respectively (Appendix 4). Soils with a clay content ≥ 15 percent are not considered to be liquefiable and are not accumulated in T_{10} , T_{15} , and T_{20} . An example of the T_{15} layer(s) is shaded in Figure A1-1; see also Table A1-1, which is the summary sheet for this borehole. Table A1-1 indicates that T_{15} for Figure A1-1 is 13.3 m.

Measured D_{50} values, (mm), are averaged in T_S , T_L , T_{10} , T_{15} , and T_{20} and assigned to the variables $D50_S$, $D50_L$, $D50_{10}$, $D50_{15}$, and $D50_{20}$, respectively (see Table A1-6, see also Table A1-1). Likewise, measured values for the percentage of fines, F, (particle size < 0.075 mm) are averaged in T_S , T_L , T_{10} , T_{15} , and T_{20} and assigned to the variables F_S , F_L , F_{10} , F_{15} , and F_{20} , respectively. Values of D_{50} and F that are interpolated between sampling intervals are not used in these averages. Also, layers that are above the water-table or soils having a clay content ≥ 15 percent are not included in these averages.

TABLE A1-5

SUMMARY OF GEOLOGICAL INDEPENDENT VARIABLES USED IN MLR

Geological

<u>Variables</u>	<u>Description</u>
T_s	Thickness of liquefied zone(s) (Simplified procedure), (m).
T_L	Thickness of liquefied zone(s) (Liao's 50% probability curve), (m).
T_{10}	Thickness of saturated cohesionless soils with $(N1)_{60} \leq 10$, (m).
T_{15}^*	Thickness of saturated cohesionless soils with $(N1)_{60} \leq 15$, (m).
T_{20}	Thickness of saturated cohesionless soils with $(N1)_{60} \leq 20$, (m).
I_s	Index of Liquefaction Potential (Simplified procedure).
I_L	Index of Liquefaction Potential (Liao's 50% probability curve).
Z_{tb}	Depth to top of liquefied zone (Simplified procedure), (m).
Z_{tl}	Depth to top of liquefied zone (Liao's 50% prob. curve), (m).
Z_{bts}	Depth to bottom of liquefied zone (Simplified procedure), (m).
Z_{btl}	Depth to bottom of liquefied zone (Liao's 50% prob. curve), (m).
Z_s	Depth to the lowest factor of safety (Simplified procedure), (m).
Z_L	Depth to the lowest factor of safety (Liao's 50% prob. curve), (m).
Z_N	Depth to lowest SPT N value in saturated cohesionless soil, (m).
Z_{N160}	Depth to lowest SPT $(N1)_{60}$ value in saturated cohesionless soil, (m).
N	Lowest SPT N value in saturated cohesionless sediments.
$N1_{60}$	Lowest SPT $(N1)_{60}$ value in saturated cohesionless sediments.
J_s	Lowest factor of safety below water table (Simplified procedure).
J_L	Lowest factor of safety below water table (Liao 50% prob. curve).
$N1_{60s}$	$(N1)_{60}$ value corresponding to J_s .
$N1_{60L}$	$(N1)_{60}$ value corresponding to J_L .
K_s	Average factor of safety in T_s .
K_L	Average factor of safety in T_L .
O_s	Average $(N1)_{60}$ in T_s .
O_L	Average factor of safety in T_L .

* Indicates independent variables used in final MLR models.

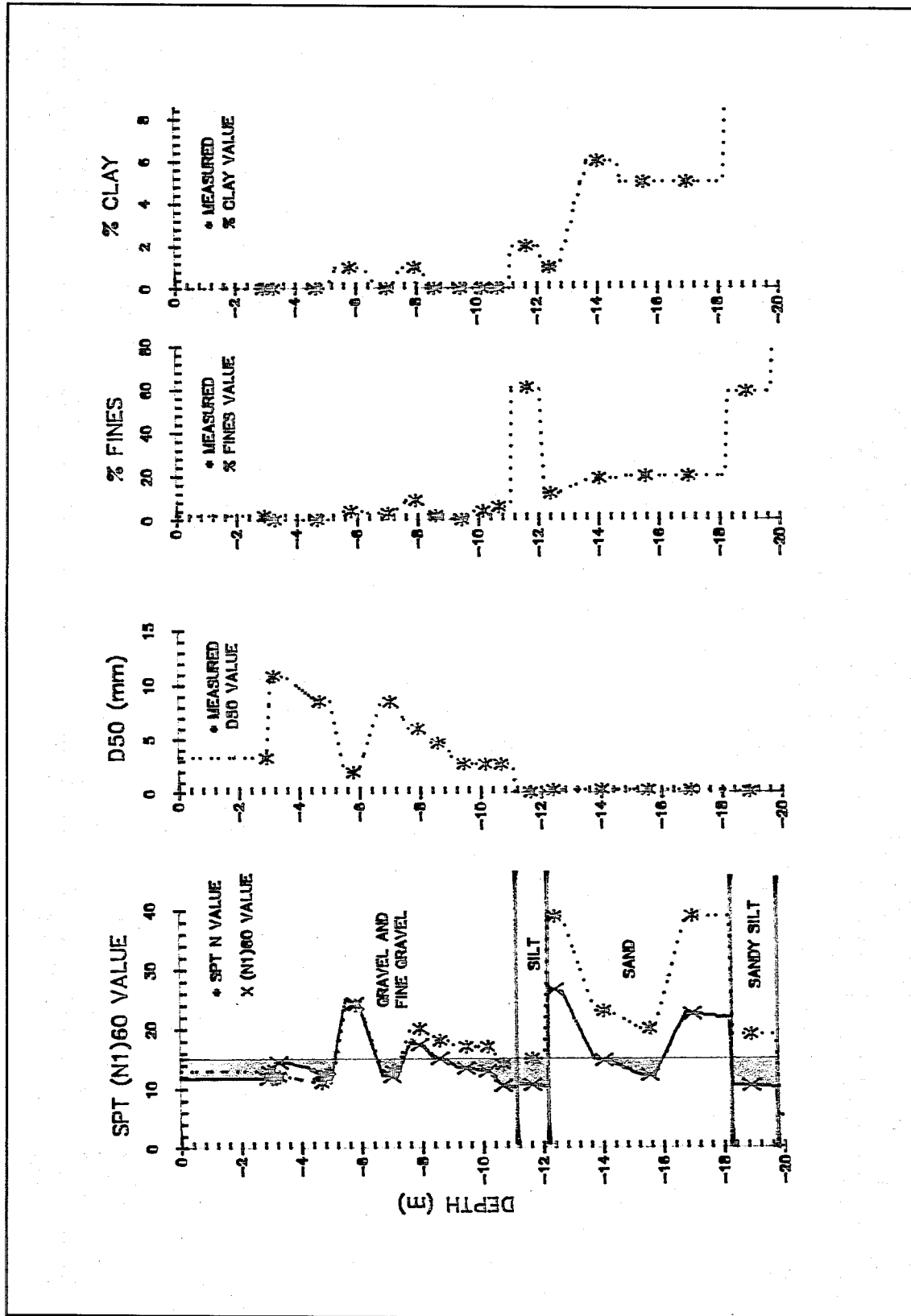


Figure A1-1 A sample SPT borehole taken at Railroad Bridge Mile Post 147.1, Matanuska River, Alaska.

The liquefaction analysis program also tabulates the lowest SPT N and (N1)₆₀ values for each soil log. These values are assigned to variables N and N1₆₀, respectively (for example, compare Table A1-1 and the borehole shown in Figure A1-1). The depth corresponding to N and N1₆₀ are also tabulated as the variables Z_N and Z_{N160}. If two intervals have equivalent N or N1₆₀ values for a given profile, the shallowest depth is assigned to Z_N and Z_{N160}. Values of N and N1₆₀ that are interpolated between sampling intervals not considered for N, N1₆₀, Z_N, and Z_{N160}. Also, N and N1₆₀ values found above the water-table or in soils with a clay content ≥ 15 percent are not considered.

TABLE A1-6
SUMMARY OF SOIL INDEPENDENT VARIABLES USED IN MLR

Soil Variables	Description
D50 _S	Average D ₅₀ in T _S , (mm).
D50 _L	Average D ₅₀ in T _L , (mm).
D50 ₁₀	Average D ₅₀ in T ₁₀ , (mm).
D50 ₁₅ *	Average D ₅₀ in T ₁₅ , (mm).
D50 ₂₀	Average D ₅₀ in T ₂₀ , (mm).
F _S	Average fines content (<0.075 mm) in T _S , (%).
F _L	Average fines content (<0.075 mm) in T _L , (%).
F ₁₀	Average fines content (<0.075 mm) in T ₁₀ , (%).
F ₁₅ *	Average fines content (<0.075 mm) in T ₁₅ , (%).
F ₂₀	Average fines content (<0.075 mm) in T ₂₀ , (%).

* Indicates independent variables used in final MLR models.

A1.3.1 Geological and Soil Measures from the Simplified Procedure

For a given (N1)₆₀ value, the liquefaction analysis program compares the cyclic stress ratio generated by the earthquake, CSRQ, to the cyclic stress ratio required to generate liquefaction in the soil profile, CSRL. If CSRQ exceeds CSRL, then the soil is assumed to have liquefied. CSRQ is a function of the earthquake magnitude, maximum ground acceleration, and the total vertical and effective vertical in-situ stresses. Based on laboratory cyclic shear tests, Seed and Idriss (1982) defined the average cyclic shear stress developed on a horizontal plane during cyclic loading as τ_h. They showed that τ_h can be approximated by:

$$\tau_h = 0.65(a_{max}/g) * \sigma_o * r_d \quad (A1.3.1.1)$$

where:

- a_{max} = maximum ground acceleration, (g)
- σ_o = in-situ vertical stress, (force/length²).
- r_d = stress reduction factor, (unitless).

The stress reduction factor, r_d, is used to decrease τ_h with increasing depth. The value of r_d is a function of depth, z, and differs according to soil type. An average value for r_d is calculated from the following equations (Liao, 1986):

$$r_d = 1 - 0.00765 z \quad (\text{for } z \leq 10 \text{ m}) \quad (A1.3.1.2)$$

$$r_d = 1.174 - 0.0276 z \quad (\text{for } z > 10 \text{ m}) \quad (A1.3.1.3)$$

To calculate the cyclic stress ratio induced by the earthquake, CSR_Q , (unitless), the value of τ_h is divided by the in-situ effective stress:

$$CSR_Q = \tau_h / \sigma_o' = 0.65(a_{max}/g) * (\sigma_o / \sigma_o') * r_d. \quad (A1.3.1.4)$$

The value of $CSRL$, (unitless), is calculated from $(N_1)_{60}$ and is adjusted for σ_o' , the amount of energy delivered by the driving hammer, and the fines content of the soil (particle size ≤ 0.075 mm). To calculate $CSRL$, each SPT N must first be normalized to an effective stress of 100 kPa by using the equation:

$$N_1 = C_N * N \quad (A1.3.1.5)$$

where:

N_1 = the normalized blow count

C_N = an overburden correction factor.

The value of C_N is estimated from (NRC, 1985):

$$C_N = (\sigma_o')^{1/2} / 10 \quad (A1.3.1.6)$$

where:

σ_o' = the in-situ effective stress, kPa.

Each N_1 value must also be corrected for the measured hammer energy delivered to the drill stem. A hammer energy ratio of 60 percent is used as the standard:

$$(N_1)_{60} = N / 60 * ER_m \quad (A1.3.1.7)$$

where:

ER_m = the hammer energy ratio, (%).

The value obtained from Equation A1.3.2.7 is the corrected, blow count (i.e., $(N_1)_{60}$) used to calculate $CSRL$. The liquefaction analysis program also has the capability to convert cone penetration test (CPT) data to SPT $(N_1)_{60}$ values by using a relationship developed by Seed and DeAlba (1986) and extended to larger grain sizes by Andrus and Youd (1989).

The $CSRL$ for a given earthquake magnitude is determined from $CSRL$ versus SPT $(N_1)_{60}$ curves develop by Seed et al. (1983, 1985; NRC 1985; see Figure A1-2). These curves are only valid for clean sands and must be adjusted for the fines content of the soil (particle size ≤ 0.075 mm). Figure A1-3 shows how $CSRL$ varies with fines content for a $M = 7.5$ earthquake. The liquefaction analysis program uses linear interpolation to adjust these $CSRL$ curves for various earthquake magnitudes. It also corrects $CSRL$ for the percentage of fines in the soil by linearly interpolating between the $CSRL$ curves in shown Figure A1-3. (Currently, no guidelines exist on how to extrapolate the $CSRL$ curves for soils with a fines content > 35 percent. For these soils, $CSRL$ values are not extrapolated beyond the 35 percent fines content $CSRL$ curve, but are set equal to this curve by the liquefaction analysis program.)

The liquefaction analysis program also calculates a factor of safety against liquefaction, FS (unitless), for each $(N_1)_{60}$ value:

$$FS = CSRL / CSR_Q. \quad (A1.3.1.8)$$

where:

$CSRL$ and CSR_Q are previously defined.

Increments in granular layers located below the water-table and with $FS < 1.0$ are identified as potentially liquefiable. Increments not found to be susceptible to liquefaction according to the criteria given by Seed and Idriss (1983; see also Section 2.2) are not marked as liquefiable.

Figure A1-4 is an illustration of a liquefaction analysis for the borehole shown in Figure A1-1 and summarized in Table A1-1. The left side of the diagram shows SPT $(N1)_{60}$ values versus depth. The right side of the diagram is a plot of CSRQ and CSRL versus depth. The solid line on the right side of the diagram is CSRQ, and the dotted line is CSRL. Layers that are susceptible to liquefaction are indicated in zones where the dotted line falls on the left side of the solid line (i.e., $FS < 1$).

Table A1-7 is an example of the computer printout for the liquefaction analysis shown in Figure A1-4. Printouts of this type are included in Appendix 4 for all of SPT boreholes included in this study. These analyses are printed in ASCII format and are grouped together according to earthquake (see Table A1-2). Each printout lists the borehole identification number, earthquake, site name, SPT and soil data, and the input parameters for the analysis. The last three columns of the printout give the values of CSRL, CSRQ and the factor of safety against liquefaction, FS. The start of each liquefiable zone is identified by the letter "S", and the end of each liquefiable zone is marked with an "E" (Table A1-7).

We reduced and tested several thickness, depth, SPT N, factor of safety, and soil measures (i.e., T_s , I_s , Z_{TLS} , Z_{BLS} , Z_s , J_s , $N1_{60s}$, K_s , O_s , $D50_s$, and F_s) using the simplified procedure for liquefaction analysis. The accumulative thickness of liquefiable sediments was tabulated as the variable, T_s . (For example, the value of T_s for the borehole shown in Figure A1-4 is 16.0 m; see also Tables A1-1 and A1-7.) Soils that are not liquefiable according to the criteria given by Seed et al. (see Section 2.2) were not accumulated. We also calculated an "Index of Liquefaction Potential," I_s , for each SPT profile (Hamada et al., 1986). This index measures the liquefaction susceptibility of the profile and is a function of FS and T_s :

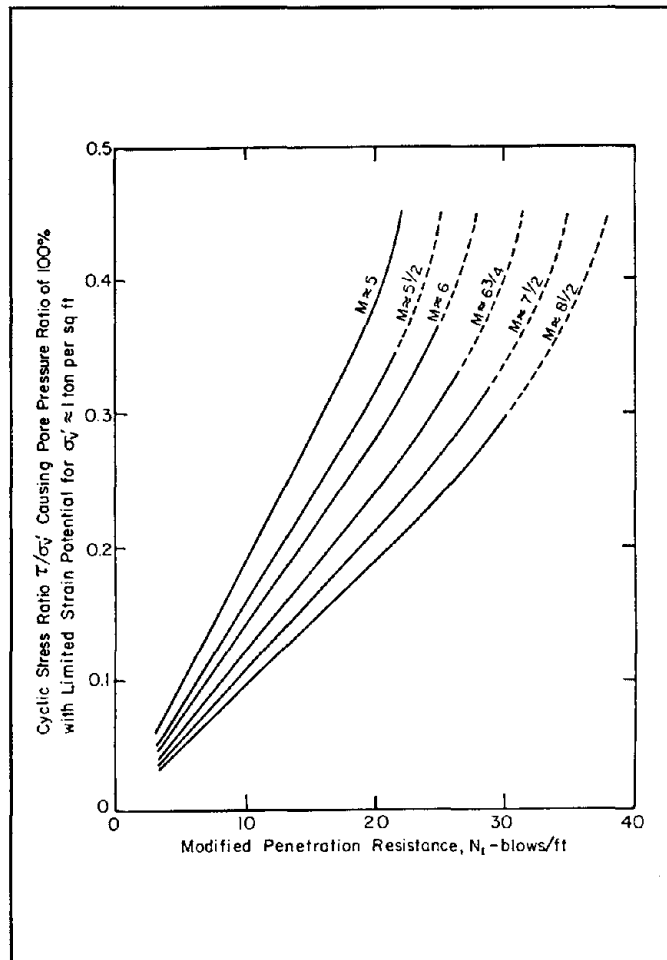


Figure A1-2 Chart for evaluation of CSRL of sands for earthquakes of different magnitudes (NRC, 1985).

$$I_s = \Sigma(1-FS)dz$$

(A1.3.1.9)

where:

$\Sigma(1-FS)$ is evaluated at 0.1 m increments for all liquefiable zone(s) in the profile.

In general, thick, highly susceptible profiles have high values of I_s and thin, marginally susceptible profiles have low values. If liquefaction analyses indicated that no liquefaction occurred in a given profile, then I_s was set equal to zero.

We also compiled several depth measures and tested them in our MLR models. The variables Z_{TLS} and Z_{BLS} were assigned to the depth, (m), to the top and bottom of the liquefied zone, respectively. If more than one zone was shown to be potentially liquefiable, then the tabulated value of Z_{TLS} corresponded to the top of the uppermost zone, and Z_{BLS} corresponded to the bottom of the deepest zone. (The values of Z_{TLS} and Z_{BLS} are 0.0 and 19.8 m, respectively for the analysis shown in Table A1-7.) We also compiled and tested the depth, Z_s , (m), that corresponded to the lowest FS in the profile. (For example, Z_s is 3.05 m for the borehole given in Table A1-7.)

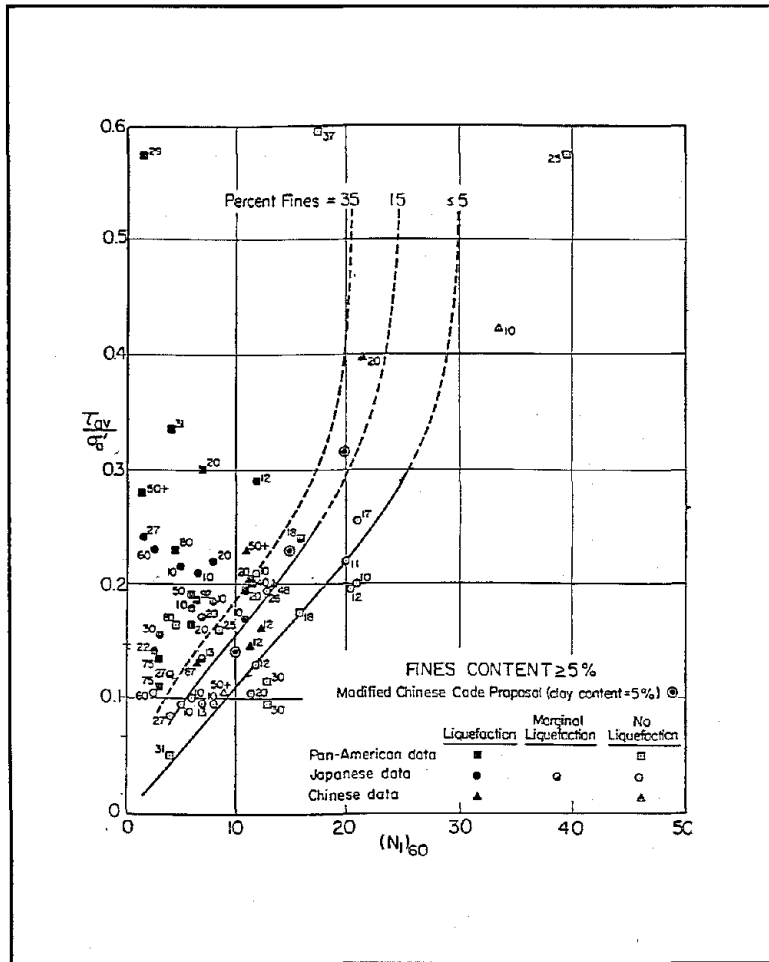


Figure A1-3 Relationship between CSRL and $N_{1,60}$ values for silty sands for $M = 7.5$ earthquakes (NRC, 1985).

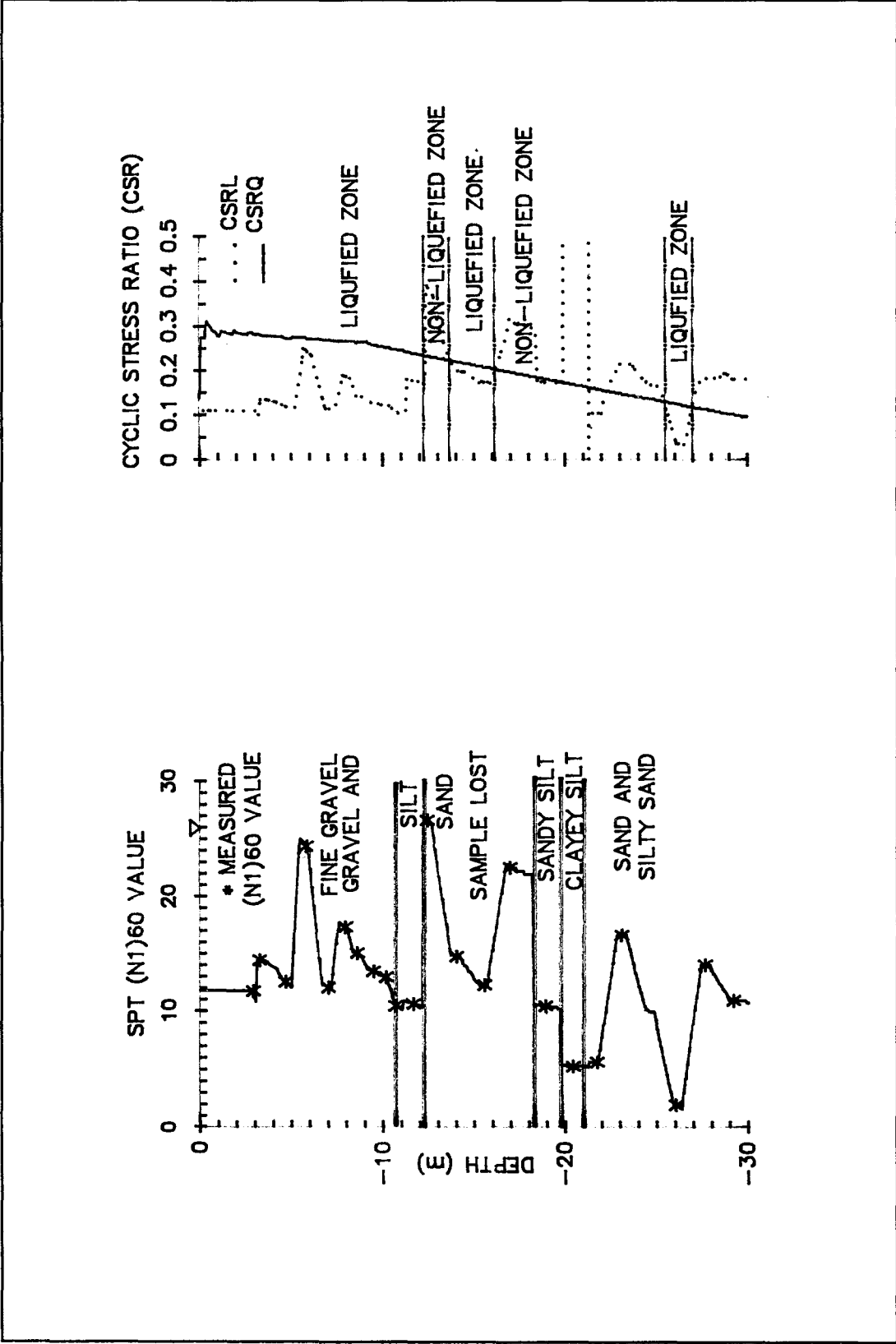


Figure A1-4 SPT (N1)₆₀ values and cyclic stress ratios (CSR) for SPT borehole at Railroad Bridge Milepost 147.1, Matanuska River, Alaska.

Several low and average FS, N, $(N_1)_{60}$ variables were also tested in our MLR models. The lowest factor of safety in the liquefied profile was tabulated as the variable J_s . (The value of J_s for the borehole in Table A1-7 is 0.35.) We also defined $N_{1_{60s}}$ as the $(N_1)_{60}$ value corresponding to J_s . ($N_{1_{60s}}$ for our example is 10.8 (Table A1-7)). We also calculated the average factor of safety in T_s and tabulated it as the variable K_s . Values of FS corresponding to interpolated values of N were not included in this average. (K_s for the sample borehole is 0.60 (see Tables A1-7 and A1-1)). Additionally, we calculated the average $(N_1)_{60}$ value in T_s and tabulated it as the variable O_s . (The value of O_s for the example borehole is 13.6, see Tables A1-7 and A1-1). Interpolated $(N_1)_{60}$ values were not included in this average.

Measured values of the mean grain size, D_{50} (mm), were also averaged in T_s and assigned to the variable $D50_s$ (see Tables A1-1 and A1-7). Likewise, measured values of the percentage of fines (particles size < 0.075 mm) were averaged in T_s and assigned to the variable F_s . Interpolated values of D_{50} and the percentage of fines were not used in these averages. Also layers located above the water-table or soils with a clay content ≥ 15 percent were not included in these averages.

A1.3.2 Liao's Probability Curves for the Simplified Procedure

Liao (1986) analyzed 278 sites of liquefaction or non-liquefaction to develop a best-fit, probabilistic model to predict liquefaction susceptibility. In Liao's procedure, CSRQ is normalized for the magnitude of the earthquake instead of CSRL:

$$CSR_{QN} = CSRQ/MNF \quad (A1.3.2.1)$$

where:

CSR_{QN} = normalized cyclic stress ratio, (unitless)
 MNF = magnitude normalization factor, (unitless).

The value of MNF is given by:

$$MNF = 0.032 M^2 - 0.631 M + 3.9334 \quad (A1.3.2.2)$$

where:

M = earthquake magnitude.

Liao formulated a set of probability curves to determine CSRL based on SPT $(N_1)_{60}$ values (Figure A1-5). For this study, we selected the 50 percent probability of liquefaction curve to calculate our independent variables. The 50 percent probability curve for soils with a percentage of fines ≤ 12 percent is:

$$CSRL = \text{EXP}((0.39760((N_1)_{60}) - 16.447)/6.4603). \quad (A1.3.2.3)$$

The 50 percent probability of liquefaction curve for soils with a percentage of fines > 12 percent is:

$$CSRL = \text{EXP}((0.18190((N_1)_{60}) - 6.4831)/2.6854). \quad (A1.3.2.4)$$

The liquefaction program uses these curves to calculate FS. Zones in the profile below the water table where FS < 1.0 are marked as liquefiable.

TABLE A1-7
EXAMPLE OF SPT DATA AND LIQUEFACTION ANALYSIS FOUND IN APPENDIX 4

LIQUEFACTION ANALYSIS

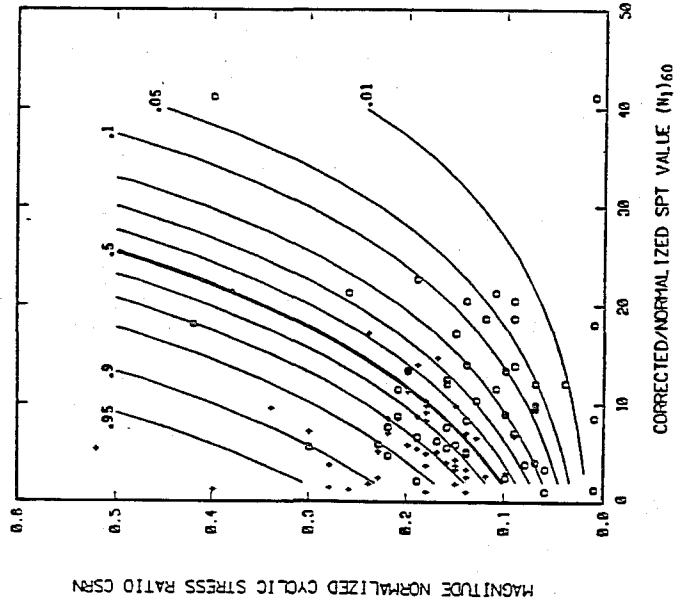
BOREHOLE ID. NO.: 13
 EARTHQUAKE: 1964 ALASKA
 SITE: RAILROAD BRIDGE MP 147.1
 HAMMER ENERGY RATIO: 45 ?
 MAGNITUDE: 9.2
 BORING: M-4
 DEPTH TO GROUNDWATER: 0.00 ?
 MAX. ACCELERATION AT SITE: 0.21 ?
SIMPLIFIED PROCEDURE CURVES

FIELD BLOW COUNT DATA, BOUNDARIES AND LIQUEFIABLE ZONES

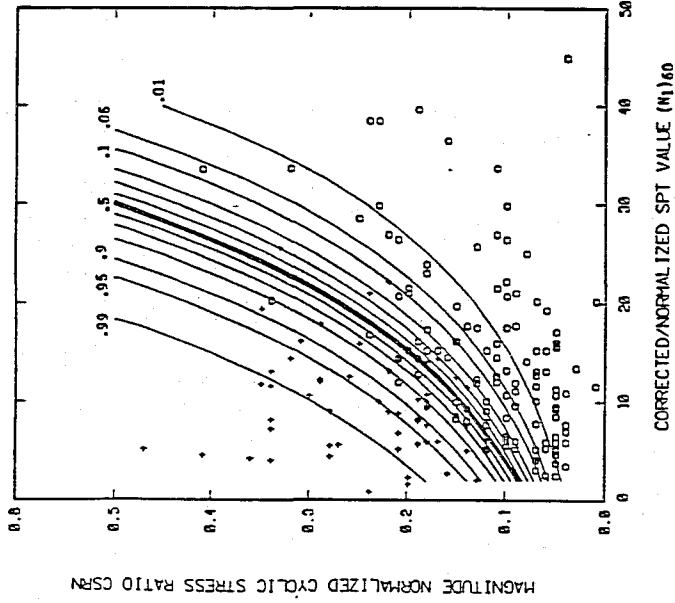
	DEPTH (m)	LC	SOIL DESCRIPTION	N	N160	%F	%C	D50 (mm)	DRY UNIT WT (kN/m ³)	MOIST UNIT WT (kN/m ³)	RATIO FOR LIQ CSRL	RATIO FROM QUAKE CSRQ	FS
*S	0.00	.F.	BOUNDARY	13.0	11.7	2	0	3.269	14.150	18.080	0.109	0.137	0.80
*	-2.44	.F.	FINE GRAVEL - C. SAND	13.0	11.7	2	0	3.269	14.150	18.080	0.109	0.282	0.39
*	-3.05	.F.	GRAVEL, A-1-a	12.0	10.8	0	0	10.847	14.930	18.080	0.100	0.282	0.35
*	-4.57	.F.	GRAVEL, A-1-a	11.0	12.6	0	0	8.514	14.930	18.860	0.117	0.276	0.42
*	-5.49	.F.	FINE GRAVEL, A-1-b	24.0	25.0	4	1	1.932	14.930	19.650	0.248	0.275	0.90
*	-6.71	.F.	GRAVEL, A-1-a	13.0	12.2	3	0	8.467	14.930	19.650	0.113	0.270	0.42
*	-7.62	.F.	GRAVEL, A-1-a	20.0	17.7	9	1	5.938	14.930	19.650	0.188	0.266	0.71
*	-8.38	.F.	GRAVEL, A-1-a	18.0	15.1	2	0	4.613	14.930	19.650	0.141	0.265	0.53
*	-9.15	.F.	SAMPLE LOST	17.0	13.6	0	0	2.700	15.720	19.650	0.126	0.260	0.48
*	-9.76	.F.	FINE GRAVEL - C. SAND	17.0	13.1	4	0	2.655	15.720	19.650	0.121	0.254	0.48
*	-10.67	.F.	FINE GRAVEL - C. SAND	14.0	10.4	6	0	2.647	15.720	19.650	0.102	0.247	0.41
*	-11.13	.F.	BOUNDARY	15.0	10.8	61	2	0.063	15.720	19.650	0.178	0.245	0.73
*	-11.13	.F.	SILT A-4(5)	15.0	10.8	61	2	0.063	15.720	19.650	0.178	0.245	0.73
E	-12.15	.F.	SILT A-4(5)	15.0	10.3	61	2	0.063	15.720	19.650	0.170	0.235	0.72
*	-12.20	.F.	BOUNDARY	39.0	26.9	12	1	0.262	15.880	19.810	0.392	0.235	1.67
*	-12.20	.F.	SAND A-2-4	39.0	26.9	12	1	0.262	15.880	19.810	0.392	0.235	1.67
S	-13.57	.F.	SAND A-2-4	25.2	16.4	18	5	0.291	15.410	18.860	0.215	0.223	0.96
*	-13.72	.F.	SAND A-2-4	23.0	14.8	19	6	0.296	14.930	18.080	0.197	0.223	0.88
*	-15.24	.F.	LOST	20.0	12.3	20	5	0.250	15.720	19.650	0.173	0.209	0.83
E	-15.90	.F.	LOST	23.6	14.2	20	5	0.250	15.720	19.650	0.192	0.206	0.93
*	-16.77	.F.	LOST	39.0	22.8	20	5	0.250	15.720	19.650	0.315	0.197	1.60
*S	-18.29	.F.	BOUNDARY	19.0	10.5	59	9	0.061	16.660	20.590	0.173	0.186	0.93
*	-18.29	.F.	SANDY SILT A-4(5)	19.0	10.5	59	9	0.061	16.660	20.590	0.173	0.186	0.93
E	-19.81	.F.	SANDY SILT A-4(5)	19.0	10.1	59	9	0.061	16.660	20.590	0.172	0.174	0.99
*	-19.82	.T.	BOUNDARY	19.0	10.1	59	9	0.061	16.660	20.590	9.999	0.174	99.99

* = DATA LINE INPUT BY USER
 ? = ESTIMATED OR INTERPOLATED VALUE
 LC = LIQUEFACTION CODE, T = MARKED BY USER AS NONLIQUEFIABLE LAYER,
 F = MARKED BY USER AS POSSIBLY LIQUEFIABLE
 %F = PERCENT FINES (<0.075mm), %C = PERCENT CLAY (<0.005mm)
 S = START OF LIQUEFIED ZONE, E = END LIQUEFIED ZONE

LIQUEFACTION POTENTIAL: 6.32



(a) Clean Sand (FC < 12%)



(b) Silty sand (FC > 12%)

Figure A1-5 Contours of equal probability of liquefaction for: (a) clean sands (i.e. fines content $\leq 12\%$), and (b) silty sands (i.e., fines content $> 12\%$) (Liao, 1986).

We used the 50 percent probability of liquefaction curves to determine the values of T_L , I_L , Z_{TLL} , Z_{BLL} , Z_L , J_L , N_{160L} , K_L , O_L , $D50_L$, and F_L in the same manner as we did for the simplified procedure (see Section A1.3.1). The results of these analyses are tabulated on the summary sheets in Appendix 4 (for an example of these summary sheets, see Table A1-1). In general, preliminary MLR models based on variables determined from the simplified procedure curves and Liao's 50 percent probability curves were comparable. We have not included the liquefaction analyses printouts using Liao's 50 percent probability curve in Appendix 4 because none of the variables determined from this procedure were used in our final MLR model. However, the summary sheets found in Appendix 4 summarize the results of these analyses (for example, see the bottom of Table A1-1).

A1.4 Weighted Averaging Routine

For many of the liquefaction sites, more than one SPT borehole was located within the failure zone. Thus, we needed a systematic method of assigning borehole measures to individual displacement vectors. We selected an inverse-distance, linearly-weighted average to interpolate all geological and soil factors listed in Tables A1-5 and A1-6 between boreholes. This averaging scheme assigns the largest weight to the borehole(s) located closest to the displacement vector:

$$X_{AVG} = W_1 * X_1 + W_2 * X_2 + \dots + W_n * X_n \quad (A1.4.1)$$

where:

X_{AVG} = weighted average
 W_1, \dots, W_n are the weights.

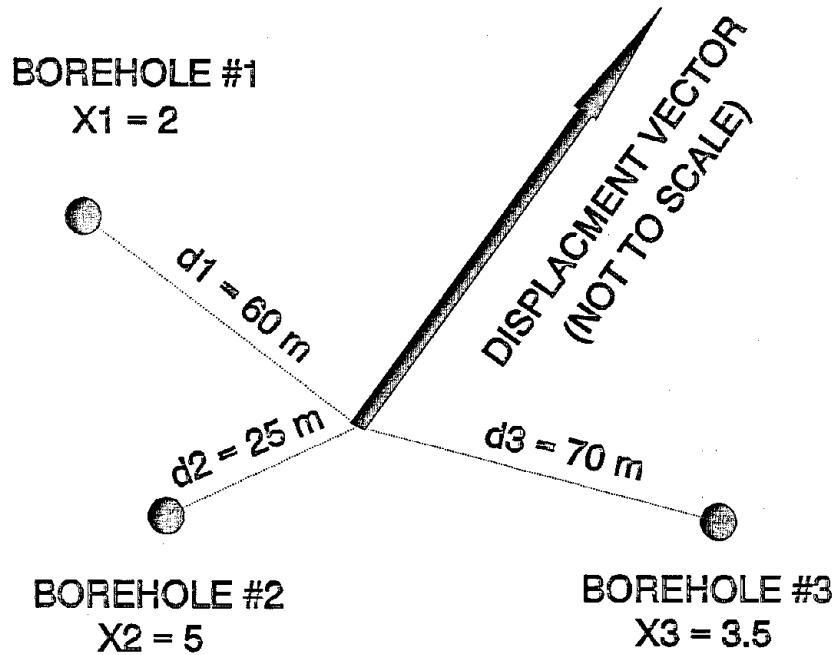
These weights are calculated from:

$$W_i = 1/d_i / \sum(1/d_i) \quad (A1.4.2)$$

where:

d_i = distance from i^{th} borehole to the displacement vector of interest (see Figure A1-6).

The geological and soil measures tabulated in MLR.DAT were averaged using Equation A1.4.1. A dBase program was written to perform the interpolation and was designed to include up to 4 boreholes in the weighted average. Appendix 3, MLR.DAT, lists the borehole identification numbers (BOREID#) for each of the boreholes used in the weighted average. The corresponding SPT logs and liquefaction analyses are found in Appendix 4 and are identified by the same identification number. Also, the distances from the displacement vector to each of the boreholes (i.e., the d_i 's) are tabulated in MLR.DAT in Appendix 3 as the variables BOREDIST1, BOREDIST2, BOREDIST3, and BOREDIST4.



$$X_{\text{avg}} = W_1 X_1 + \dots + W_n X_n$$

where

$$W_i = \frac{1/d_i}{\sum_{i=1}^n (1/d_i)}$$

example:

$$W_1 = 1/60 / (1/60 + 1/25 + 1/70) = 0.235$$

$$W_2 = 1/25 / (1/60 + 1/25 + 1/70) = 0.564$$

$$W_3 = 1/70 / (1/60 + 1/25 + 1/70) = 0.201$$

$$X_{\text{avg}} = \sum_{i=1}^n W_i X_i = 0.235(2) + 0.564(5) + 0.201(3.5)$$

Figure A1-6 Weighted average used to assign borehole measurements to displacement vectors.

APPENDIX 2
MINITAB ANALYSES

A2.1 Minitab Analysis for Equation 3.4.10

MINITAB OUTPUT FOR EQUATION 3.4.10 (FREE FACE MODEL FOR NIIGATA, JAPAN)

MTB > REGRESS LOG DH ON 5 LOG W, T15, F15, D5015, N160S

The regression equation is
 $\text{LOG DH} = 0.610 + 0.572 \text{ LOG W} + 0.0247 \text{ T15} - 0.0278 \text{ F15} - 1.61 \text{ D5015} - 0.0315 \text{ N160S}$

Predictor	Coef	Stdev	t-ratio	p
Constant	0.6101	0.1890	3.23	0.002
LOG W	0.57166	0.05058	11.30	0.000
T15	0.024721	0.005485	4.51	0.000
F15	-0.027827	0.004190	-6.64	0.000
D5015	-1.6074	0.3422	-4.70	0.000
N160S	-0.031502	0.009331	-3.38	0.001

s = 0.1870 R-sq = 72.4% R-sq(adj) = 71.3%

Analysis of Variance

SOURCE	DF	SS	MS	F	p
Regression	5	12.1792	2.4358	69.65	0.000
Error	133	4.6513	0.0350		
Total	138	16.8305			

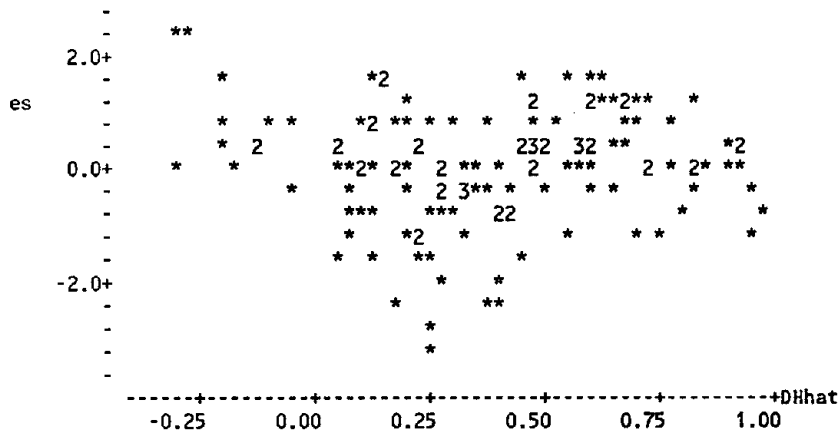
SOURCE	DF	SEQ SS
LOG W	1	6.3875
T15	1	4.1223
F15	1	0.5958
D5015	1	0.6750
N160S	1	0.3986

Unusual Observations

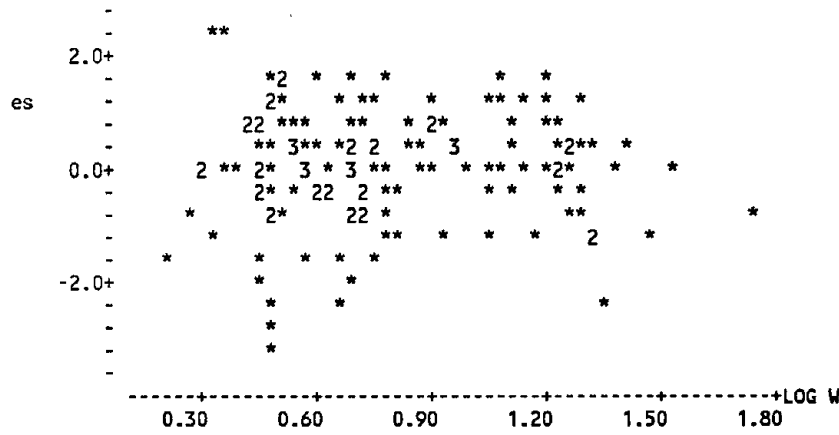
Obs.	LOG W	LOG DH	Fit	Stdev.Fit	Residual	St.Resid
6	0.48	-0.3767	0.2381	0.0294	-0.6148	-3.33R
7	0.49	-0.2518	0.2537	0.0292	-0.5055	-2.74R
8	0.68	-0.0915	0.2835	0.0622	-0.3750	-2.13R
11	0.65	-0.2757	0.1787	0.0428	-0.4544	-2.50R
44	0.45	0.0899	-0.0525	0.0748	0.1424	0.83 X
67	0.32	0.1206	-0.3090	0.0593	0.4296	2.42R
71	0.36	0.1399	-0.2700	0.0663	0.4099	2.34R
72	1.35	-0.0555	0.3746	0.0677	-0.4301	-2.47RX
114	0.22	-0.2076	0.0553	0.0837	-0.2629	-1.57 X
133	0.49	0.0043	0.4115	0.0313	-0.4072	-2.21R
139	0.45	0.0043	0.3885	0.0323	-0.3842	-2.09R

R denotes an obs. with a large st. resid.
X denotes an obs. whose X value gives it large influence.

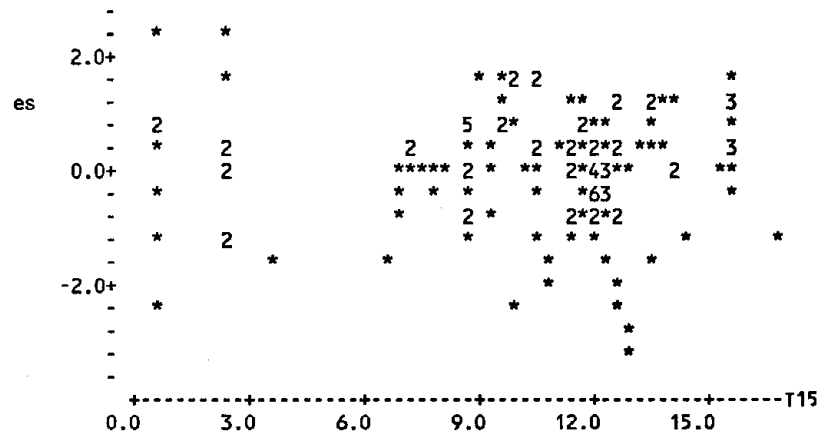
MTB > STANDARDIZED RESIDUAL PLOT FOR EQUATION 3.4.10



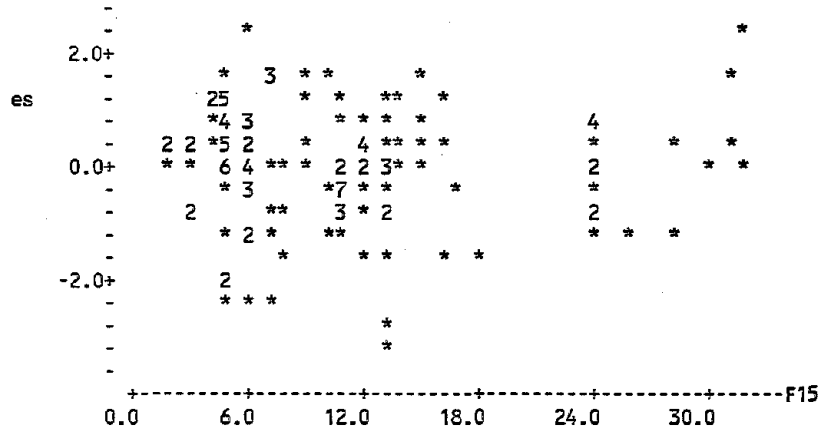
MTB > STANDARDIZED RESIDUAL PLOT FOR EQUATION 3.4.10



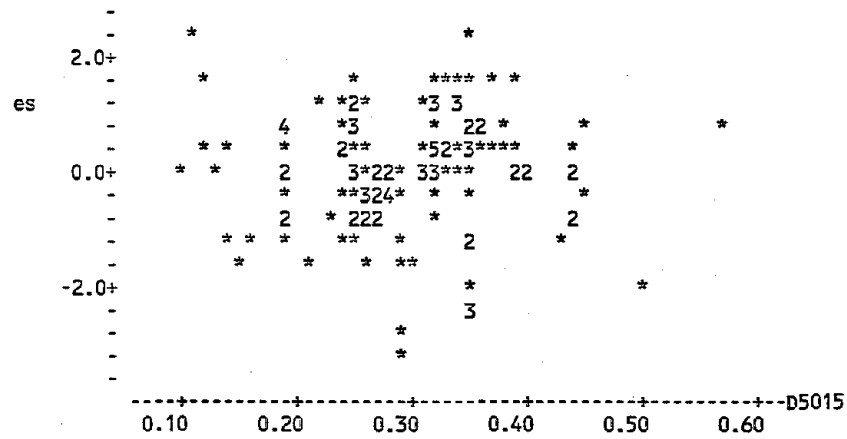
MTB > STANDARDIZED RESIDUAL PLOT FOR EQUATION 3.4.10



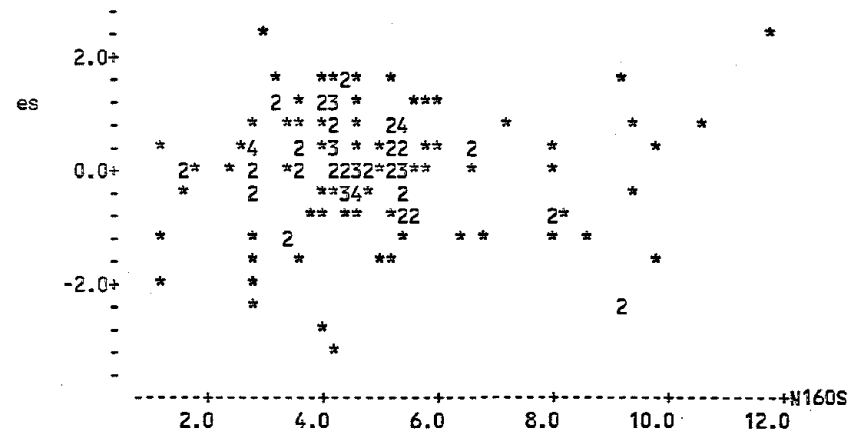
MTB > STANDARDIZED RESIDUAL PLOT FOR EQUATION 3.4.10



MTB > STANDARDIZED RESIDUAL PLOT FOR EQUATION 3.4.10



MTB > STANDARDIZED RESIDUAL PLOT FOR EQUATION 3.4.10



A2.2 Minitab Analysis for Equation 3.5.3

MINITAB OUTPUT FOR EQUATION 3.5.3 (GROUND SLOPE MODEL FOR NIIGATA AND NOSHIO, JAPAN)

MTB > REGRESS LOG DH ON 4 LOG S, T15, F15, D5015

The regression equation is

LOG DH = 0.698 + 0.378 LOG S + 0.0362 T15 - 0.0326 F15 - 0.929 D5015

Predictor	Coef	Stdev	t-ratio	p
Constant	0.69815	0.07338	9.51	0.000
LOG S	0.37764	0.03867	9.77	0.000
T15	0.036228	0.005179	7.00	0.000
F15	-0.032553	0.005333	-6.10	0.000
D5015	-0.9292	0.1921	-4.84	0.000

s = 0.1454 R-sq = 54.2% R-sq(adj) = 53.4%

Analysis of Variance

SOURCE	DF	SS	MS	F	P
Regression	4	5.6834	1.4208	67.17	0.000
Error	227	4.8020	0.0212		
Total	231	10.4854			

SOURCE	DF	SEQ SS
LOG S	1	4.4126
T15	1	0.3993
F15	1	0.3767
D5015	1	0.4947

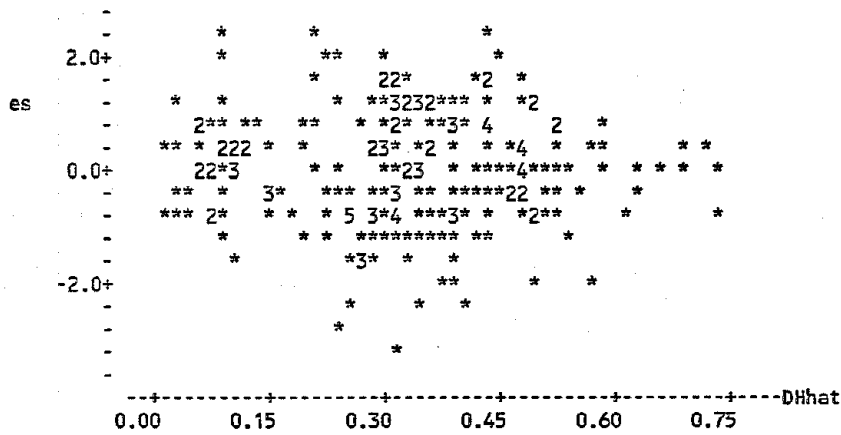
Unusual Observations

Obs.	LOG S	LOG DH	Fit	Stdev.Fit	Residual	St.Resid
24	-0.569	0.43933	0.09744	0.02427	0.34190	2.38R
66	-0.538	0.54407	0.20639	0.01746	0.33768	2.34R
127	-0.194	0.15229	0.09123	0.04319	0.06107	0.44 X
136	-0.268	-0.12494	0.24063	0.04560	-0.36557	-2.65RX
137	-0.149	0.35984	0.09675	0.05145	0.26308	1.93 X
138	-0.201	-0.10790	0.10074	0.04950	-0.20865	-1.53 X
139	-0.268	0.13033	0.15804	0.04586	-0.02770	-0.20 X
140	-0.201	-0.09690	0.24899	0.03116	-0.34589	-2.43R
155	-0.337	-0.00000	0.33848	0.01291	-0.33848	-2.34R
160	-0.268	0.30750	0.38944	0.05191	-0.08195	-0.60 X
164	0.100	0.77011	0.43267	0.01612	0.33744	2.33R
182	0.155	0.03742	0.40639	0.01979	-0.36897	-2.56R
191	0.316	0.26717	0.56833	0.02052	-0.30116	-2.09R
216	-0.208	-0.14874	0.31269	0.01883	-0.46144	-3.20R
226	-0.276	0.56349	0.24722	0.01702	0.31626	2.19R

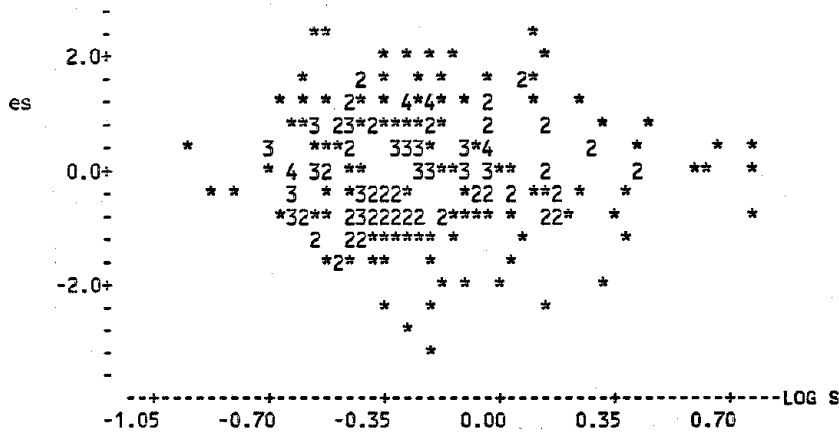
R denotes an obs. with a large st. resid.

X denotes an obs. whose X value gives it large influence.

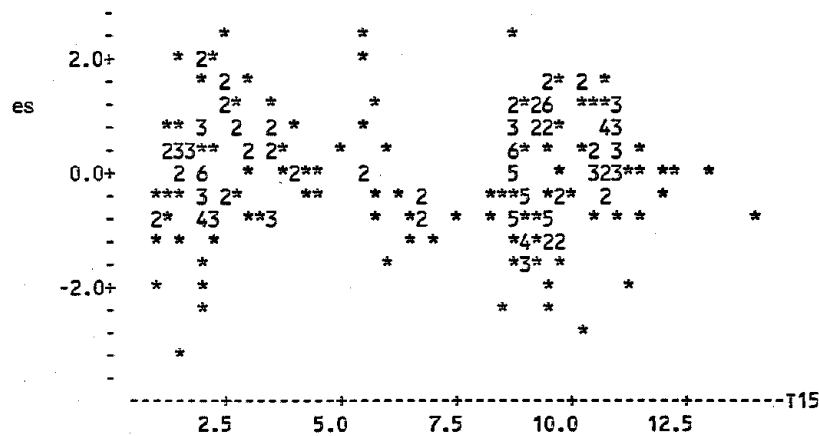
MTB > STANDARDIZED RESIDUAL PLOT FOR EQUATION 3.5.3



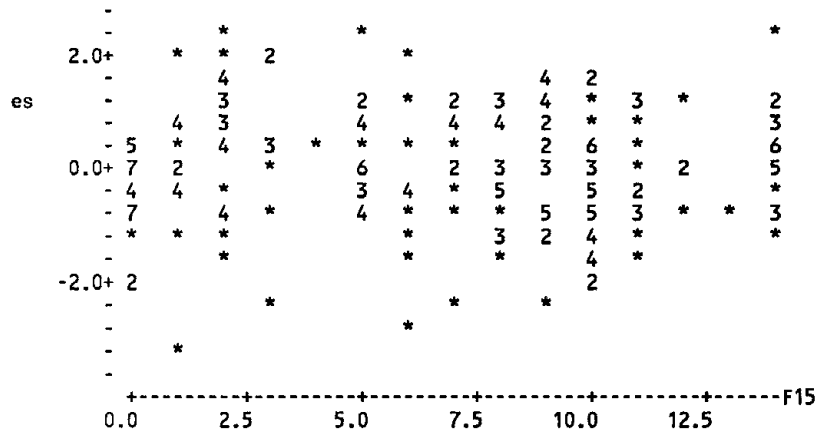
MTB > STANDARDIZED RESIDUAL PLOT FOR EQUATION 3.5.3



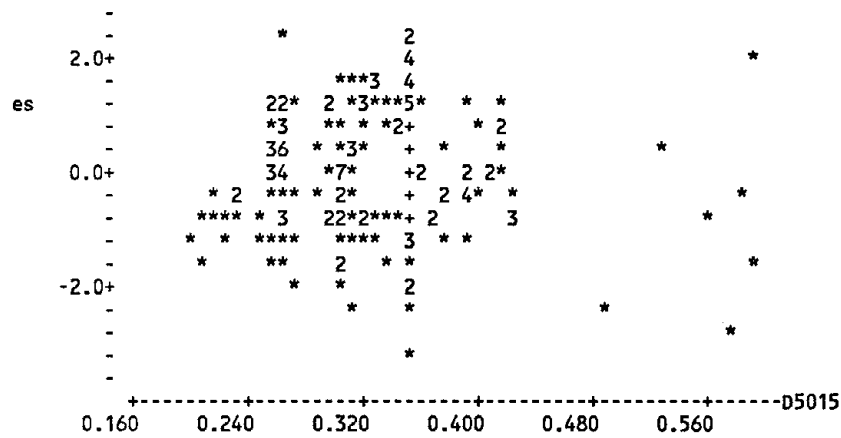
MTB > STANDARDIZED RESIDUAL PLOT FOR EQUATION 3.5.3



MTB > STANDARDIZED RESIDUAL PLOT FOR EQUATION 3.5.3



MTB > STANDARDIZED RESIDUAL PLOT FOR EQUATION 3.5.3



A2.3 Minitab Analysis for Equation 4.1.9

MINITAB OUTPUT FOR EQUATION 4.1.9 (COMBINED MODEL FOR U.S. AND JAPAN DATA)

MTB > REGRESS LOG(DH+0.01) ON 9 BOff, M, LOG R, R, LOG Wff, LOG Sgs,
LOG T15, LOG (100-F15), D5015

The regression equation is

LOG DH = - 15.8 - 0.579 BOff + 1.18 M - 0.927 LOG R - 0.0133 R + 0.657 LOG Wff
+ 0.429 LOG Sgs + 0.348 LOG T15 + 4.53 LOG(100-F15) - 0.922 D5015

Predictor	Coef	Stdev	t-ratio	p
Constant	-15.7869	0.4752	-33.22	0.000
BOff	-0.57884	0.04504	-12.85	0.000
M	1.17818	0.04274	27.57	0.000
LOG R	-0.92745	0.04819	-19.24	0.000
R	-0.013289	0.001231	-10.79	0.000
LOG Wff	0.65716	0.04570	14.38	0.000
LOG Sgs	0.42932	0.04484	9.57	0.000
LOG T15	0.34833	0.03140	11.09	0.000
LOG(100-F15)	4.5270	0.2005	22.58	0.000
D5015	-0.9223	0.1092	-8.45	0.000

s = 0.2086 R-sq = 82.6% R-sq(adj) = 82.3%

Analysis of Variance

SOURCE	DF	SS	MS	F	P
Regression	9	94.633	10.515	241.75	0.000
Error	457	19.877	0.043		
Total	466	114.510			

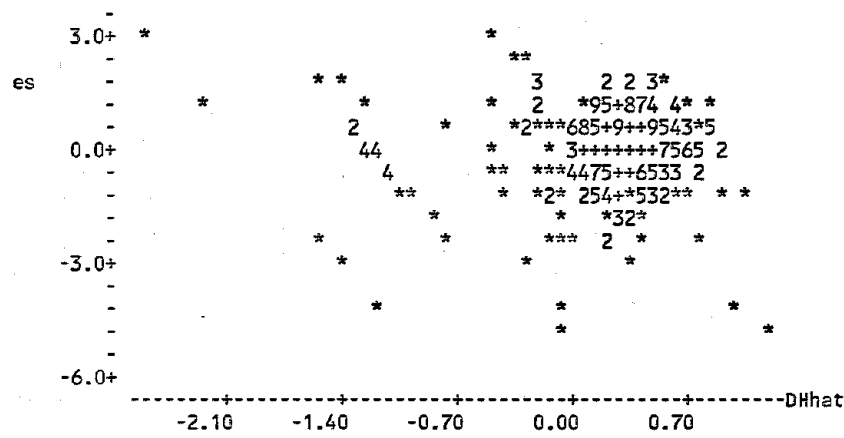
SOURCE	DF	SEQ SS
BOff	1	0.477
M	1	11.604
LOG R	1	13.880
R	1	28.419
LOG Wff	1	5.538
LOG Sgs	1	4.681
LOG T15	1	7.841
LOG(100-F15)	1	19.087
D5015	1	3.105

Unusual Observations

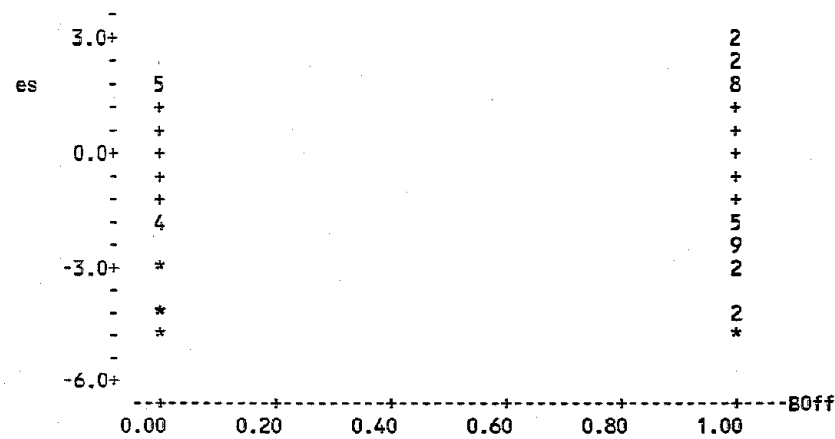
Obs.	BOff	LOG DH	Fit	Stdev.Fit	Residual	St.Resid
1	1.00	-0.03621	0.43331	0.04353	-0.46952	-2.30R
2	0.00	0.17898	1.16221	0.03632	-0.98323	-4.79R
3	0.00	0.17898	0.99455	0.02609	-0.81557	-3.94R
4	1.00	0.26482	0.74533	0.03425	-0.48051	-2.34R
5	1.00	0.13988	0.05827	0.07990	0.08161	0.42 X
6	1.00	0.28330	0.17724	0.10318	0.10606	0.59 X
7	1.00	0.26951	0.47337	0.10022	-0.20386	-1.11 X
8	1.00	0.19866	0.20391	0.11030	-0.00525	-0.03 X
9	0.00	-0.50864	-0.40477	0.08985	-0.10387	-0.55 X
10	0.00	-0.50864	-0.52308	0.08487	0.01444	0.08 X
11	0.00	0.38917	0.34106	0.09785	0.04811	0.26 X
12	1.00	-1.04576	-0.08657	0.03592	-0.95919	-4.67R
13	1.00	-0.53760	-0.07156	0.03604	-0.46604	-2.27R
33	1.00	-0.95861	-0.08889	0.03378	-0.86972	-4.23R
34	1.00	-0.58503	-0.11530	0.03467	-0.46973	-2.28R
35	0.00	0.22789	-0.17576	0.05433	0.40365	2.00RX
36	0.00	-0.28400	-0.17576	0.05433	-0.10824	-0.54 X
37	0.00	0.08991	-0.17576	0.05433	0.26567	1.32 X
38	0.00	0.22789	-0.17576	0.05433	0.40365	2.00RX
39	0.00	0.22789	-0.17576	0.05433	0.40365	2.00RX
40	0.00	-2.00000	-2.22700	0.08273	0.22700	1.19 X
41	0.00	-2.00000	-1.42365	0.05572	-0.57635	-2.87RX
42	1.00	-2.00000	-2.56716	0.09161	0.56716	3.03RX
43	1.00	-2.00000	-1.20942	0.05097	-0.79058	-3.91R
55	1.00	-0.50864	-0.03466	0.02983	-0.47398	-2.30R
68	1.00	-0.85387	-0.28663	0.02810	-0.56724	-2.74R
76	1.00	-0.95861	-1.37846	0.05107	0.41985	2.08R
77	1.00	-2.00000	-1.54092	0.04939	-0.45908	-2.27R
83	1.00	-0.37675	0.17807	0.02442	-0.55482	-2.68R
84	1.00	-0.25181	0.18622	0.02417	-0.43803	-2.11R
88	1.00	-0.27572	0.32843	0.01904	-0.60415	-2.91R
141	1.00	0.09691	-0.34849	0.03532	0.44540	2.17R
144	1.00	0.12057	-0.49544	0.04114	0.61601	3.01R
148	1.00	0.13988	-0.29364	0.04561	0.43352	2.13R
149	1.00	-0.05552	0.35687	0.04815	-0.41239	-2.03R
432	0.00	-0.14267	0.27199	0.02443	-0.41466	-2.00R
449	1.00	-1.22185	-0.74737	0.05403	-0.47448	-2.36RX
450	0.00	-1.22185	-1.33730	0.05470	0.11545	0.57 X
451	1.00	-1.22185	-1.21864	0.05780	-0.00321	-0.02 X
452	1.00	-1.22185	-1.19877	0.06710	-0.02308	-0.12 X
453	0.00	-1.22185	-1.24779	0.06019	0.02594	0.13 X
456	1.00	-1.22185	-1.34545	0.06456	0.12360	0.62 X
458	0.00	-1.22185	-1.12997	0.05941	-0.09188	-0.46 X
459	1.00	-1.22185	-1.25156	0.07015	0.02971	0.15 X

R denotes an obs. with a large st. resid.
X denotes an obs. whose X value gives it large influence.

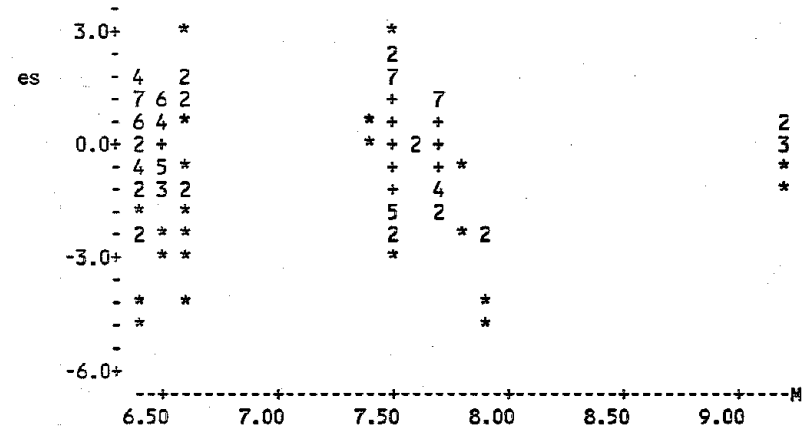
MTB > STANDARDIZED RESIDUAL PLOT FOR EQUATION 4.1.9



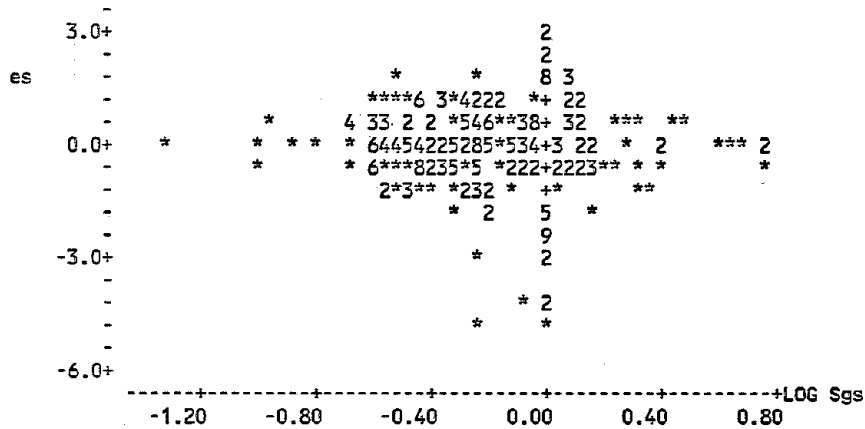
MTB > STANDARDIZED RESIDUAL PLOT FOR EQUATION 4.1.9



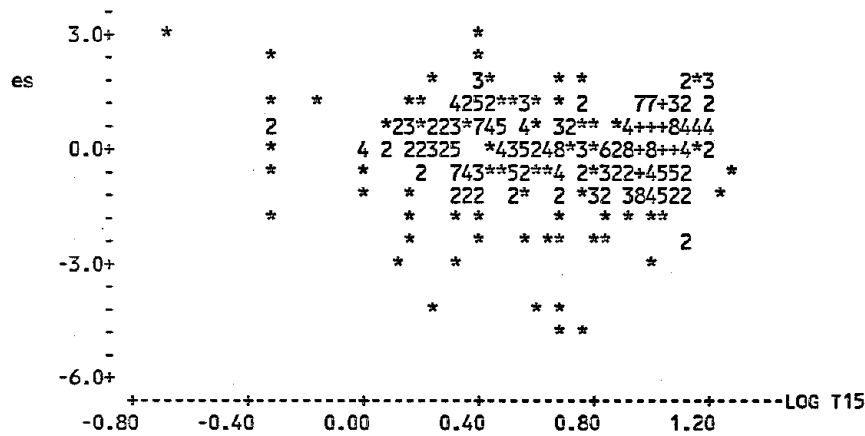
MTB > STANDARDIZED RESIDUAL PLOT FOR EQUATION 4.1.9



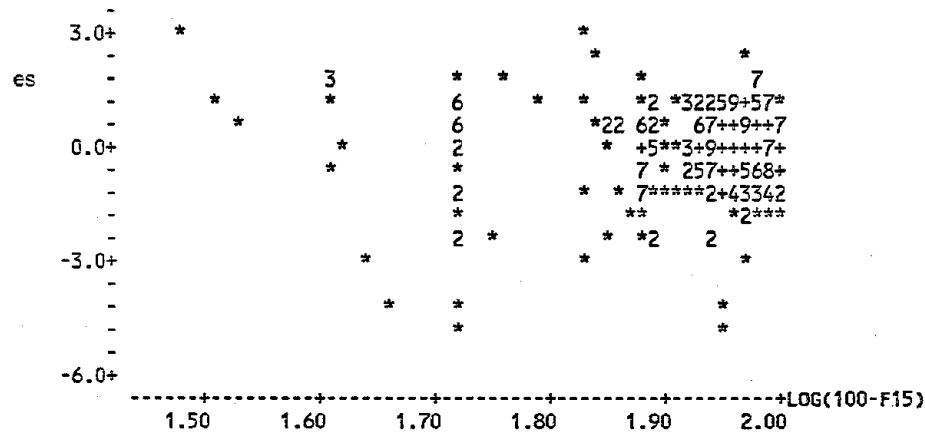
MTB > STANDARDIZED RESIDUAL PLOT FOR EQUATION 4.1.9



MTB > STANDARDIZED RESIDUAL PLOT FOR EQUATION 4.1.9



MTB > STANDARDIZED RESIDUAL PLOT FOR EQUATION 4.1.9



**NATIONAL CENTER FOR EARTHQUAKE ENGINEERING RESEARCH
LIST OF TECHNICAL REPORTS**

The National Center for Earthquake Engineering Research (NCEER) publishes technical reports on a variety of subjects related to earthquake engineering written by authors funded through NCEER. These reports are available from both NCEER's Publications Department and the National Technical Information Service (NTIS). Requests for reports should be directed to the Publications Department, National Center for Earthquake Engineering Research, State University of New York at Buffalo, Red Jacket Quadrangle, Buffalo, New York 14261. Reports can also be requested through NTIS, 5285 Port Royal Road, Springfield, Virginia 22161. NTIS accession numbers are shown in parenthesis, if available.

- NCEER-87-0001 "First-Year Program in Research, Education and Technology Transfer," 3/5/87, (PB88-134275/AS).
- NCEER-87-0002 "Experimental Evaluation of Instantaneous Optimal Algorithms for Structural Control," by R.C. Lin, T.T. Soong and A.M. Reinhorn, 4/20/87, (PB88-134341/AS).
- NCEER-87-0003 "Experimentation Using the Earthquake Simulation Facilities at University at Buffalo," by A.M. Reinhorn and R.L. Ketter, to be published.
- NCEER-87-0004 "The System Characteristics and Performance of a Shaking Table," by J.S. Hwang, K.C. Chang and G.C. Lee, 6/1/87, (PB88-134259/AS). This report is available only through NTIS (see address given above).
- NCEER-87-0005 "A Finite Element Formulation for Nonlinear Viscoplastic Material Using a Q Model," by O. Gyebe and G. Dasgupta, 11/2/87, (PB88-213764/AS).
- NCEER-87-0006 "Symbolic Manipulation Program (SMP) - Algebraic Codes for Two and Three Dimensional Finite Element Formulations," by X. Lee and G. Dasgupta, 11/9/87, (PB88-219522/AS).
- NCEER-87-0007 "Instantaneous Optimal Control Laws for Tall Buildings Under Seismic Excitations," by J.N. Yang, A. Akbarpour and P. Ghaemmaghami, 6/10/87, (PB88-134333/AS).
- NCEER-87-0008 "IDARC: Inelastic Damage Analysis of Reinforced Concrete Frame - Shear-Wall Structures," by Y.J. Park, A.M. Reinhorn and S.K. Kunnath, 7/20/87, (PB88-134325/AS).
- NCEER-87-0009 "Liquefaction Potential for New York State: A Preliminary Report on Sites in Manhattan and Buffalo," by M. Budhu, V. Vijayakumar, R.F. Giese and L. Baumgras, 8/31/87, (PB88-163704/AS). This report is available only through NTIS (see address given above).
- NCEER-87-0010 "Vertical and Torsional Vibration of Foundations in Inhomogeneous Media," by A.S. Veletsos and K.W. Dotson, 6/1/87, (PB88-134291/AS).
- NCEER-87-0011 "Seismic Probabilistic Risk Assessment and Seismic Margins Studies for Nuclear Power Plants," by Howard H.M. Hwang, 6/15/87, (PB88-134267/AS).
- NCEER-87-0012 "Parametric Studies of Frequency Response of Secondary Systems Under Ground-Acceleration Excitations," by Y. Yong and Y.K. Lin, 6/10/87, (PB88-134309/AS).
- NCEER-87-0013 "Frequency Response of Secondary Systems Under Seismic Excitation," by J.A. HoLung, J. Cai and Y.K. Lin, 7/31/87, (PB88-134317/AS).
- NCEER-87-0014 "Modelling Earthquake Ground Motions in Seismically Active Regions Using Parametric Time Series Methods," by G.W. Ellis and A.S. Cakmak, 8/25/87, (PB88-134283/AS).
- NCEER-87-0015 "Detection and Assessment of Seismic Structural Damage," by E. DiPasquale and A.S. Cakmak, 8/25/87, (PB88-163712/AS).

- NCEER-87-0016 "Pipeline Experiment at Parkfield, California," by J. Isenberg and E. Richardson, 9/15/87, (PB88-163720/AS). This report is available only through NTIS (see address given above).
- NCEER-87-0017 "Digital Simulation of Seismic Ground Motion," by M. Shinozuka, G. Deodatis and T. Harada, 8/31/87, (PB88-155197/AS). This report is available only through NTIS (see address given above).
- NCEER-87-0018 "Practical Considerations for Structural Control: System Uncertainty, System Time Delay and Truncation of Small Control Forces," J.N. Yang and A. Akbarpour, 8/10/87, (PB88-163738/AS).
- NCEER-87-0019 "Modal Analysis of Nonclassically Damped Structural Systems Using Canonical Transformation," by J.N. Yang, S. Sarkani and F.X. Long, 9/27/87, (PB88-187851/AS).
- NCEER-87-0020 "A Nonstationary Solution in Random Vibration Theory," by J.R. Red-Horse and P.D. Spanos, 11/3/87, (PB88-163746/AS).
- NCEER-87-0021 "Horizontal Impedances for Radially Inhomogeneous Viscoelastic Soil Layers," by A.S. Veletsos and K.W. Dotson, 10/15/87, (PB88-150859/AS).
- NCEER-87-0022 "Seismic Damage Assessment of Reinforced Concrete Members," by Y.S. Chung, C. Meyer and M. Shinozuka, 10/9/87, (PB88-150867/AS). This report is available only through NTIS (see address given above).
- NCEER-87-0023 "Active Structural Control in Civil Engineering," by T.T. Soong, 11/11/87, (PB88-187778/AS).
- NCEER-87-0024 "Vertical and Torsional Impedances for Radially Inhomogeneous Viscoelastic Soil Layers," by K.W. Dotson and A.S. Veletsos, 12/87, (PB88-187786/AS).
- NCEER-87-0025 "Proceedings from the Symposium on Seismic Hazards, Ground Motions, Soil-Liquefaction and Engineering Practice in Eastern North America," October 20-22, 1987, edited by K.H. Jacob, 12/87, (PB88-188115/AS).
- NCEER-87-0026 "Report on the Whittier-Narrows, California, Earthquake of October 1, 1987," by J. Pantelic and A. Reinhorn, 11/87, (PB88-187752/AS). This report is available only through NTIS (see address given above).
- NCEER-87-0027 "Design of a Modular Program for Transient Nonlinear Analysis of Large 3-D Building Structures," by S. Srivastav and J.F. Abel, 12/30/87, (PB88-187950/AS).
- NCEER-87-0028 "Second-Year Program in Research, Education and Technology Transfer," 3/8/88, (PB88-219480/AS).
- NCEER-88-0001 "Workshop on Seismic Computer Analysis and Design of Buildings With Interactive Graphics," by W. McGuire, J.F. Abel and C.H. Conley, 1/18/88, (PB88-187760/AS).
- NCEER-88-0002 "Optimal Control of Nonlinear Flexible Structures," by J.N. Yang, F.X. Long and D. Wong, 1/22/88, (PB88-213772/AS).
- NCEER-88-0003 "Substructuring Techniques in the Time Domain for Primary-Secondary Structural Systems," by G.D. Manolis and G. Juhn, 2/10/88, (PB88-213780/AS).
- NCEER-88-0004 "Iterative Seismic Analysis of Primary-Secondary Systems," by A. Singhal, L.D. Lutes and P.D. Spanos, 2/23/88, (PB88-213798/AS).
- NCEER-88-0005 "Stochastic Finite Element Expansion for Random Media," by P.D. Spanos and R. Ghanem, 3/14/88, (PB88-213806/AS).

- NCEER-88-0006 "Combining Structural Optimization and Structural Control," by F.Y. Cheng and C.P. Pantelides, 1/10/88, (PB88-213814/AS).
- NCEER-88-0007 "Seismic Performance Assessment of Code-Designed Structures," by H.H.-M. Hwang, J.-W. Jaw and H.-J. Shan, 3/20/88, (PB88-219423/AS).
- NCEER-88-0008 "Reliability Analysis of Code-Designed Structures Under Natural Hazards," by H.H.-M. Hwang, H. Ushiba and M. Shinozuka, 2/29/88, (PB88-229471/AS).
- NCEER-88-0009 "Seismic Fragility Analysis of Shear Wall Structures," by J.-W. Jaw and H.H.-M. Hwang, 4/30/88, (PB89-102867/AS).
- NCEER-88-0010 "Base Isolation of a Multi-Story Building Under a Harmonic Ground Motion - A Comparison of Performances of Various Systems," by F.-G. Fan, G. Ahmadi and I.G. Tadjbakhsh, 5/18/88, (PB89-122238/AS).
- NCEER-88-0011 "Seismic Floor Response Spectra for a Combined System by Green's Functions," by F.M. Lavelle, L.A. Bergman and P.D. Spanos, 5/1/88, (PB89-102875/AS).
- NCEER-88-0012 "A New Solution Technique for Randomly Excited Hysteretic Structures," by G.Q. Cai and Y.K. Lin, 5/16/88, (PB89-102883/AS).
- NCEER-88-0013 "A Study of Radiation Damping and Soil-Structure Interaction Effects in the Centrifuge," by K. Weissman, supervised by J.H. Prevost, 5/24/88, (PB89-144703/AS).
- NCEER-88-0014 "Parameter Identification and Implementation of a Kinematic Plasticity Model for Frictional Soils," by J.H. Prevost and D.V. Griffiths, to be published.
- NCEER-88-0015 "Two- and Three- Dimensional Dynamic Finite Element Analyses of the Long Valley Dam," by D.V. Griffiths and J.H. Prevost, 6/17/88, (PB89-144711/AS).
- NCEER-88-0016 "Damage Assessment of Reinforced Concrete Structures in Eastern United States," by A.M. Reinhorn, M.J. Seidel, S.K. Kunnath and Y.J. Park, 6/15/88, (PB89-122220/AS).
- NCEER-88-0017 "Dynamic Compliance of Vertically Loaded Strip Foundations in Multilayered Viscoelastic Soils," by S. Ahmad and A.S.M. Israil, 6/17/88, (PB89-102891/AS).
- NCEER-88-0018 "An Experimental Study of Seismic Structural Response With Added Viscoelastic Dampers," by R.C. Lin, Z. Liang, T.T. Soong and R.H. Zhang, 6/30/88, (PB89-122212/AS). This report is available only through NTIS (see address given above).
- NCEER-88-0019 "Experimental Investigation of Primary - Secondary System Interaction," by G.D. Manolis, G. Juhn and A.M. Reinhorn, 5/27/88, (PB89-122204/AS).
- NCEER-88-0020 "A Response Spectrum Approach For Analysis of Nonclassically Damped Structures," by J.N. Yang, S. Sarkani and F.X. Long, 4/22/88, (PB89-102909/AS).
- NCEER-88-0021 "Seismic Interaction of Structures and Soils: Stochastic Approach," by A.S. Veletsos and A.M. Prasad, 7/21/88, (PB89-122196/AS).
- NCEER-88-0022 "Identification of the Serviceability Limit State and Detection of Seismic Structural Damage," by E. DiPasquale and A.S. Cakmak, 6/15/88, (PB89-122188/AS). This report is available only through NTIS (see address given above).
- NCEER-88-0023 "Multi-Hazard Risk Analysis: Case of a Simple Offshore Structure," by B.K. Bhartia and E.H. Vanmarcke, 7/21/88, (PB89-145213/AS).

- NCEER-88-0024 "Automated Seismic Design of Reinforced Concrete Buildings," by Y.S. Chung, C. Meyer and M. Shinozuka, 7/5/88, (PB89-122170/AS). This report is available only through NTIS (see address given above).
- NCEER-88-0025 "Experimental Study of Active Control of MDOF Structures Under Seismic Excitations," by L.L. Chung, R.C. Lin, T.T. Soong and A.M. Reinhorn, 7/10/88, (PB89-122600/AS).
- NCEER-88-0026 "Earthquake Simulation Tests of a Low-Rise Metal Structure," by J.S. Hwang, K.C. Chang, G.C. Lee and R.L. Ketter, 8/1/88, (PB89-102917/AS).
- NCEER-88-0027 "Systems Study of Urban Response and Reconstruction Due to Catastrophic Earthquakes," by F. Kozin and H.K. Zhou, 9/22/88, (PB90-162348/AS).
- NCEER-88-0028 "Seismic Fragility Analysis of Plane Frame Structures," by H.H.-M. Hwang and Y.K. Low, 7/31/88, (PB89-131445/AS).
- NCEER-88-0029 "Response Analysis of Stochastic Structures," by A. Kardara, C. Bucher and M. Shinozuka, 9/22/88, (PB89-174429/AS).
- NCEER-88-0030 "Nonnormal Accelerations Due to Yielding in a Primary Structure," by D.C.K. Chen and L.D. Lutes, 9/19/88, (PB89-131437/AS).
- NCEER-88-0031 "Design Approaches for Soil-Structure Interaction," by A.S. Veletsos, A.M. Prasad and Y. Tang, 12/30/88, (PB89-174437/AS). This report is available only through NTIS (see address given above).
- NCEER-88-0032 "A Re-evaluation of Design Spectra for Seismic Damage Control," by C.J. Turkstra and A.G. Tallin, 11/7/88, (PB89-145221/AS).
- NCEER-88-0033 "The Behavior and Design of Noncontact Lap Splices Subjected to Repeated Inelastic Tensile Loading," by V.E. Sagan, P. Gergely and R.N. White, 12/8/88, (PB89-163737/AS).
- NCEER-88-0034 "Seismic Response of Pile Foundations," by S.M. Mamoon, P.K. Banerjee and S. Ahmad, 11/1/88, (PB89-145239/AS).
- NCEER-88-0035 "Modeling of R/C Building Structures With Flexible Floor Diaphragms (IDARC2)," by A.M. Reinhorn, S.K. Kunnath and N. Panahshahi, 9/7/88, (PB89-207153/AS).
- NCEER-88-0036 "Solution of the Dam-Reservoir Interaction Problem Using a Combination of FEM, BEM with Particular Integrals, Modal Analysis, and Substructuring," by C-S. Tsai, G.C. Lee and R.L. Ketter, 12/31/88, (PB89-207146/AS).
- NCEER-88-0037 "Optimal Placement of Actuators for Structural Control," by F.Y. Cheng and C.P. Pantelides, 8/15/88, (PB89-162846/AS).
- NCEER-88-0038 "Teflon Bearings in Aseismic Base Isolation: Experimental Studies and Mathematical Modeling," by A. Mokha, M.C. Constantinou and A.M. Reinhorn, 12/5/88, (PB89-218457/AS). This report is available only through NTIS (see address given above).
- NCEER-88-0039 "Seismic Behavior of Flat Slab High-Rise Buildings in the New York City Area," by P. Weidlinger and M. Ettouney, 10/15/88, (PB90-145681/AS).
- NCEER-88-0040 "Evaluation of the Earthquake Resistance of Existing Buildings in New York City," by P. Weidlinger and M. Ettouney, 10/15/88, to be published.
- NCEER-88-0041 "Small-Scale Modeling Techniques for Reinforced Concrete Structures Subjected to Seismic Loads," by W. Kim, A. El-Attar and R.N. White, 11/22/88, (PB89-189625/AS).

- NCEER-88-0042 "Modeling Strong Ground Motion from Multiple Event Earthquakes," by G.W. Ellis and A.S. Cakmak, 10/15/88, (PB89-174445/AS).
- NCEER-88-0043 "Nonstationary Models of Seismic Ground Acceleration," by M. Grigoriu, S.E. Ruiz and E. Rosenblueth, 7/15/88, (PB89-189617/AS).
- NCEER-88-0044 "SARCF User's Guide: Seismic Analysis of Reinforced Concrete Frames," by Y.S. Chung, C. Meyer and M. Shinozuka, 11/9/88, (PB89-174452/AS).
- NCEER-88-0045 "First Expert Panel Meeting on Disaster Research and Planning," edited by J. Pantelic and J. Stoyke, 9/15/88, (PB89-174460/AS).
- NCEER-88-0046 "Preliminary Studies of the Effect of Degrading Infill Walls on the Nonlinear Seismic Response of Steel Frames," by C.Z. Chrysostomou, P. Gergely and J.F. Abel, 12/19/88, (PB89-208383/AS).
- NCEER-88-0047 "Reinforced Concrete Frame Component Testing Facility - Design, Construction, Instrumentation and Operation," by S.P. Pessiki, C. Conley, T. Bond, P. Gergely and R.N. White, 12/16/88, (PB89-174478/AS).
- NCEER-89-0001 "Effects of Protective Cushion and Soil Compliancy on the Response of Equipment Within a Seismically Excited Building," by J.A. HoLung, 2/16/89, (PB89-207179/AS).
- NCEER-89-0002 "Statistical Evaluation of Response Modification Factors for Reinforced Concrete Structures," by H.H-M. Hwang and J-W. Jaw, 2/17/89, (PB89-207187/AS).
- NCEER-89-0003 "Hysteretic Columns Under Random Excitation," by G-Q. Cai and Y.K. Lin, 1/9/89, (PB89-196513/AS).
- NCEER-89-0004 "Experimental Study of 'Elephant Foot Bulge' Instability of Thin-Walled Metal Tanks," by Z-H. Jia and R.L. Ketter, 2/22/89, (PB89-207195/AS).
- NCEER-89-0005 "Experiment on Performance of Buried Pipelines Across San Andreas Fault," by J. Isenberg, E. Richardson and T.D. O'Rourke, 3/10/89, (PB89-218440/AS).
- NCEER-89-0006 "A Knowledge-Based Approach to Structural Design of Earthquake-Resistant Buildings," by M. Subramani, P. Gergely, C.H. Conley, J.F. Abel and A.H. Zaghw, 1/15/89, (PB89-218465/AS).
- NCEER-89-0007 "Liquefaction Hazards and Their Effects on Buried Pipelines," by T.D. O'Rourke and P.A. Lane, 2/1/89, (PB89-218481).
- NCEER-89-0008 "Fundamentals of System Identification in Structural Dynamics," by H. Imai, C-B. Yun, O. Maruyama and M. Shinozuka, 1/26/89, (PB89-207211/AS).
- NCEER-89-0009 "Effects of the 1985 Michoacan Earthquake on Water Systems and Other Buried Lifelines in Mexico," by A.G. Ayala and M.J. O'Rourke, 3/8/89, (PB89-207229/AS).
- NCEER-89-R010 "NCEER Bibliography of Earthquake Education Materials," by K.E.K. Ross, Second Revision, 9/1/89, (PB90-125352/AS).
- NCEER-89-0011 "Inelastic Three-Dimensional Response Analysis of Reinforced Concrete Building Structures (IDARC-3D), Part I - Modeling," by S.K. Kunnath and A.M. Reinhorn, 4/17/89, (PB90-114612/AS).
- NCEER-89-0012 "Recommended Modifications to ATC-14," by C.D. Poland and J.O. Malley, 4/12/89, (PB90-108648/AS).
- NCEER-89-0013 "Repair and Strengthening of Beam-to-Column Connections Subjected to Earthquake Loading," by M. Corazao and A.J. Durrani, 2/28/89, (PB90-109885/AS).

- NCEER-89-0014 "Program EXKAL2 for Identification of Structural Dynamic Systems," by O. Maruyama, C-B. Yun, M. Hoshiya and M. Shinozuka, 5/19/89, (PB90-109877/AS).
- NCEER-89-0015 "Response of Frames With Bolted Semi-Rigid Connections, Part I - Experimental Study and Analytical Predictions," by P.J. DiCorso, A.M. Reinhorn, J.R. Dickerson, J.B. Radzinski and W.L. Harper, 6/1/89, to be published.
- NCEER-89-0016 "ARMA Monte Carlo Simulation in Probabilistic Structural Analysis," by P.D. Spanos and M.P. Mignolet, 7/10/89, (PB90-109893/AS).
- NCEER-89-P017 "Preliminary Proceedings from the Conference on Disaster Preparedness - The Place of Earthquake Education in Our Schools," Edited by K.E.K. Ross, 6/23/89.
- NCEER-89-0017 "Proceedings from the Conference on Disaster Preparedness - The Place of Earthquake Education in Our Schools," Edited by K.E.K. Ross, 12/31/89, (PB90-207895). This report is available only through NTIS (see address given above).
- NCEER-89-0018 "Multidimensional Models of Hysteretic Material Behavior for Vibration Analysis of Shape Memory Energy Absorbing Devices, by E.J. Graesser and F.A. Cozzarelli, 6/7/89, (PB90-164146/AS).
- NCEER-89-0019 "Nonlinear Dynamic Analysis of Three-Dimensional Base Isolated Structures (3D-BASIS)," by S. Nagarajaiah, A.M. Reinhorn and M.C. Constantinou, 8/3/89, (PB90-161936/AS). This report is available only through NTIS (see address given above).
- NCEER-89-0020 "Structural Control Considering Time-Rate of Control Forces and Control Rate Constraints," by F.Y. Cheng and C.P. Pantelides, 8/3/89, (PB90-120445/AS).
- NCEER-89-0021 "Subsurface Conditions of Memphis and Shelby County," by K.W. Ng, T-S. Chang and H-H.M. Hwang, 7/26/89, (PB90-120437/AS).
- NCEER-89-0022 "Seismic Wave Propagation Effects on Straight Jointed Buried Pipelines," by K. Elhadi and M.J. O'Rourke, 8/24/89, (PB90-162322/AS).
- NCEER-89-0023 "Workshop on Serviceability Analysis of Water Delivery Systems," edited by M. Grigoriu, 3/6/89, (PB90-127424/AS).
- NCEER-89-0024 "Shaking Table Study of a 1/5 Scale Steel Frame Composed of Tapered Members," by K.C. Chang, J.S. Hwang and G.C. Lee, 9/18/89, (PB90-160169/AS).
- NCEER-89-0025 "DYNA1D: A Computer Program for Nonlinear Seismic Site Response Analysis - Technical Documentation," by Jean H. Prevost, 9/14/89, (PB90-161944/AS). This report is available only through NTIS (see address given above).
- NCEER-89-0026 "1:4 Scale Model Studies of Active Tendon Systems and Active Mass Dampers for Aseismic Protection," by A.M. Reinhorn, T.T. Soong, R.C. Lin, Y.P. Yang, Y. Fukao, H. Abe and M. Nakai, 9/15/89, (PB90-173246/AS).
- NCEER-89-0027 "Scattering of Waves by Inclusions in a Nonhomogeneous Elastic Half Space Solved by Boundary Element Methods," by P.K. Hadley, A. Askar and A.S. Cakmak, 6/15/89, (PB90-145699/AS).
- NCEER-89-0028 "Statistical Evaluation of Deflection Amplification Factors for Reinforced Concrete Structures," by H.H.M. Hwang, J-W. Jaw and A.L. Ch'ng, 8/31/89, (PB90-164633/AS).
- NCEER-89-0029 "Bedrock Accelerations in Memphis Area Due to Large New Madrid Earthquakes," by H.H.M. Hwang, C.H.S. Chen and G. Yu, 11/7/89, (PB90-162330/AS).

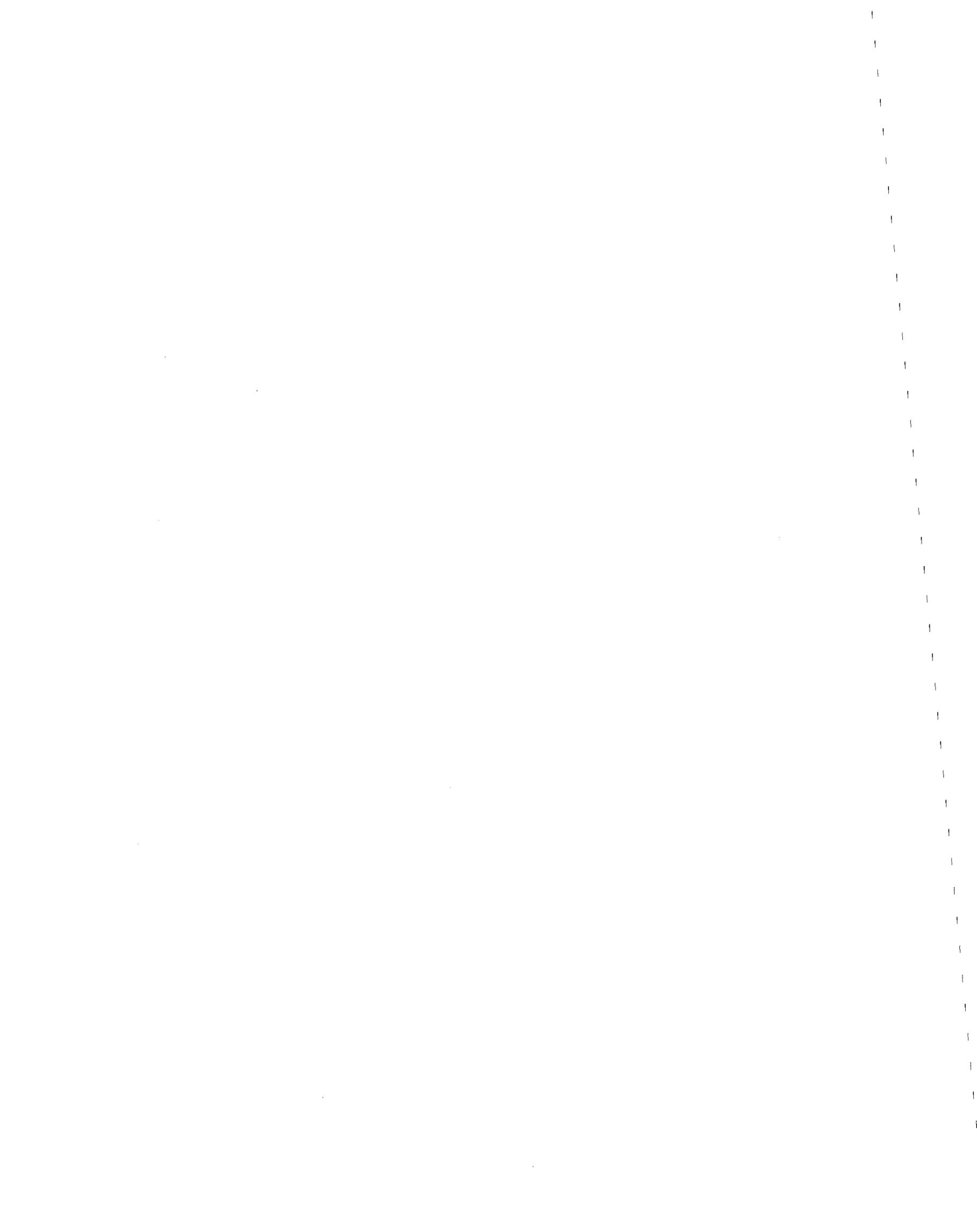
- NCEER-89-0030 "Seismic Behavior and Response Sensitivity of Secondary Structural Systems," by Y.Q. Chen and T.T. Soong, 10/23/89, (PB90-164658/AS).
- NCEER-89-0031 "Random Vibration and Reliability Analysis of Primary-Secondary Structural Systems," by Y. Ibrahim, M. Grigoriu and T.T. Soong, 11/10/89, (PB90-161951/AS).
- NCEER-89-0032 "Proceedings from the Second U.S. - Japan Workshop on Liquefaction, Large Ground Deformation and Their Effects on Lifelines, September 26-29, 1989," Edited by T.D. O'Rourke and M. Hamada, 12/1/89, (PB90-209388/AS).
- NCEER-89-0033 "Deterministic Model for Seismic Damage Evaluation of Reinforced Concrete Structures," by J.M. Bracci, A.M. Reinhorn, J.B. Mander and S.K. Kunnath, 9/27/89.
- NCEER-89-0034 "On the Relation Between Local and Global Damage Indices," by E. DiPasquale and A.S. Cakmak, 8/15/89, (PB90-173865).
- NCEER-89-0035 "Cyclic Undrained Behavior of Nonplastic and Low Plasticity Silts," by A.J. Walker and H.E. Stewart, 7/26/89, (PB90-183518/AS).
- NCEER-89-0036 "Liquefaction Potential of Surficial Deposits in the City of Buffalo, New York," by M. Budhu, R. Giese and L. Baumgrass, 1/17/89, (PB90-208455/AS).
- NCEER-89-0037 "A Deterministic Assessment of Effects of Ground Motion Incoherence," by A.S. Veletsos and Y. Tang, 7/15/89, (PB90-164294/AS).
- NCEER-89-0038 "Workshop on Ground Motion Parameters for Seismic Hazard Mapping," July 17-18, 1989, edited by R.V. Whitman, 12/1/89, (PB90-173923/AS).
- NCEER-89-0039 "Seismic Effects on Elevated Transit Lines of the New York City Transit Authority," by C.J. Costantino, C.A. Miller and E. Heymsfield, 12/26/89, (PB90-207887/AS).
- NCEER-89-0040 "Centrifugal Modeling of Dynamic Soil-Structure Interaction," by K. Weissman, Supervised by J.H. Prevost, 5/10/89, (PB90-207879/AS).
- NCEER-89-0041 "Linearized Identification of Buildings With Cores for Seismic Vulnerability Assessment," by I-K. Ho and A.E. Aktan, 11/1/89, (PB90-251943/AS).
- NCEER-90-0001 "Geotechnical and Lifeline Aspects of the October 17, 1989 Loma Prieta Earthquake in San Francisco," by T.D. O'Rourke, H.E. Stewart, F.T. Blackburn and T.S. Dickerman, 1/90, (PB90-208596/AS).
- NCEER-90-0002 "Nonnormal Secondary Response Due to Yielding in a Primary Structure," by D.C.K. Chen and L.D. Lutes, 2/28/90, (PB90-251976/AS).
- NCEER-90-0003 "Earthquake Education Materials for Grades K-12," by K.E.K. Ross, 4/16/90, (PB91-113415/AS).
- NCEER-90-0004 "Catalog of Strong Motion Stations in Eastern North America," by R.W. Busby, 4/3/90, (PB90-251984)/AS.
- NCEER-90-0005 "NCEER Strong-Motion Data Base: A User Manual for the GeoBase Release (Version 1.0 for the Sun3)," by P. Friberg and K. Jacob, 3/31/90 (PB90-258062/AS).
- NCEER-90-0006 "Seismic Hazard Along a Crude Oil Pipeline in the Event of an 1811-1812 Type New Madrid Earthquake," by H.H.M. Hwang and C-H.S. Chen, 4/16/90(PB90-258054).
- NCEER-90-0007 "Site-Specific Response Spectra for Memphis Sheahan Pumping Station," by H.H.M. Hwang and C.S. Lee, 5/15/90, (PB91-108811/AS).

- NCEER-90-0008 "Pilot Study on Seismic Vulnerability of Crude Oil Transmission Systems," by T. Ariman, R. Dobry, M. Grigoriu, F. Kozin, M. O'Rourke, T. O'Rourke and M. Shinozuka, 5/25/90, (PB91-108837/AS).
- NCEER-90-0009 "A Program to Generate Site Dependent Time Histories: EQGEN," by G.W. Ellis, M. Srinivasan and A.S. Cakmak, 1/30/90, (PB91-108829/AS).
- NCEER-90-0010 "Active Isolation for Seismic Protection of Operating Rooms," by M.E. Talbott, Supervised by M. Shinozuka, 6/8/9, (PB91-110205/AS).
- NCEER-90-0011 "Program LINEARID for Identification of Linear Structural Dynamic Systems," by C-B. Yun and M. Shinozuka, 6/25/90, (PB91-110312/AS).
- NCEER-90-0012 "Two-Dimensional Two-Phase Elasto-Plastic Seismic Response of Earth Dams," by A.N. Yiagos, Supervised by J.H. Prevost, 6/20/90, (PB91-110197/AS).
- NCEER-90-0013 "Secondary Systems in Base-Isolated Structures: Experimental Investigation, Stochastic Response and Stochastic Sensitivity," by G.D. Manolis, G. Juhn, M.C. Constantinou and A.M. Reinhorn, 7/1/90, (PB91-110320/AS).
- NCEER-90-0014 "Seismic Behavior of Lightly-Reinforced Concrete Column and Beam-Column Joint Details," by S.P. Pessiki, C.H. Conley, P. Gergely and R.N. White, 8/22/90, (PB91-108795/AS).
- NCEER-90-0015 "Two Hybrid Control Systems for Building Structures Under Strong Earthquakes," by J.N. Yang and A. Danielians, 6/29/90, (PB91-125393/AS).
- NCEER-90-0016 "Instantaneous Optimal Control with Acceleration and Velocity Feedback," by J.N. Yang and Z. Li, 6/29/90, (PB91-125401/AS).
- NCEER-90-0017 "Reconnaissance Report on the Northern Iran Earthquake of June 21, 1990," by M. Mehrain, 10/4/90, (PB91-125377/AS).
- NCEER-90-0018 "Evaluation of Liquefaction Potential in Memphis and Shelby County," by T.S. Chang, P.S. Tang, C.S. Lee and H. Hwang, 8/10/90, (PB91-125427/AS).
- NCEER-90-0019 "Experimental and Analytical Study of a Combined Sliding Disc Bearing and Helical Steel Spring Isolation System," by M.C. Constantinou, A.S. Mokha and A.M. Reinhorn, 10/4/90, (PB91-125385/AS).
- NCEER-90-0020 "Experimental Study and Analytical Prediction of Earthquake Response of a Sliding Isolation System with a Spherical Surface," by A.S. Mokha, M.C. Constantinou and A.M. Reinhorn, 10/11/90, (PB91-125419/AS).
- NCEER-90-0021 "Dynamic Interaction Factors for Floating Pile Groups," by G. Gazetas, K. Fan, A. Kaynia and E. Kausel, 9/10/90, (PB91-170381/AS).
- NCEER-90-0022 "Evaluation of Seismic Damage Indices for Reinforced Concrete Structures," by S. Rodriguez-Gomez and A.S. Cakmak, 9/30/90, PB91-171322/AS).
- NCEER-90-0023 "Study of Site Response at a Selected Memphis Site," by H. Desai, S. Ahmad, E.S. Gazetas and M.R. Oh, 10/11/90, (PB91-196857/AS).
- NCEER-90-0024 "A User's Guide to Strongmo: Version 1.0 of NCEER's Strong-Motion Data Access Tool for PCs and Terminals," by P.A. Friberg and C.A.T. Susch, 11/15/90, (PB91-171272/AS).
- NCEER-90-0025 "A Three-Dimensional Analytical Study of Spatial Variability of Seismic Ground Motions," by L-L. Hong and A.H.-S. Ang, 10/30/90, (PB91-170399/AS).

- NCEER-90-0026 "MUMOID User's Guide - A Program for the Identification of Modal Parameters," by S. Rodriguez-Gomez and E. DiPasquale, 9/30/90, (PB91-171298/AS).
- NCEER-90-0027 "SARCF-II User's Guide - Seismic Analysis of Reinforced Concrete Frames," by S. Rodriguez-Gomez, Y.S. Chung and C. Meyer, 9/30/90, (PB91-171280/AS).
- NCEER-90-0028 "Viscous Dampers: Testing, Modeling and Application in Vibration and Seismic Isolation," by N. Makris and M.C. Constantinou, 12/20/90 (PB91-190561/AS).
- NCEER-90-0029 "Soil Effects on Earthquake Ground Motions in the Memphis Area," by H. Hwang, C.S. Lee, K.W. Ng and T.S. Chang, 8/2/90, (PB91-190751/AS).
- NCEER-91-0001 "Proceedings from the Third Japan-U.S. Workshop on Earthquake Resistant Design of Lifeline Facilities and Countermeasures for Soil Liquefaction, December 17-19, 1990," edited by T.D. O'Rourke and M. Hamada, 2/1/91, (PB91-179259/AS).
- NCEER-91-0002 "Physical Space Solutions of Non-Proportionally Damped Systems," by M. Tong, Z. Liang and G.C. Lee, 1/15/91, (PB91-179242/AS).
- NCEER-91-0003 "Seismic Response of Single Piles and Pile Groups," by K. Fan and G. Gazetas, 1/10/91, (PB92-174994/AS).
- NCEER-91-0004 "Damping of Structures: Part I - Theory of Complex Damping," by Z. Liang and G. Lee, 10/10/91, (PB92-197235/AS).
- NCEER-91-0005 "3D-BASIS - Nonlinear Dynamic Analysis of Three Dimensional Base Isolated Structures: Part II," by S. Nagarajaiah, A.M. Reinhorn and M.C. Constantinou, 2/28/91, (PB91-190553/AS).
- NCEER-91-0006 "A Multidimensional Hysteretic Model for Plasticity Deforming Metals in Energy Absorbing Devices," by E.J. Graesser and F.A. Cozzarelli, 4/9/91, (PB92-108364/AS).
- NCEER-91-0007 "A Framework for Customizable Knowledge-Based Expert Systems with an Application to a KBES for Evaluating the Seismic Resistance of Existing Buildings," by E.G. Ibarra-Anaya and S.J. Fenves, 4/9/91, (PB91-210930/AS).
- NCEER-91-0008 "Nonlinear Analysis of Steel Frames with Semi-Rigid Connections Using the Capacity Spectrum Method," by G.G. Deierlein, S-H. Hsieh, Y-J. Shen and J.F. Abel, 7/2/91, (PB92-113828/AS).
- NCEER-91-0009 "Earthquake Education Materials for Grades K-12," by K.E.K. Ross, 4/30/91, (PB91-212142/AS).
- NCEER-91-0010 "Phase Wave Velocities and Displacement Phase Differences in a Harmonically Oscillating Pile," by N. Makris and G. Gazetas, 7/8/91, (PB92-108356/AS).
- NCEER-91-0011 "Dynamic Characteristics of a Full-Size Five-Story Steel Structure and a 2/5 Scale Model," by K.C. Chang, G.C. Yao, G.C. Lee, D.S. Hao and Y.C. Yeh," 7/2/91.
- NCEER-91-0012 "Seismic Response of a 2/5 Scale Steel Structure with Added Viscoelastic Dampers," by K.C. Chang, T.T. Soong, S-T. Oh and M.L. Lai, 5/17/91 (PB92-110816/AS).
- NCEER-91-0013 "Earthquake Response of Retaining Walls; Full-Scale Testing and Computational Modeling," by S. Alampalli and A-W.M. Elgarnal, 6/20/91, to be published.
- NCEER-91-0014 "3D-BASIS-M: Nonlinear Dynamic Analysis of Multiple Building Base Isolated Structures," by P.C. Tsopelas, S. Nagarajaiah, M.C. Constantinou and A.M. Reinhorn, 5/28/91, (PB92-113885/AS).

- NCEER-91-0015 "Evaluation of SEAOC Design Requirements for Sliding Isolated Structures," by D. Theodossiou and M.C. Constantinou, 6/10/91, (PB92-114602/AS).
- NCEER-91-0016 "Closed-Loop Modal Testing of a 27-Story Reinforced Concrete Flat Plate-Core Building," by H.R. Somaprasad, T. Toksoy, H. Yoshiyuki and A.E. Aktan, 7/15/91, (PB92-129980/AS).
- NCEER-91-0017 "Shake Table Test of a 1/6 Scale Two-Story Lightly Reinforced Concrete Building," by A.G. El-Attar, R.N. White and P. Gergely, 2/28/91, (PB92-222447/AS).
- NCEER-91-0018 "Shake Table Test of a 1/8 Scale Three-Story Lightly Reinforced Concrete Building," by A.G. El-Attar, R.N. White and P. Gergely, 2/28/91.
- NCEER-91-0019 "Transfer Functions for Rigid Rectangular Foundations," by A.S. Veletsos, A.M. Prasad and W.H. Wu, 7/31/91.
- NCEER-91-0020 "Hybrid Control of Seismic-Excited Nonlinear and Inelastic Structural Systems," by J.N. Yang, Z. Li and A. Danielians, 8/1/91, (PB92-143171/AS).
- NCEER-91-0021 "The NCEER-91 Earthquake Catalog: Improved Intensity-Based Magnitudes and Recurrence Relations for U.S. Earthquakes East of New Madrid," by L. Seeber and J.G. Armbruster, 8/28/91, (PB92-176742/AS).
- NCEER-91-0022 "Proceedings from the Implementation of Earthquake Planning and Education in Schools: The Need for Change - The Roles of the Changemakers," by K.E.K. Ross and F. Winslow, 7/23/91, (PB92-129998/AS).
- NCEER-91-0023 "A Study of Reliability-Based Criteria for Seismic Design of Reinforced Concrete Frame Buildings," by H.H.M. Hwang and H-M. Hsu, 8/10/91, (PB92-140235/AS).
- NCEER-91-0024 "Experimental Verification of a Number of Structural System Identification Algorithms," by R.G. Ghanem, H. Gavin and M. Shinozuka, 9/18/91, (PB92-176577/AS).
- NCEER-91-0025 "Probabilistic Evaluation of Liquefaction Potential," by H.H.M. Hwang and C.S. Lee, 11/25/91, (PB92-143429/AS).
- NCEER-91-0026 "Instantaneous Optimal Control for Linear, Nonlinear and Hysteretic Structures - Stable Controllers," by J.N. Yang and Z. Li, 11/15/91, (PB92-163807/AS).
- NCEER-91-0027 "Experimental and Theoretical Study of a Sliding Isolation System for Bridges," by M.C. Constantinou, A. Kartoum, A.M. Reinhorn and P. Bradford, 11/15/91, (PB92-176973/AS).
- NCEER-92-0001 "Case Studies of Liquefaction and Lifeline Performance During Past Earthquakes, Volume 1: Japanese Case Studies," Edited by M. Hamada and T. O'Rourke, 2/17/92, (PB92-197243/AS).
- NCEER-92-0002 "Case Studies of Liquefaction and Lifeline Performance During Past Earthquakes, Volume 2: United States Case Studies," Edited by T. O'Rourke and M. Hamada, 2/17/92, (PB92-197250/AS).
- NCEER-92-0003 "Issues in Earthquake Education," Edited by K. Ross, 2/3/92, (PB92-222389/AS).
- NCEER-92-0004 "Proceedings from the First U.S. - Japan Workshop on Earthquake Protective Systems for Bridges," 2/4/92, to be published.
- NCEER-92-0005 "Seismic Ground Motion from a Haskell-Type Source in a Multiple-Layered Half-Space," A.P. Theoharis, G. Deodatis and M. Shinozuka, 1/2/92, to be published.
- NCEER-92-0006 "Proceedings from the Site Effects Workshop," Edited by R. Whitman, 2/29/92, (PB92-197201/AS).

- NCEER-92-0007 "Engineering Evaluation of Permanent Ground Deformations Due to Seismically-Induced Liquefaction," by M.H. Baziar, R. Dobry and A-W.M. Elgamal, 3/24/92, (PB92-222421/AS).
- NCEER-92-0008 "A Procedure for the Seismic Evaluation of Buildings in the Central and Eastern United States," by C.D. Poland and J.O. Malley, 4/2/92, (PB92-222439/AS).
- NCEER-92-0009 "Experimental and Analytical Study of a Hybrid Isolation System Using Friction Controllable Sliding Bearings," by M.Q. Feng, S. Fujii and M. Shinozuka, 5/15/92.
- NCEER-92-0010 "Seismic Resistance of Slab-Column Connections in Existing Non-Ductile Flat-Plate Buildings," by A.J. Durrani and Y. Du, 5/18/92.
- NCEER-92-0011 "The Hysteretic and Dynamic Behavior of Brick Masonry Walls Upgraded by Ferrocement Coatings Under Cyclic Loading and Strong Simulated Ground Motion," by H. Lee and S.P. Prawel, 5/11/92, to be published.
- NCEER-92-0012 "Study of Wire Rope Systems for Seismic Protection of Equipment in Buildings," by G.F. Demetriades, M.C. Constantinou and A.M. Reinhorn, 5/20/92.
- NCEER-92-0013 "Shape Memory Structural Dampers: Material Properties, Design and Seismic Testing," by P.R. Witting and F.A. Cozzarelli, 5/26/92.
- NCEER-92-0014 "Longitudinal Permanent Ground Deformation Effects on Buried Continuous Pipelines," by M.J. O'Rourke, and C. Nordberg, 6/15/92.
- NCEER-92-0015 "A Simulation Method for Stationary Gaussian Random Functions Based on the Sampling Theorem," by M. Grigoriu and S. Balopoulou, 6/11/92, (PB93-127496/AS).
- NCEER-92-0016 "Gravity-Load-Designed Reinforced Concrete Buildings: Seismic Evaluation of Existing Construction and Detailing Strategies for Improved Seismic Resistance," by G.W. Hoffmann, S.K. Kunnath, J.B. Mander and A.M. Reinhorn, 7/15/92, to be published.
- NCEER-92-0017 "Observations on Water System and Pipeline Performance in the Limón Area of Costa Rica Due to the April 22, 1991 Earthquake," by M. O'Rourke and D. Ballantyne, 6/30/92, (PB93-126811/AS).
- NCEER-92-0018 "Fourth Edition of Earthquake Education Materials for Grades K-12," Edited by K.E.K. Ross, 8/10/92.
- NCEER-92-0019 "Proceedings from the Fourth Japan-U.S. Workshop on Earthquake Resistant Design of Lifeline Facilities and Countermeasures for Soil Liquefaction," Edited by M. Hamada and T.D. O'Rourke, 8/12/92.
- NCEER-92-0020 "Active Bracing System: A Full Scale Implementation of Active Control," by A.M. Reinhorn, T.T. Soong, R.C. Lin, M.A. Riley, Y.P. Wang, S. Aizawa and M. Higashino, 8/14/92, (PB93-127512/AS).
- NCEER-92-0021 "Empirical Analysis of Horizontal Ground Displacement Generated by Liquefaction-Induced Lateral Spreads," by S.F. Bartlett and T.L. Youd, 8/17/92.



REPORT DOCUMENTATION PAGE	1. REPORT NO. NCEER-92-0021	2.	3. PB93-188241
4. Title and Subtitle Empirical Analysis of Horizontal Ground Displacement Generated by Liquefaction-Induced Lateral Spreads		5. Report Date August 17, 1992	
7. Author(s) S.F. Bartlett and T.L. Youd		6.	
9. Performing Organization Name and Address Department of Civil Engineering Brigham Young University Provo, Utah 84602		8. Performing Organization Report No.	
12. Sponsoring Organization Name and Address National Center for Earthquake Engineering Research State University of New York at Buffalo Red Jacket Quadrangle Buffalo, New York 14261		10. Project/Task/Work Unit No.	
		11. Contract(C) or Grant(G) No. (C) BCS 90-25010 (G) NEC-91029	
		13. Type of Report & Period Covered Technical Report	
15. Supplementary Notes This research was conducted at Brigham Young University and was partially supported by the National Science Foundation under Grant No. BCS 90-25010 and the New York State Science and Technology Foundation under Grant No. NEC-91029.		14.	
16. Abstract (Limit: 200 words) This report describes empirical models used to estimate the horizontal ground displacement caused by liquefaction-induced lateral spreads. The models were developed from earthquake, geological, topographic, and soil factors that affect ground displacement. Case histories of lateral spreading from the following earthquakes were used: 1) 1906 San Francisco; 2) 1964 Alaska; 3) 1964 Niigata, Japan; 4) 1971 San Fernando, California; 5) 1979 Imperial Valley, California; 6) 1983 Nihonkai-Chubu, Japan; 7) 1983 Borah Peak, Idaho; and 8) 1987 Superstition Hills, California. A multiple linear regression (MLR) is used to develop the empirical models from the compiled data. Two general models are derived: one for free face failures and one for ground slope failures. The predictive performance of the proposed empirical models is determined by a compari- son of the predicted displacements with those actually measured at the case history sites. The first appendix presents a discussion of the independent variables used in the MLR analyses. The minitab analyses are presented in the second appendix. (Adapted from authors' abstract).			
17. Document Analysis a. Descriptors SOIL DEPTH. SATURATED SOIL. EPICENTRAL DISTANCE. LAYERED SOILS. STANDARD PENETRATION VALUES. b. Identifiers/Open-Ended Terms EARTHQUAKE ENGINEERING. LIQUEFACTION. EMPIRICAL MODELS. LATERAL SPREADING. PERMANENT GROUND DISPLACEMENT. REGRESSION ANALYSIS. CASE STUDIES. SAN FRANCISCO, CALIFORNIA EARTHQUAKE, 1906. GROUND SLOPE. ANCHORAGE, ALASKA EARTHQUAKE, 1964. NIIGATA, JAPAN EARTHQUAKE, 1964. SAN FERNANDO, CALIFORNIA EARTHQUAKE, 1971. IMPERIAL VALLEY, CALIFORNIA EARTHQUAKE, 1979. BORAH PEAK, IDAHO EARTHQUAKE, 1983. SUPERSTITION HILLS, c. COSATI Field/Group CALIFORNIA, 1987. MOMENT MAGNITUDE FREE FACE RATIO.			
18. Availability Statement Release Unlimited		19. Security Class (This Report) Unclassified	21. No. of Pages
		20. Security Class (This Page) Unclassified	22. Price

